Elucidation of the Role of VraTSR and Lipid Metabolism in the Development of Resistance Phenotypes in *Staphylococcus aureus*

Tianwei Shen

A dissertation

submitted in partial fulfillment of the

requirements for the degree of

Doctor of Philosophy

University of Washington

2024

Reading Committee:

Libin Xu, Chair

Brian J. Werth

Michelle Reniere

Program Authorized to Offer Degree:

Medicinal Chemistry

University of Washington

Abstract

Elucidation of the Role of VraTSR and Lipid Metabolism in the Development of Resistance Phenotypes in *Staphylococcus aureus*

Tianwei Shen

Chair of the Supervisory Committee:

Associate Professor Libin Xu

Medicinal Chemistry

Staphylococcus aureus is a gram-positive bacterium, which has developed resistance to many antimicrobials. Methicillin-resistant *S. aureus* (MRSA) was first isolated in 1961. Since then, glycopeptides (*e.g.* vancomycin), lipopeptides (*e.g.* daptomycin), and long-acting lipoglycopeptides (*e.g.* dalbavancin) have been developed. MRSA, however, has developed resistance against all three types of antimicrobials over time. VraSR is one two-component system (TCS) out of the 16 prototypical TCSs in *S. aureus*, which is activated in response to cell-envelope-targeting antimicrobials, such as vancomycin and β-lactams. A third component, VraT, has been shown to be essential for VraSR full activation, making it a three-component regulatory system VraTSR. The molecular inducer of VraTSR has been proposed to be the inhibition of transglycosylation in the peptidoglycan layer, and hundreds of genes have been shown to be in the VraR regulon, including those related to cell wall synthesis. On the other hand, cell wall

synthesis has been hypothesized to crosstalk with cell membrane metabolism *via* three potential ways: lipoteichoic acids (LTAs), acetyl-CoA, and lipid II. In fact, overall decreased levels of lipid abundance have been observed in multiple *S. aureus* strains that have developed resistance against vancomycin, daptomycin, or dalbavancin, some of which harbor mutations in VraTSR along with other mutations. None of the strains, nevertheless, have mutations only in VraTSR until we isolated S7-D2 from the parent S7 strain by serial passage against dalbavancin. S7-D2 has a non-synonymous mutation in *vraT* (c. 377C>T; p. P126L) compared to S7. We hypothesized this mutation to be gain-of-function. By using this strain pair and *vraTSR* loss-of-function mutants, we aim to elucidate the contribution of *vraTSR* to the remodeling of the cell envelope and the modulation of antimicrobial susceptibility.

Chapter 1 provides background on *S. aureus* and bacterial TCSs and their relation to antimicrobial susceptibility. In Chapter 2, we applied a multi-omics methodology (transcriptomics, metabolomics, and lipidomics), along with various phenotypic characterization, to assess the role of VraTSR. We found that the loss-of-function mutations in VraTSR resulted in a general increase in antimicrobial susceptibility and that an increase in only limited lipid species was unexpectedly observed. On the contrary, the gain-of-function mutant S7-D2 (confirmed by transcriptomics) exhibited characteristic decreased levels of lipids. We also showed from the multi-omics studies several aspects that could have implications in resistance modulation, *e.g.*, decreased membrane fluidity and upregulated arginine deiminase pathway and betaine biosynthesis pathway, and in crosstalk between cell wall and cell membrane, *e.g.* LTAs and acetyl-CoA. We proposed several future experiments to follow up on the observations from the multi-omics studies. From a practical standpoint, inhibiting the lipid synthesis with AFN-1252

and the VraTSR with histidine kinase inhibitors appear promising in modulating resistance to cell-envelope-targeting antimicrobials, and more studies are warranted.

The *agr* system is another TCS in *S. aureus* that plays critical roles in quorum sensing and virulence. The phenol-soluble modulins (PSMs) produced from Agr and released by *S. aureus* have been suggested to antagonize the lipid shedding mechanism of daptomycin inactivation by binding to the released lipids. Others have shown that *S. aureus* survival in the presence of daptomycin is enhanced with loss of the Agr function. In Chapter 3, we examined several pairs of *S. aureus* strains with dysfunctional Agr (KO or mutants) for their survival with exposure to daptomycin and their lipid profile (released and membrane lipids) in static time-kill experiments and *in vitro* pharmacokinetic/pharmacodynamic (PK/PD) modeling. We found that the contribution of dysfunctional Agr to enhanced survival varied depending on the genetic background or the type of mutations and that the enhanced survival did not correlate with the released lipids. We proposed that PSMs might not be the only molecules released by *S. aureus* that contributed to the antagonizing effects. Studying other released factors might help shed light on the variations among the Agr dysfunctional mutants in terms of enhanced survival against daptomycin. Chapter 4 summarizes the overall findings and proposes future directions.

Acknowledgments

In this Ph.D. journey that lasted for seven years, there are many people who have come along and become an invaluable part of it. Firstly, I would like to express my deepest gratitude to my advisor, Dr. Libin Xu. Thank you for the opportunity to work on such a thought-provoking project, for your exceptional guidance in navigating the complexities of the research project, and for your unwavering patience and encouragement in and outside the lab. Looking back, these seven years have not been easy, especially since my father passed away during the pandemic years, but your tremendous support has kept me going through those hard times. Your expertise in mass spectrometry has also been a treasure from which to get first-hand learning experience. At the same time, I would like to extend the same heartfelt gratitude to my co-advisor, Dr. Brian Werth. Thank you for your dedication to teaching me everything bacteria-related, for the intriguing discussions on microbes, and for the opportunities to participate in projects other than my dissertation project. I probably have spent more time in your lab than in the Xu lab, and I will never forget the small but cozy old lab space. It is a real honor to be a student of both of you.

I am also grateful to the past and current members of the Xu lab and the Werth lab for the collaborative environment they have fostered. I would especially like to mention a great mentor and a good friend of mine, Dr. Hideaki Tomita, who introduced me to the interesting world of molecular biology and has continued to guide and inspire me even after he started his new job in Japan. Thanks especially to Dr. Kelly Hines for her insights into mass spectrometry; to Dr. Rutan Zhang for the rides home and his help with mass spectrometry; to Dr. Amy Li for her willingness to always listen and help, especially with RNAseq data analysis; to Hung Phan for his proficient programming skills in RNAseq data analysis; to the past and current members of the Werth lab (Nate Ashford, Ismael Barreras, Ethan Ahrendt, and Melanie Foreman) for their diligence in

maintaining the lab stocks and an overall tidy and comfortable lab space to work in; and to Qingyu Guo for his hard work as an excellent undergraduate mentee. I would also like to take this opportunity to acknowledge the time and efforts Ismael Barreras spent on the time-kill experiments with AFN-1252; thank you for your help.

Special thanks go to the members of my committee, Dr. Kelly Lee, Dr. Rheem Totah, Dr. Michelle Reniere, Dr. Brian Werth, and Dr. Libin Xu, for their constructive feedback during the committee meetings and their expert advice that have significantly contributed to the quality of this work. I would also like to thank Dr. Lauren Shull in the Reniere lab for guiding me through the *Staphylococcus aureus* mutant generation step-by-step and Dr. Kelsi Penewit, Dr. Elizabeth Holmes, and Dr. Adam Waalkes in the laboratory of Dr. Stephen Salipante for sharing with me their expert knowledge in CRISPR-Cas9 editing of the bacterial genome, total RNA isolation and RNAseq data analysis. My research efforts have been greatly facilitated by the Department of Medicinal Chemistry and the Department of Pharmaceutics staff. Their assistance with resources and facilities was crucial for the completion of this dissertation. Fundings from NIH R01AI136979, the School of Pharmacy Innovation Fund, and the University of Washington Royalty Research Fund are gratefully acknowledged.

Finally, I would like to express my profound appreciation to my mom, dad, and boyfriend. Although we are almost 10,000 km apart from each other, your love and encouragement have been the bedrock of my resilience and determination. Thank you for sharing in the ups and downs of this academic pursuit and beyond with unswerving companionship and understanding. And to all my friends, you know who you are; thank you for being there whenever I need you.

Long Live the Rabbit!

TABLE OF CONTENTS

LIST OF FIGURES

LIST OF TABLES

Chapter 1 Introduction

1.1 *Staphylococcus aureus* and Methicillin-Resistant *S. aureus*

Staphylococcus aureus is a gram-positive bacterium. The cell envelope structure of a gram-positive bacterium is composed of the plasma membrane, the periplasmic space, and the peptidoglycan layer (**Figure 1.1**). The peptidoglycan layer is a mesh of two sugars, *N*-acetylglucosamine (NAG) and *N*-acetylmuramic acid (NAM), connected by the pentaglycine cross-links on the amino acid side chains. Teichoic acids and lipoteichoic acids are also integral parts of the gram-positive cell wall, the latter of which has a lipid anchor inserted in the bacterial membrane. Methicillin-resistant *S. aureus* (MRSA) was first reported in 1961 from the United Kingdom (1), invalidating almost all antimicrobials including the most potent β-lactams at the time (2). Although several antimicrobials in the categories of glycopeptides, lipopeptides, and lipoglycopeptides have been developed after methicillin resistance appeared in the 1970s (1), MRSA has developed resistance to these drugs (3–5) and still causes a wide range of infections, commonly involving the skin, soft tissue, bone, joints, and the infections associated with indwelling catheters or prosthetic devices (6). The Centers for Disease Control and Prevention (CDC) categorizes MRSA as a serious threat and has reported 323,700 cases of MRSA and 10,600 deaths in the United States in 2019 (7). As a result, there is an urgent need to study MRSA and its resistance mechanisms to the antimicrobials developed after methicillin resistance appeared.

1.1.1. Cell Envelope-Targeting Drugs against MRSA

Vancomycin (**Figure 1.2A**), a glycopeptide, is a first-line anti-MRSA antibiotic which targets peptidoglycan synthesis. The amino acids (*D*-Ala-*D*-Ala), where the pentaglycine cross-links form, are exactly where vancomycin targets (**Figure 1.1**) (8, 9). When the cross-links

break, the bacteria cannot resist turgor pressure and is less likely to survive. Clinical and Laboratory Standards Institute (CLSI) has established laboratory breakpoints for defining vancomycin resistance in MRSA. MRSA is divided into three categories based on their minimum inhibitory concentrations (MICs): vancomycin-susceptible (VSSA; MIC≤2 μg/mL), vancomycin-intermediate (VISA; MIC=4-8 μg/mL), and vancomycin-resistant *S. aureus* (VRSA; MIC≥16 μg/mL) (10). Heteroresistant VISA (hVISA) has also been reported (11–17) and can be identified by modified population analysis profiling (PAP) (12).

A VRSA strain was first identified in 1997 from Japan (17), and since then efforts have been made to develop alternatives to vancomycin. Lipopeptides (*e.g.* daptomycin, **Figure 1.2B**) have been developed as last-resort antimicrobials to treat MRSA (18). Unlike vancomycin, daptomycin binds with Ca^{2+} in the growth medium to become a de facto cationic peptide that is electrostatically attracted to the negatively charged membrane (**Figure 1.1**) (19). It then inserts its hydrophobic tail into the membrane and oligomerizes (19). There has been conflicting evidence on the precise mechanism of bacterial death mediated by daptomycin, but membrane depolarization through loss of K^+ ions and delocalization of key peripheral proteins are consistently observed (19). Alternatively, dalbavancin is a long-acting lipoglycopeptide derived from teicoplanin and dosed once weekly because of its extended half-life (20, 21). Regarding structure (Figure 1.1C), dalbavancin can be viewed as a combination of glycopeptide and lipopeptide; hence, it has been shown to interact with both the cell wall and the cell membrane (20). Although the *D*-Ala-*D*-Ala in the peptidoglycan layer of the cell wall and anionic lipids in the cell membrane seem to be different targets, cross-resistance among vancomycin, daptomycin, and dalbavancin has been observed, where increases in vancomycin resistance generally correlate with increases in daptomycin and dalbavancin resistance (22–24). In addition,

downregulation of cell wall autolysis and/or upregulated synthesis of cell wall components are consistently observed in *S. aureus* strains that are resistant to vancomycin and/or daptomycin (23, 25–30). Such observations in strains resistant to daptomycin suggest that crosstalk between cell wall synthesis and cell membrane metabolism might exist in *S. aureus*, possibly acting together to develop resistance to cell-envelope-targeting antimicrobials.

1.1.2. Crosstalk between Cell Membrane and Cell Wall Synthesis in *S. aureus*

S. aureus synthesizes three major classes of phospholipids: phosphatidylglycerols (PGs), lysyl-PGs, and cardiolipins (CLs) (31–33). A schematic of the lipid synthesis pathway is shown in **Figure 1.3**. Lipid synthesis starts with glycerol 3-phosphates (GPs) and fatty acids from the FASII fatty acid synthesis pathway to form phosphatidic acids (PAs) (34). PGs can be produced from PAs *via* several steps in the lipid metabolism pathway. PGs can, in turn, result in the formation of CLs through the action of cardiolipin synthase (Cls) and the formation of lysyl-PGs through the action of phosphatidylglycerol lysyltransferase (MprF) (35, 36). PGs and lysyl-PGs are negatively charged and are the major targets of daptomycin. Furthermore, PGs can donate their GP headgroups to lipoteichoic acids (LTAs), forming the backbone of LTAs and leaving the diacylglycerols (DAGs) as the by-product. DAGs can accept glucose molecules and serve as the lipid anchor for LTAs (36–38).

As can be seen above, LTAs are a major connection between cell wall synthesis and lipid synthesis in *S. aureus*, in that their backbone and lipid anchor can be generated from the lipid metabolism pathway (**Figure 1.3**). There are two other routes through which lipid synthesis is metabolically closely connected with cell wall synthesis. Firstly, acetyl-CoA is essential for both the synthesis of fatty acids (34) and the synthesis of NAGs and NAMs in the formation of the peptidoglycan layer (9) (**Figure 1.3**). Secondly, a polyisoprenoid lipid (lipid II; structure shown

in **Figure 1.4**) serves as an anchor to transport peptidoglycan precursors from cytosol to outside (8, 39, 40). The crosstalk between cell wall synthesis and lipid metabolism in *S. aureus* might be an underlying mechanism behind the observed cross-resistance (22–24).

1.2 Cell Envelope Stress Response and Resistance to Peptide Antimicrobials

1.2.1. Bacterial Two-Component Regulatory Systems

Two-component systems (TCS) are one of the major signal transfer mechanisms in prokaryotes, such as bacteria and many archaea (41–43). They enable microorganisms to sense, respond and adapt to a wide range of environments, including but not limited to pH, nutrient level, redox state, osmotic pressure, and antimicrobials (44, 45). TSCs control various aspects of bacterial cell physiology, *e.g.* cell division, biofilm formation, quorum sensing, and sporulation (41, 45). They also play important roles in the expression of virulence factors, toxin production and secretion, invasion, and antimicrobial resistance (41, 45–47). Several databases are available for the identification and analysis of microbial signal transduction and TCS proteins. For instance, the P2CS database (Prokaryotic 2-Component Systems) makes accessible 164,651 TCS proteins from 2,758 prokaryotic genomes (48) and the microbial signal transduction (MiST) 4.0 database allows for the profiling of signaling systems with metagenomic functions (49).

A prototypical TCS consists of a dimeric sensor histidine kinase (HK) and its cognate response regulator (RR) (41, 50, 51). Although the structures of HKs are diverse (50–52), an HK typically harbors an *N*-terminal extracytoplasmic or periplasmic sensor domain, a transmembrane domain, and usually one or more intracellular signal domains (41, 53). On the *C*-terminal of an HK is a catalytic core consisting of a DHp (dimerization and histidine phosphorylation) domain and a CA (catalytic and ATP-binding) domain (41, 53). On the other hand, an RR is composed of a phosphoacceptor receiver (REC) domain and a DNA-binding

output domain (50, 53). Upon exposure to inducers, the signal is perceived in the sensor domain and transmitted through the transmembrane and intracellular signal domains, eventually to the catalytic core where APT binds to the CA domain and autophosphorylates the conserved histidine residue in the DHp domain (41, 50, 53). The phosphoryl group is then transferred to the conserved aspartic acid residue in the REC domain of the cognate RR (41, 50, 53). The phosphorylated RRs most frequently inform downstream target genes by binding to the promoter region (41, 50, 53). In some instances, RRs can also bind to RNA and proteins or exert enzymatic activities (41, 53). In addition to the kinase property of HKs, most HKs can also dephosphorylate their cognate RRs, controlling the levels of phosphorylated RRs and, therefore, downstream responses to external stimuli (41). The structures and functions of HKs vary and have been comprehensively reviewed in (54–56). On the other hand, RRs can be divided into four subfamilies based on the structures of the DNA-binding domains (50): OmpR subfamily (winged-helix DNA-binding domain) (57), LuxR subfamily (helix-turn-helix DNA-binding domain) (58), AraC subfamily (helix-turn-helix DNA-binding domain) (58), and LytR subfamily (10-stranded β-folds DNA-binding domain) (59). The OmpR subfamily is the largest among the four (50, 57).

1.2.2. Two-Component Regulatory Systems in *S. aureus*

There are 16 prototypical TCSs in the core genome of *S. aureus*, among which WalKR (also known as YycGF or VicKR) is the only one essential for bacterial survival under normal growth conditions (60) and has been linked to cell-wall metabolism (61). The other 15 TCSs are nonessential (50). They, nevertheless, have been associated with a variety of cellular functions, such as antimicrobial resistance (VraSR, BraSR, and GraSR) (30, 62–64), virulence (SaeSR and AgrCA) (65, 66), bacterial respiration, nitrate metabolism and fermentation (SrrBA, NreBC, and

AirSR) (67–70), cell-wall metabolism (ArlSR and LytSR) (71, 72), and nutrient sensing and metabolism (HssSR, PhoRP, and KdpDE) (50, 73–75). A review of the structural families, main target genes, functions, known stimuli, and trans-strain conservation of the TCSs in *S. aureus* has been detailed in (50).

Other sensory systems than the 16 TCSs also exist in *S. aureus*. The *bla* operon consists of the *blaZ*, *blaI*, and *blaR1* genes, which code for β-lactamase, repressor, and sensor transducers, and is located on the mobile genetic element or genomic DNA (50, 76). Eukaryote-like serine/threonine kinases (STK) and phosphatase (STP) are also present in *S. aureus* (77, 78). The bacterium has one major STK (Stk1, also denoted as PknB or PkrC) and one major STP (Stp1) (77, 78). In some *S. aureus* strains, *e.g.* N315 and Mu50, a second hypothetical cytoplasmic STK has also been found in the *SCCmec* element (77, 78). Stk1/Stp1 does not have a cognate RR, but it has been shown to be capable of phosphorylating the RRs in the VraSR and the GraSR TCSs, VraR and GraR, respectively (50, 77, 79). Additionally, Stk1 has been implicated in virulence regulation and has been shown to possess regulatory effects on cell signaling, central metabolism, stress response, purine biosynthesis, cell-wall metabolism, autolysis, and glutamine synthesis (50, 77, 80–84). It has also been associated with vancomycin susceptibility (85, 86).

1.2.3. The VraTSR Three-Component Regulatory System in *S. aureus*

The VraSR TCS has a third component, VraT, and together the three component regulatory system VraTSR is named for its association with vancomycin resistance and may be especially important for responding to cell-envelope-targeting antimicrobials, such as vancomycin and β-lactams (87). VraS is the HK, and VraR is the RR (88). As with prototypical TCSs, VraS is capable of undergoing autophosphorylation, and its phosphoryl group is rapidly

transferred to VraR. Only phosphorylated VraR dimerizes and becomes biologically active, and thus VraS confers tight control on the phosphorylation states of VraR through rapid phosphorylation and dephosphorylation (88). A proposed scheme of the phosphotransfer-mediated VraTSR signaling pathway is shown in **Figure 1.5** (87). It has been shown that cell wall synthesis-associated genes, *pbp2*, *murZ*/*murA*, and *sgtB*, are regulated by the direct binding of VraR to their respective promoters (89), and that the transcription of over 200 genes are affected by the induction of the VraTSR system (28).

Although it was shown that VraT is required for the functioning of VraS and VraR (87), the role of VraT is not yet entirely understood. Fernandes et al. (90) have demonstrated that VraT is membrane-bound (87, 90) and harbors an extracellular C-terminal domain (90). The molecular signal for the induction of the VraTSR system is unknown but has been proposed to be the damage inflicted to cell wall peptidoglycan by antimicrobials (88). Fernandes et al. (90) have narrowed down the potential inducers of the VraTSR system and have suggested that the inhibition of transglycosylase activity, instead of the changes in the amount of lipid-linked peptidoglycan precursors (*e.g.* lipid II), seems to play important roles in the activation of the VraTSR system (90).

1.2.4. VraTSR, WalKR, Antimicrobial Resistance, and the Associated Phenotypic Changes

In strains of *S. aureus* that have developed resistance to vancomycin and/or daptomycin, mutations or increased expression of *vraTSR* are frequently observed (26–28, 91–94). Although inactivating *vraTSR* increases susceptibility to cell wall antimicrobials (87, 95), mutations in *vraT* and *vraS* are common in resistant strains, likely because they lead to increased expression of *vraR* (27, 93). On the other hand, WalKR is often mutated in strains resistant to daptomycin and/or vancomycin (96–98). WalKR is known to regulate cell wall metabolism by affecting cell

wall degradation (99, 100). In *S. pneumoniae*, the induction of *yycF* (or *walR*) elevates the expression of fatty acid synthesis genes, such as *fabKDGF* and *accABC* (101, 102). Whole genome sequencing of daptomycin-resistant *S. aureus*, both clinical and laboratory strains, has also revealed mutations in genes related to lipid metabolism, including *mprF* (the most commonly observed) (94, 103), *cls*, and *pgsA* (104, 105). Notably, upregulation of *vraSR* have been linked to cell wall thickening in these strains, indicating a connection between altered lipid metabolism and increased cell wall thickness (94). In addition to cell wall thickness, , cell surface charge tends to be more positive in strains resistant to daptomycin, possibly due to weaker association with the drug based on electrostatic repulsion (106–108).

1.3 The Agr System, Lipid Shedding and Daptomycin Tolerance

Most of our work has focused on correlating changes in membrane composition with changes in antimicrobial susceptibility. However, others have put forth a theory by which shed cell envelop components may affect drug activity against bacterial cells (109). In fact, bacteria can release a diverse array of molecules to intercept antibiotics, including monomeric PGs, capsular polysaccharides, aminoglycosides, and outer-membrane vesicles (109). Monomeric PGs and other lipids released by *S. aureus* upon daptomycin exposure have been proposed to inactivate daptomycin as a novel mechanism of daptomycin tolerance (110). The authors found that amphipathic peptides called phenol soluble modulins (PSMs) can bind the released lipids and thus prevent the inactivation of daptomycin (110). PSMs are produced by the accessory gene regulatory (Agr) system (**Figure 1.6**), which also controls the secretion of multiple virulence factors through the action of RNAIII (111). The regulator of the Agr system is the cyclic peptide AIP, which is produced from its linear peptide precursor AgrD by the endopeptidase AgrB (111). Binding of AIP to the histidine kinase AgrC initiates phosphorylation of the RR AgrA and leads

to the upregulation of RNAII (P2 promoter), RNAIII (P3 promoter) and PSMs (111). Pader et al. (2016) suggested that loss of the Agr quorum-sensing system enhances *S. aureus* survival during daptomycin treatment because the absence of PSMs in Agr-defective *S. aureus* allows daptomycin to be sequestered in the released lipids. However, the authors failed to elucidate the detailed composition of the membrane lipids and the shed lipids, in that they profiled the lipid composition with the fluorescent probe FM-4-64 (110), which is designed to bind the outer leaflet of the plasma membrane and has not been demonstrated for binding of discrete lipids in solution (112). Additionally, the authors did not examine the effects of lipid shedding on daptomycin activity under clinically relevant kinetic drug exposures. Hence, we aim to assess the detailed lipid composition by hydrophilic interaction liquid chromatography-ion mobility-mass spectrometry (HILIC-IM-MS)-based lipidomics and the impacts on daptomycin tolerance by static time-kills and *in vitro* pharmacokinetic/pharmacodynamic (PK/PD) modeling to better understand the contribution of lipid shedding to daptomycin tolerance.

1.4 Dissertation Overview

In this thesis, I have applied a multi-omics approach in evaluating the roles of a specific regulatory system, the VraTSR system, in the development of resistance phenotypes in *S. aureus*. Analyses of the transcriptome, metabolome and lipidome have been performed to gain insights into how the VraTSR system and, more importantly, VraT lead to characteristic metabolic changes with decreased susceptibility to cell-envelope-targeting antimicrobials, *e.g.* vancomycin, daptomycin and dalbavancin. I have also examined the effects of small molecule inhibitors on the killing effects of the cell-envelope-targeting antimicrobials. These studies have shed light on various metabolic routes governed by the VraTSR system, which lead to the observed susceptibility changes. However, limited studies have been conducted on VraT, and our results

warrant further research on this membrane-bound protein. In addition, I have also examined the role of lipid shedding in daptomycin tolerance in various *S. aureus* strains as well as in a clinical PK/PD model of daptomycin. This allows for a different angle of inspection of the lipid metabolism and its effects on the resistance phenotypes in *S. aureus*.

Chapter 2 focuses on the VraTSR system. It describes the lipid profile and resistance phenotypes of *vraTSR* loss-of-function mutations, followed by the multi-omics results of the *S. aureus* strain with a gain-of-function mutation in *vraT*. Multiple follow-up experiments to the omics studies are detailed, and the modulation of resistance phenotypes by small molecule inhibitors is also examined in Chapter 2. Chapter 3 focuses on lipid shedding and its relationship with daptomycin tolerance in *S. aureus* strains defective in the Agr system. Finally, Chapter 4 summarizes the overall findings and the future directions.

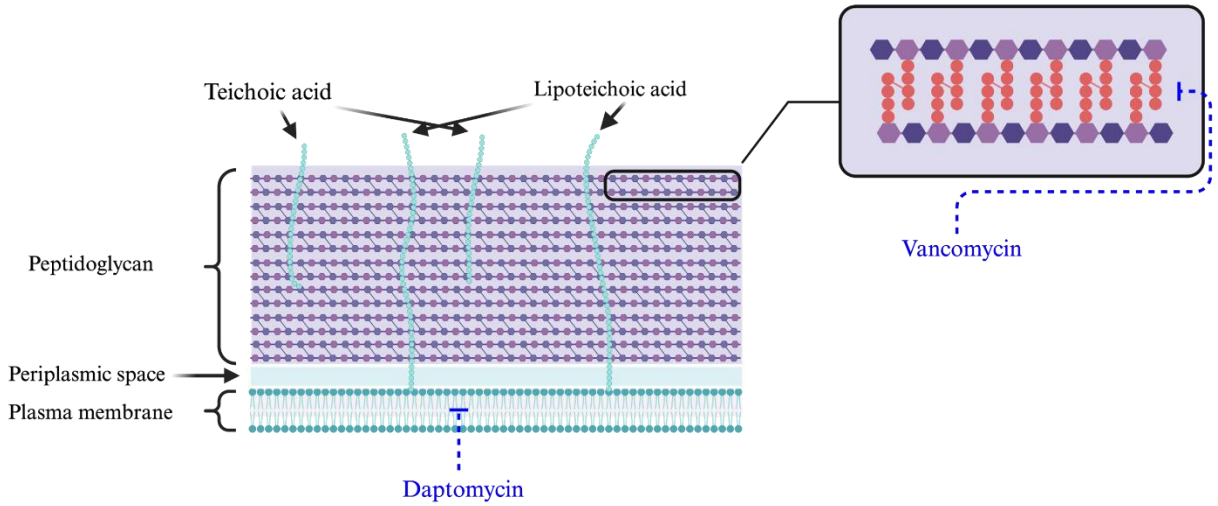

Figure 1.1 Illustration of a gram-positive cell envelope structure, consisting of the plasma membrane, periplasmic space, peptidoglycan layer, teichoic acids, and lipoteichoic acids. Targets of vancomycin and daptomycin are labeled: *D*-Ala-*D*-Ala of the amino acid side chain in the peptidoglycan layer and lipids in the cell membrane. Created with BioRender.com.

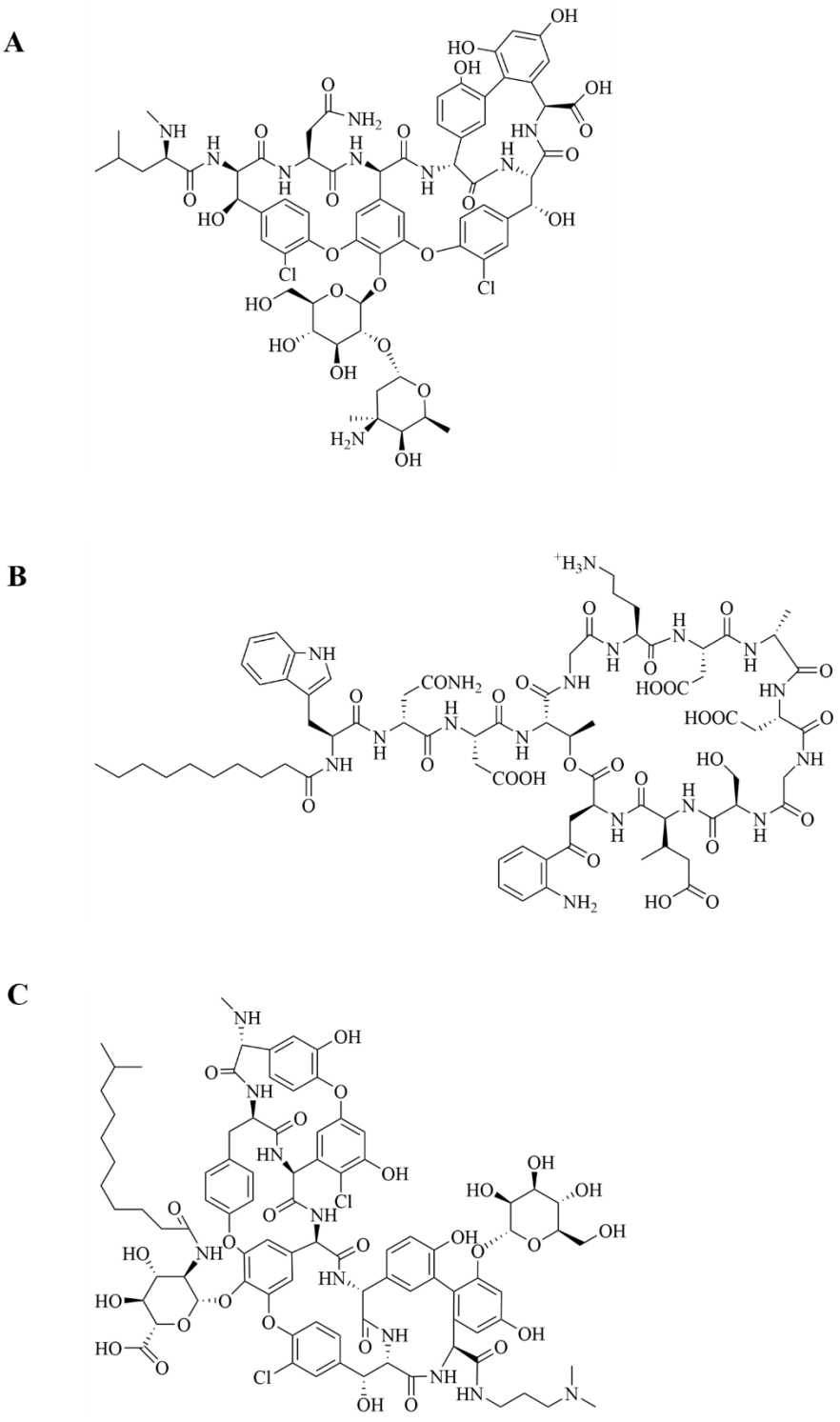

Figure 1.2 Chemical structures of **A**) vancomycin (glycopeptide), **B**) daptomycin (lipopeptide), and **C**) dalbavancin (lipoglycopeptide).

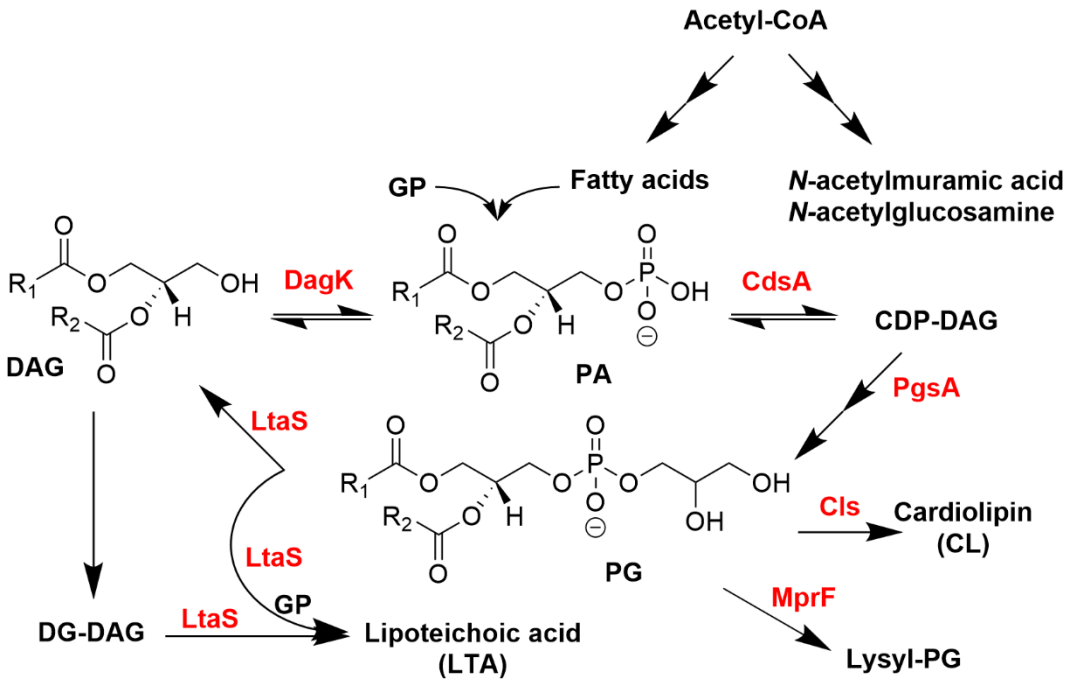

Figure 1.3 Lipid metabolic pathway in *S. aureus*. DagK, diacylglycerol kinase; CdsA, phosphatidate cytidylyltransferase; PgsA, phosphatidylglycerol phosphate synthase; Cls, cardiolipin synthase; MprF, lysyl-PG synthase; LtaS, LTA synthase; GP, glycerol 3-phosphate; PA, phosphatidic acid; PG, phosphatidylglycerol; DAG, diacylglycerol; DG-DAG, diglucosyl-DAG; R1, R2: fatty acid chain. Schematic credit to Dr. Libin Xu.

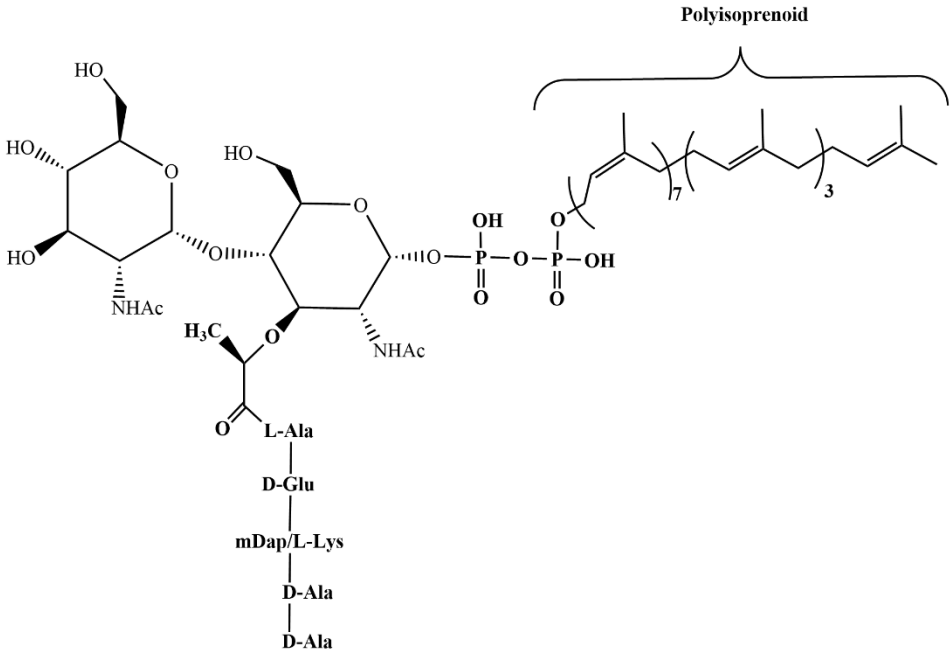

Figure 1.4 Chemical structure of lipid II, a polyisoprenoid lipid.

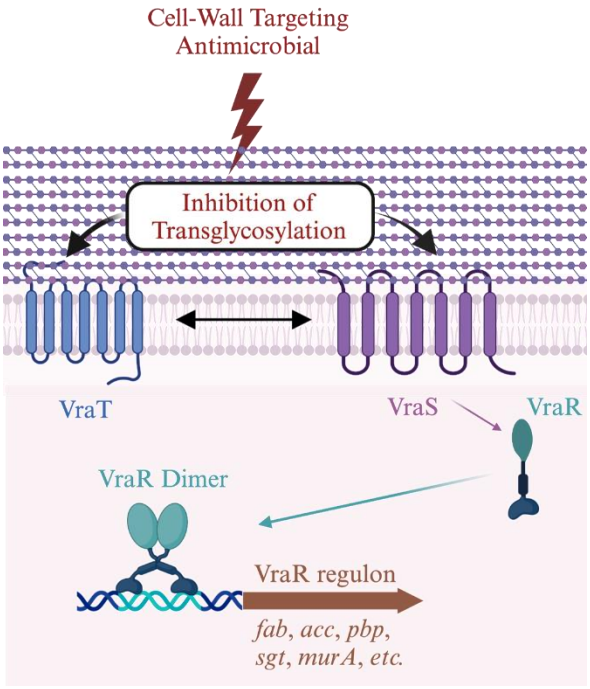

Figure 1.5 Scheme of the *vraTSR* signaling pathway. Upon exposure to cell-wall acting antimicrobials, inhibition of transglycosylation serves as a possible molecular inducer of *vraTSR*. VraS relays the phosphorylation signal to VraR. VraT is required to activate vraTSR fully. Created with BioRender.com. Adapted and reprinted with permission from **(87)**. Copyright 2013 American Society for Microbiology.

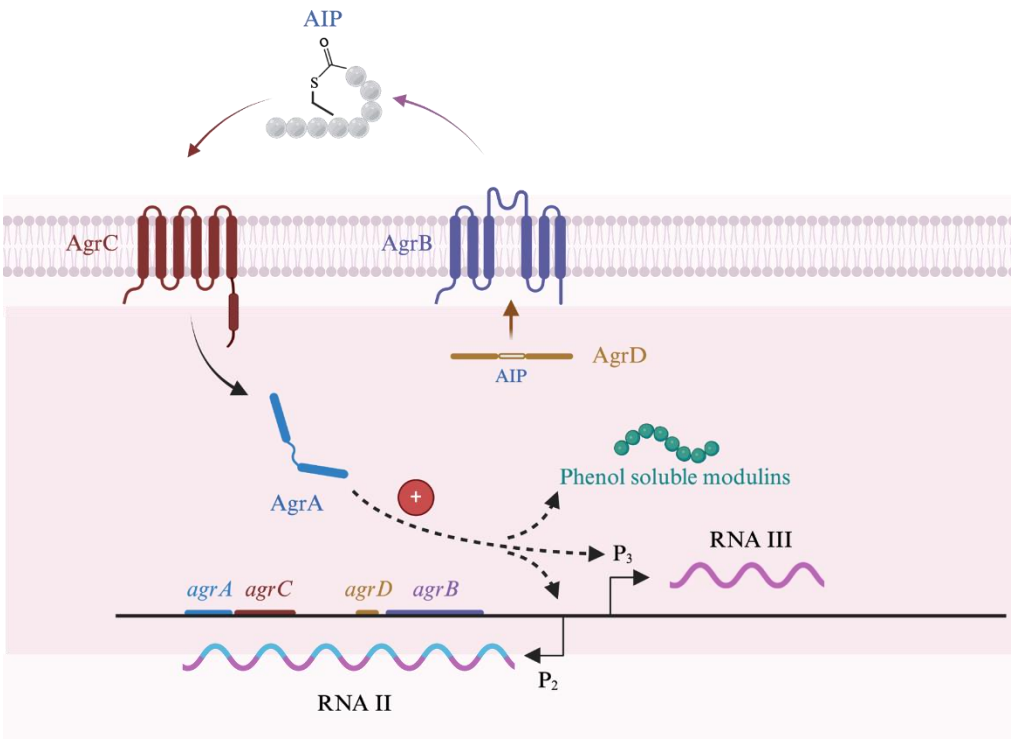

Figure 1.6 Schematic of the Agr system in *S. aureus*. Activation of the system positively regulates RNAII, RNAIII and phenol soluble modulins (PSMs). RNAIII is the primary effector and turns on the secretion of virulence factors. Created with BioRender.com. Adapted and reprinted with permission from (111). Copyright 2011 American Chemical Society.

Chapter 2 Contributions of the VraTSR Three-Component Regulatory System to the Susceptibility to Cell-Envelope-Targeting Antimicrobials in *Staphylococcus aureus*

2.1 Introduction

When cell-wall active antimicrobials, *e.g.* glycopeptides, lipopeptides, lipoglycopeptides and *β*-lactams, damage the cell wall, *Staphylococcus aureus* can mount a response in an effort to counteract the drug exposure. There are 16 known two-component systems (TCSs) that help *S. aureus* to detect and respond to cell envelope stress, including WalKR, GraRS, ArlRS, AirRS, BraRS, and VraSR (50, 95, 113–116). There is a third component to the VraSR TCS, VraT, and the phosphorelay signal transduction of the VraTSR system has been detailed in Section 1.2.3. Briefly, VraS phosphorylates VraR upon exposure to cell-envelope active antimicrobials, which regulates lots of genes including those involved in cell wall synthesis (28, 87–89). The membrane-bound VraT is required for the full activation of VraTSR, which is likely to be induced by the inhibition of transglycosylation activity (87, 90).

Point mutations and/or upregulations in the *vraTSR* system are commonly observed in *S. aureus* that have developed resistance against vancomycin and/or daptomycin (26–28, 91–94). We previously also observed *vraTSR* mutations in the JE2 *S. aureus* strains that were isolated after exposure to multistage escalated concentrations of vancomycin or dalbavancin (24, 117). Additionally, we showed that the levels of the membrane lipids, phosphatidylglycerols (PGs), correlated with the susceptibility to vancomycin, daptomycin and dalbavancin (24, 117). We also examined another MRSA strain, N315 (104, 118), and clinical MRSA isolates that are part of the Werth Lab strain collection, including W308 (117) and VAPH-884 (119). The increased resistance to vancomycin, daptomycin and/or dalbavancin in the *S. aureus* strains after serial passage or *in vitro* pharmacokinetic/pharmacodynamic (PK/PD) modeling generally correlated

with decreased levels of membrane lipids, except in some instances involving *β*-lactam seesaw effects where there were increased levels of membrane lipids even when the vancomycin, daptomycin and/or dalbavancin resistance increased (24). Most of the resistant strains harbored more than one mutation, except the studies with W308 as the parent strain where a couple of dalbavancin-nonsusceptible strains isolated from *in vitro* PK/PD modeling had point mutations in only the *walK* or *walR* gene (117). Some of the resistant strains had mutations in *vraTSR*, but none of the *vraTSR* mutations occurred by themselves (24, 118).

Previously in our lab, we isolated a vancomycin-susceptible MRSA strain, S72982 (S7; vancomycin MIC: 1 μg/mL), from a patient with MRSA bacteremia who was treated with a vancomycin and dalbavancin-containing regimen (120). By exposing this strain to multistage escalated concentrations of dalbavancin until the dalbavancin minimum inhibitory concentration (MIC) was 1 μg/mL, we were able to isolate a vancomycin-intermediate *S. aureus* (VISA) strain S7-D2 with a vancomycin MIC of 4 μg/mL and with only one point mutation in *vraT* (c. 377C>T; p. P126L) as compared to S7 by whole-genome sequencing (120). This strain pair served as a good starting point for studying the role of the *vraTSR* system in producing resistance to cell-envelope-targeting antimicrobials, not only because it harbored only one point mutation but also because the mutation was in the not-well-studied *vraT* gene.

For this Chapter, we hypothesized that *vraTSR* contributed to the remodeling of cell envelope to modulate susceptibility. This hypothesis was based on the following two aspects: 1) the *vraT* mutation in S7-D2 has been associated with vancomycin and dalbavancin resistance (120); and 2) characteristic changes to lipid metabolism have been observed in *S. aureus* strains with mutations in *vraTSR* and increased resistance to cell-envelope-targeting antimicrobials (24, 118). Furthermore, we hypothesized that small molecule modulators of lipid metabolism or *vraS*-

targeting histidine kinase inhibitors could directly modulate susceptibility to cell-envelope-targeting antimicrobials. Lipid synthesis inhibitors have been developed as antimicrobials over the past few decades. For example, HDSF is a bacterial phospholipase inhibitor (121), statins are polyisoprenoid synthesis inhibitors, and compound 1771 is a known inhibitor of lipoteichoic acid (122). FASII inhibitors, on the other hand, target the FASII fatty acid synthesis pathway (34, 123). Among them, cerulenin acts where the fatty acid chains are elongated (FabF inhibitor), while triclosan and AFN-1252 act where the precursors to lipid synthesis are formed (FabI inhibitor) (34, 123). These compounds are potential modulators of lipid metabolism in *S. aureus*. It would be of interest to determine how the lipid synthesis inhibitors would affect the lipid metabolism and if the lipid synthesis inhibitors could favor a susceptible phenotype.

Histidine kinase inhibitors are another potential modulator of the VraTSR system and antimicrobial resistance. Histidine kinases, such as VraS, are unique in bacteria, and therefore histidine kinase inhibitors would not target human kinases. We propose to examine the histidine kinase inhibitors developed by Dr. Michael E. Johnson's group (Center for Biomolecular Sciences and Department of Medicinal Chemistry & Pharmacognosy, University of Illinois at Chicago, Chicago IL) (124). Those histidine kinase inhibitors were designed to specifically target the VraTSR three-component regulatory system, and have been shown to exhibit synergy with oxacillin, a β-lactam cell-wall active antimicrobial (124). With demonstrated synergy with oxacillin, those inhibitors hold promise in being synergistic with other cell-envelope active antimicrobials, such as vancomycin, daptomycin and dalbavancin. Among the developed histidine kinase inhibitors, we chose to examine F1374-0037 specifically due to its demonstrated binding to VraS (and not VraR or some other histidine kinases) (124) and its relatively high solubility in the aqueous environment.

In this Chapter, we will first examine how the loss-of-function mutations of the *vraTSR* system might affect the resistance phenotypes and the lipid metabolism, using the JE2 transposon strains and the in-house generated N315 *vraS* knock-out (KO) strain. We will then focus on the S7 and S7-D2 strain pair. Presumably, the 377C>T non-synonymous mutation in S7-D2 is likely a gain-of-function mutation because the vancomycin and dalbavancin MIC significantly increased in S7-D2 (120). Hence, including *vraTSR* loss-of-function mutants in our studies is necessary to get a more complete view of the effects of the regulatory system on antimicrobial resistance. For the S7 strain pair, a multi-omics approach (transcriptomics, metabolomics and lipidomics) will be applied. We believe that such an approach will reveal insights into how the *vraTSR* regulatory system functions on different levels in the context of antimicrobial resistance, with a specific focus on vancomycin, daptomycin, and dalbavancin. Finally, we will determine the effects of the lipid synthesis inhibitors (cerulenin and AFN-1252) and the histidine kinase inhibitor (F1374-0037) on modulating the resistance phenotypes of S7 and S7-D2. Results from these studies will shed light on the role of the VraTSR system in the development of resistance to cell-envelope-targeting antimicrobials and suggest potential modulators of the resistance.

2.2 Results

2.2.1. *vraTSR* loss-of-function mutants exhibited varied lipid metabolism and resistance phenotypes

The 377C>T point mutation in S7-D2 could be loss-of-function or gain-of-function. Although we hypothesized the mutation to be the latter, we started with transposon mutants and KOs to test the effects of loss-of-function mutations in *vraTSR* on antimicrobial resistance and lipid synthesis. We obtained the *vraT, vraS*, and *vraR* transposon mutants (*vraT*::Tn, *vraS*::Tn, and *vraR*::Tn) from the Nebraska Transposon Mutant Library (125). These transposon mutants

were derived from the USA300 JE2 strain (125). We performed broth microdilution MIC tests on the three transposon mutants and population analysis profiling (PAP) on *vraS* and *vraR* transposon mutants to characterize their resistance to vancomycin, daptomycin, and dalbavancin compared to the WT. By definition, the broth microdilution MIC measurements report the minimum concentration of antimicrobials at which bacterial growth is inhibited (10). Alternatively, PAP is the gold standard for the identification of heteroresistant VISA (hVISA) (12, 126), but in this case, it allows for the detection of bacterial killing profiles at different antimicrobial concentrations and the assessment of overall susceptibility by comparing the area under the curve (AUC). We found that JE2 transposon mutants of *vraT*, *vraS*, and *vraR* were more susceptible to dalbavancin by broth microdilution (>2-fold decrease in MIC for *vraT*::Tn and >4-fold decrease for *vraS*::Tn and *vraR*::Tn) and that *vraT*::Tn was also more susceptible to daptomycin (a 4-fold decrease in MIC) (**Table 2.1**). No significant changes were observed in susceptibility to vancomycin in the broth microdilution tests (**Table 2.1**). PAP revealed that the *vraS* and *vraR* transposon mutants were more susceptible to vancomycin and daptomycin (**Figure 2.1**), although the change in daptomycin susceptibility was minimal. Combining the broth microdilution and PAP results, the JE2 *vraT*, *vraS*, and *vraR* transposon mutants showed increased susceptibility to vancomycin, daptomycin, and dalbavancin, except for *vraT*::Tn whose vancomycin PAP has not been quantified. Furthermore, we did not test high enough daptomycin concentrations to confirm what the necessary concentration was to eliminate any growth in PAP. More experiments investigating these two aspects would be noteworthy.

To examine the role of the VraTSR system in a different genetic background, we chose the well-studied MRSA strain, N315 (2). Using the *p*IMAY plasmid (127), we successfully generated a *vraS* KO in N315. The polymerase chain reaction (PCR) product of the *vraS* KO was

expected to have 1340 bp of nucleic acids, consistent with what the agarose gel image showed in **Figure 2.3**. The *vraS* KO was subsequently subjected to MIC measurements using the broth microdilution method. Its vancomycin and daptomycin MICs were not significantly changed as compared to the WT, which coincided with the JE2 *vraS*::Tn (**Table 2.1**). The dalbavancin MIC of the N315 *vraS* KO was unfortunately not adequately determined (**Table 2.1**) and should be verified in future experiments. The general trend that increase in susceptibility to vancomycin, daptomycin, and dalbavancin was observed in the *vraS* KO and the JE2 transposon mutants led us to believe that the *vraTSR* mutations were possibly gain-of-function in the *S. aureus* strains with increased resistance to cell-envelope-targeting antimicrobials (detailed in Section 2.1), especially S7-D2.

In addition to the resistance phenotypes, we compared the lipid metabolism of the JE2 *vraT*, *vraS* and *vraR* transposon mutants to that of the WT by the untargeted hydrophilic interaction liquid chromatography-ion mobility-mass spectrometry (HILIC-IM-MS) method. We aimed to determine if the overall lipid abundance increased in the loss-of-function mutants because of the following two reasons: 1) we previously observed the reversed trend in the resistant *S. aureus* strains from the serial-passage experiments and *in vitro* PK/PD modeling (24, 104, 117–119); and 2) we hypothesized that at least a portion of those resistant strains possessed gain-of-function mutations in *vraTSR*. The lipid profile (**Figure 2.2**) demonstrated that, compared with the WT, the levels of PGs (the major lipid species) and lysyl-PGs in *vraS*::Tn and *vraR*::Tn generally decreased, while those in *vraT*::Tn were not significantly different except for PG 30:0, which also significantly decreased. On the other hand, the levels of FAs generally increased in all three mutants, especially the most abundant FA 20:0. As for DGDGs, several species significantly decreased (DGDG 30:0 in *vraT*::Tn; DGDG 30:0, 31:0, and 32:0 in

vraS::Tn and *vraR*::Tn), while DGDG 34:0 significantly increased in *vraT*::Tn and *vraS*::Tn. Taken together, we observed from the lipid profile that *vraT*::Tn showed only increase in limited lipid species, *e.g.* FA 20:0 and DGDG 34:0, and that *vraS*::Tn or *vraR*::Tn led to decrease in lipids other than FAs, and increases only in the same small number of lipid species as for *vraT*::Tn. These observations were not entirely consistent with our expectations and could indicate that loss-of-function *vraT* mutations are not sufficient to lead to lipid changes, but gain-of-function point mutations might. Such an implication furthers the need to examine the S7 and S7-D2 strain pair. The observations could also indicate that the WalKR TCS may be more important in governing lipid metabolism upon exposure to cell-envelope active antimicrobials, as mutations in this system have been observed, standalone or with mutations in other genes, in multiple *S. aureus* strains that developed resistance to vancomycin, daptomycin, or dalbavancin over time *via* serial-passage or *in vitro* PK/PD modeling (24, 104, 117–119). Those strains have further been shown to have modulation effects on lipid metabolism (24, 104, 117–119).

2.2.2. S7-D2 had a growth defect and a more rigid bacterial membrane

The increased antimicrobial susceptibility of the *vraTSR* loss-of-function mutants supported our hypothesis (section 2.1) that the *vraT* mutation in the S7-D2 strain is a gain-of-function mutation. As a result, we next examined the S7 and S7-D2 strain pair. Because vancomycin resistance is frequently associated with loss of fitness (128, 129), we started with comparing the growth curve of S7-D2 with its parent strain S7 over a 24-h period. The growth curves (**Figure 2.4A**) indicated that S7-D2 had a prolonged lag phase compared with the vancomycin and dalbavancin susceptible parent, S7. The parameters of the linear regression of the mid-exponential phase were also shown in **Figure 2.4A**, and demonstrated that S7-D2 had a

slower growth rate (increase in OD_{600} by 0.1329 per hour) compared with S7 (increase in OD_{600} by 0.2048 per hour).

Daptomycin susceptibility is associated with membrane fluidity (130–132) and to the best of our knowledge, this commonly observed attribute has not been clearly linked with *vraT* activities. Hence, we used the fluorescent membrane probe TMA-DPH (1-(4-trimethylammoniumphenyl)-6-phenyl-1,3,5-hexatriene *p*-toluenesulfonate) (excitation and emission wavelengths of 360 and 426 nm) (133–135) to measure membrane fluidity of the S7 strain pair at the stationary phase as previously described (134). TMA-DPH inserts into the bacterial membrane after incubation, and when excited by light, TMA-DPH emits light in both vertical and horizontal directions relative to the excitation light, denoted as $F\perp$ and $F\parallel$ respectively. A metric for membrane fluidity is the fluorescence polarization, defined as the ratio of $(F\parallel - F\perp)$ to $(F\parallel + F\perp)$. When the membrane is rigid, the TMA-DPH molecule cannot move around easily in the membrane. Thus, the emission light in the vertical direction tends to be smaller, and the fluorescence polarization is closer to 1. Simply put, the fluorescence polarization is inversely proportional to membrane fluidity. In our experiment, as shown in **Figure 2.4B**, the membrane of S7-D2 is significantly more rigid than S7, which could be due to decreased levels of branched-chain lipids and/or decreases in membrane fluidity-increasing lipids, such as cardiolipins (136).

2.2.3. Transcriptomics analysis of S7 and S7-D2

RNA sequencing has been proven to generate quantitative results as quantitative reverse transcription PCR (RT-qPCR) (137, 138). In an effort to gain insights into how *vraT* gain-of-function mutations could alter gene expression, the total RNA of S7 and S7-D2 during mid-exponential phase growth (**Table 2.2**) was sequenced, and bioinformatics tools were utilized to

assess for differentially expressed genes (DEGs) and functional clustering of the DEGs. Because we wanted to limit our analyses to genes with a high magnitude of change and to findings that were less likely due to chances (139), we set a cutoff for $\log_2$fold change to be greater than 1 or less than -1 and a cutoff for adjusted *p* to be less than 0.05, although we briefly touched upon some genes that fell out of those thresholds to get a more complete view of certain pathways.

With the annotation in the reference genome USA300-FPR3757, the bioinformatics analysis resulted in a total of 486 DEGs with adjusted *p* less than 0.05, 71 of which had $\log_2$fold change greater than 1 and 68 had $\log_2$fold change less than -1. Using VolcaNoseR (140), we generated a volcano plot of the DEGs (**Figure 2.5A**) and labeled the top 15 DEGs ranked by Manhattan distance from the origin. We also included on the plot ten genes of interest to us (*argF*, *betA*, *fabH*, *lytM, thrB*, *thrC*, *vraS*, *vraR*, *purE*, and *purK*). *lytM* codes for an autolytic enzyme involved in the growth and division of *S. aureus*, which hydrolyzes the pentaglycine cross-bridge of the staphylococcal peptidoglycan layer (141, 142). *thrB* and *thrC* are constituents of threonine synthesis, and the synthesis of threonine has been shown to support *S. aureus* growth in serum and has implications for host adaptation and pathogenesis (143). Purine synthesis, where *purE* and *purK* play roles, has been implicated in virulence and persistent MRSA bacteremia (144–147). The remaining genes (*argF*, *betA*, *fabH*, *vraS*, and *vraR*) are detailed in the following sections and are related to stress response and fatty acid synthesis.

Because *vraT* is not annotated in the reference genome, we repeated the data processing with the same reference genome, using the locus tags instead of the annotated gene names. We specifically identified *vraR*, *vraS* and *vraT* from the locus tags (SAUSA300_1865, SAUSA300_1866, and SAUSA300_1867, respectively). The individual counts, fold changes, and adjusted *p*-values of the three genes were shown in **Figure 2.5B**, which demonstrated that

their levels were significantly increased in S7-D2 and confirmed our hypothesis that the single point mutation in S7-D2 (*vraT* 377C>T) was indeed gain-of-function. All other transcriptomics analyses were still performed using the annotated results. Notably, the locus tag method outputs 1,497 DEGs with adjusted *p* less than 0.05, compared to 486 DEGs with adjusted *p* less than 0.05 using annotation. Such a huge difference suggested that large numbers of unannotated hypothetical proteins might be missing from our annotated analyses. This is a limitation until a better annotated *S. aureus* genome can be obtained.

In **Table 2.3**, we listed a selection of genes related to the cell wall synthesis and their respective $\log_2$fold changes, adjusted *p*-values, and the proteins they encode. The *pbp* and *sgt* genes are involved in transpeptidase and glycosyltransferase activities in peptidoglycan synthesis (148). Penicillin-binding protein (PBP) 1, PBP3, and PBP4 are transpeptidases, among which PBP1 is required for the survival of *S. aureus* (149). Unlike the previous 3 PBPs, PBP2 has bifunctional transpeptidase and glycosyltransferase activities, and the alternative PBP2A (transpeptidase) is additionally needed for β-lactam resistance in MRSA strains (150, 151). SgtA and SgtB are nonessential monofunctional glycosyltransferases (149). Although SgtA and SgtB have shown glycosyltransferase activity *in vitro*, only SgtB can support the growth of *S. aureus* in the absence of the main glycosyltransferase PBP2 (148, 152, 153). SgtB alone, however, cannot support the growth of *S. aureus* in the presence of β-lactam antimicrobials when an interaction between PBP2 and PBP2A is needed (148, 152, 153). In our transcriptomics results, we observed an overall increase in the *pbp* genes and the *sgt* genes, especially *pbp2* and *sgtB* ($\log_2$fold change=0.965 and 1.18, respectively). There was also a general increase in the expression of the *mur* genes, as shown in **Table 2.3**, except *murA* which significantly decreased in S7-D2 ($\log_2$fold change=-0.415). The Mur enzyme family is also involved in the

peptidoglycan synthesis, of which MurA-MurF is responsible for the conversion from UDP-*N*-acetyl-glucosamine to UDP-*N*-acetylmuramoyl-pentapeptide (**Figure 2.6**) (154–156) and MurG functions to add the pentapeptide moiety to Lipid I and generate Lipid II (157). Considering the increase in *pbp*, *sgt*, and *mur* genes, the results suggested that the peptidoglycan synthesis was likely to be upregulated in S7-D2, which might lead to the decreased susceptibility to vancomycin and daptomycin in S7-D2.

In **Table 2.4**, we also listed a selection of genes involved in the FASII fatty acid synthesis pathway (**Figure 2.7**), which might affect downstream lipid synthesis and, ultimately, cell membrane synthesis. The *fab* genes and *acc* genes witnessed an overall increase in their expression levels, with *fabH* (also shown in **Figure 2.5A**), *fabF*, *accB* and *accC* being the top four with the largest increase ($\log_2$fold change=1.21, 0.939, 0.859 and 0.797, respectively). FabH and AccBC initiate the FASII fatty acid synthesis pathway, while FabF elongates the fatty acid chains (**Figure 2.7**). On the contrary, the expression level of *fabZ*, which forms *trans*-2-enoly-ACP from 2-hydroxyacyl-ACP and ultimately leads to the formation of acyl-ACP before exiting the FASII fatty acid synthesis pathway (**Figure 2.7**), was significantly decreased in S7-D2. It would be interesting to compare the expression levels of the fatty acid synthesis genes with the lipidomics results to get more insights into how lipid metabolism might be modulated by the VraTSR system. Based on the select list of fatty acid synthesis genes, we would expect to observe elongated fatty acid acyl chains due to elevated *fabF* levels and decreased lipid abundance owing to lowered *fabZ* levels along with elevated *fabH* and *accBC* levels.

Furthermore, we performed functional annotation clustering with the Database for Annotation, Visualization and Integrated Discovery (DAVID) (158), using *S. aureus* subspecies USA300 as the background genome. With an input of 852 genes (all DEGs from the annotated

analysis without cut-offs), DAVID was able to match 374 gene IDs to their database, and the results found four functional annotation clusters. Among the four clusters, clusters 1 and 2 possessed categories with adjusted *p*-values less than 0.05, as shown in **Table 2.5**. The individual genes involved in each cluster are shown in **Figure 2.8**, with *sdrE*, *fnbB*, *sbi* appearing in both clusters. As can be seen from **Figure 2.8**, cluster 1 was mostly involved in adhesion and the genes involved showed an overall decrease in S7-D2. Notably, *sdrD* and *sbi* in cluster 1 also appeared on the upper left corner of the volcano plot (**Figure 2.5A**), further suggesting that S7-D2 might have decreased adhesion capability. Cluster 2 had genes mostly involved in TCSs associated with virulence, which also demonstrated an overall decrease in S7-D2 (**Figure 2.8**). However, the caveat with the DAVID clustering results lay in the fact that only 374 out of 852 genes were matched and that only 3 categories from 2 clusters were significantly enriched, each with a few gene counts. While the DAVID results shed light on the group of genes possibly enriched, manual clustering would be of utmost importance as a future step.

To further confirm the cell adhesion capabilities of S7 and S7-D2, we measured the degree of biofilm formation, as biofilm formation starts with the attachment of bacterial cells to a surface in the current five-stage model (159, 160). With the crystal violet assay (161), we found that S7-D2 formed a thinner layer of biofilm than S7 over a 24-h growth period (**Figure 2.9**). This result was consistent with the transcriptomics results, suggesting decreased level of adhesion in S7-D2.

2.2.4. Metabolomics analysis of S7 and S7-D2

Because changes in the levels of gene expression do not directly translate to changes in the levels of the metabolites, we opted to analyze the metabolomics of S7 and S7-D2 to obtain a more meta-level understanding of the *vraTSR* effects. The bacterial strains were grown to late

mid-exponential phase (**Table 2.2**), as well as stationary phase, because gene expression changes typically precede metabolic changes. Each sample was analyzed by targeted and untargeted metabolomics, the latter of which served to calculate a normalization factor for the former. The targeted metabolomics was performed by Dr. Haiwei Gu's group (College of Health Solutions, Arizona State University). After the results from the targeted metabolomics were normalized, a list of compounds with p-value <0.05 (Student's t-test, two-tailed, equal variance) was generated. One compound prominent from the list of significantly altered metabolites was UNAG, as it is one of the key components of the peptidoglycan layer. **Figure 2.10** demonstrated that UNAG significantly decreased in S7-D2 during both mid-exponential and stationary phases.

Significantly enriched pathways were then identified in MetaboAnalyst (162), using N315 as the reference strain because it was the only one available for *S. aureus* at the time of analysis. Herein we will denote the pathways with $-\log_{10}p$ no less than 1.5 as "top pathways" (**Figure 2.11** for the mid-exponential phase; **Figure 2.19** for the stationary phase). The significantly altered metabolites for each pathway were shown in **Figure 2.12** – **Figure 2.18** for the mid-exponential phase and **Figure 2.20** – **Figure 2.29** for the stationary phase. Common top pathways which appeared in both phases were: purine metabolism (KEGG: SAU00230 (163)), aminoacyl-*t*RNA biosynthesis (KEGG: SAU00970 (163)), arginine biosynthesis (KEGG: SAU00220 (163)), glycine, serine and threonine metabolism (KEGG: SAU00260 (163)), alanine, aspartate and glutamate metabolism (KEGG: SAU00250 (163)), and β-alanine metabolism (KEGG: SAU00410 (163)). Furthermore, four top pathways were unique to the stationary phase: glyoxylate and dicarboxylate metabolism (KEGG: SAU00630 (163)), cyanoamino acid metabolism (KEGG: SAU00460 (163)), pyrimidine metabolism (KEGG: SAU00240 (163)) and TCA cycle (KEGG: SAU00020 (163)).

The betaine biosynthesis module (KEGG: SAU_M00555 (163)) in the glycine, serine and threonine metabolism pathway and the arginine biosynthesis module (KEGG: SAU_M00844 (163)) in the arginine biosynthesis pathway were detailed below in Section 2.2.3.1 and Section 2.2.3.2, respectively. The decrease in all the metabolites across the panels in the purine pathway (mid-exponential: **Figure 2.12**; stationary: **Figure 2.21**) and the pyrimidine pathway (stationary: **Figure 2.27**) was consistent with the growth defect in S7-D2 as discussed in Section 2.2.2. Moreover, the decrease in the levels of valine and isoleucine (mid-exponential: **Figure 2.15**; stationary: **Figure 2.22**) was in line with the increased rigidity of the bacterial membrane of S7-D2 as discussed in Section 2.2.2. The branched-chain amino acids valine and isoleucine (and leucine) are precursors to membrane branched-chain fatty acids in *S. aureus* (164, 165), and their decreased levels might relate to decreased levels of branched-chain lipids in the bacterial membrane and the observed decrease in membrane fluidity in S7-D2.

To better understand how certain variations on the gene level between S7 and S7-D2 translate to metabolic changes, we decided to take a combined look at the transcriptomics and metabolomics results.

2.2.3.1 The betaine biosynthesis pathway

The first pathway that stood out was the betaine biosynthesis pathway (a simplified view of the pathway shown in **Figure 2.30A**). *S. aureus* can take up betaine or choline *via* multiple transporters, *e.g.* BccT, OpuB(ab), OpuC(abcd), OpuD, OpuD2 and ProP (166, 167) (**Figure 2.30A**). Betaine can also be synthesized from choline through the action of BetA (oxygen-dependent choline dehydrogenase) and BetB (aldehyde dehydrogenase), with betaine aldehyde as the intermediate (166, 167). Several of the transporters mentioned above were upregulated or downregulated in S7-D2 (**Figure 2.5A** and **Table 2.6**), among which the upregulated *bccT*

exhibited the largest log_2fold change. The genes encoding for the enzymes that convert choline to betaine, *betA* and *betB*, were also upregulated in S7-D2. Despite the mixed changes in the transporter genes, the metabolomics results (**Figure 2.30B**) demonstrated that choline and betaine were significantly increased in S7-D2 during the mid-exponential phase, while only choline did so during the stationary phase and its abundance was less different between S7 and S7-D2 comparing the stationary phase with the mid-exponential phase.

Since betaine protects *S. aureus* against osmotic pressure (168, 169), we determined if S7-D2 was capable of tolerating higher osmotic pressure exerted by the hyperosmotic agent maltodextrin (170). Maltodextrin reduces water activity in cells and their environment (170, 171) and has been used to experimentally in combination with vancomycin to enhance the killing of *S. aureus* biofilms (170, 172). We subjected S7 and S7-D2 to five concentrations of maltodextrin (10 mg/mL, 25 mg/mL, 50 mg/mL, 75 mg/mL, 100 mg/mL), and compared the growth curves over a 30-h period, with S7 or S7-D2 alone as controls. The OD_{600} of the maltodextrin by itself at different concentrations was also measured (**Figure 2.31**), which was relatively consistent over the 30-h period and served as decent background subtractions for the growth curves. The growth curves of S7 and S7-D2 with or without exposure to maltodextrin are shown in **Figure 2.32A**. There was a general trend of increased growth inhibition as the maltodextrin concentration increased. The AUC was calculated to account for the total growth over the entire growth period, shown in **Figure 2.32B**. We then calculated the ratio of the AUC at each maltodextrin concentration relative to the AUC of S7 or S7-D2 alone for comparison between S7 and S7-D2, because S7-D2 has a growth defect at baseline (**Figure 2.4A** and **Figure 2.32A**). As can be seen from **Figure 2.32B**, the total growth over the 30-h period was decreased to a larger extent for S7-

D2 than S7 at each maltodextrin concentration. Counter to our initial hypothesis, these findings suggested that S7-D2 may have lower osmotic tolerance than S7.

Because of the observed differences in choline and betaine abundance during the mid-exponential *vs.* the stationary phase (**Figure 2.30B**), another metric, the growth rate, was calculated by performing linear regression on a 2-h period during each mid-exponential growth phase (**Table 2.7**). Although the growth rate of S7-D2 alone was higher than that calculated in **Figure 2.4A**, it was still significantly lower than the growth rate of S7 ($p<0.0001$; Student's *t*-test, unpaired, two-tailed, equal variance). Hence, the growth defect in S7-D2 was also confirmed in this experiment. Based on the growth rates, a percentage was again calculated to account for the growth difference between S7 and S7-D2. The results were similar to those from the AUC measurements: S7-D2 showed lower osmotic tolerance even just during the mid-exponential phase. Taken together, the increase in the levels of choline and betaine failed to provide a growth advantage to S7-D2 in the context of osmotic pressure exerted by maltodextrin, indicating that maltodextrin might inhibit *S. aureus* growth through mechanisms other than osmotic pressure. Another possibility is that S7-D2 could be less osmotically tolerant than S7, so the choline and betaine were upregulated to compensate, but the upregulation still could not fully make up for the lowered osmotic tolerance in S7-D2.

2.2.3.2 The arginine deiminase pathway

Another pathway that seemed prominent was the arginine deiminase pathway (ADI) coupled with the urea cycle (**Figure 2.33A**), because several components of the pathway, namely *arcABCD* and *arcR*, had large fold changes as seen from the volcano plot in **Figure 2.5A**. ADI is the main bacterial arginine catabolic pathway, encoded by the *arc* operon (173). It converts arginine to citrulline and ammonia in the presence of water *via* the action of ArcA (arginine

deiminase). A phosphate group is added to citrulline to form ornithine and carbamoyl phosphate *via* the action of ArgF and ArcB (carbamoyl transferases). Finally, through the action of ArcC (carbamate kinase), carbamoyl phosphate is converted into ammonia and hydrogencarbonate, with the concurrent production of 1 mol ATP per mol of arginine consumed. Another gene in the *arc* operon is *arcD*, which encodes a membrane-bound arginine/ornithine antiporter. All four genes, *arcABDC*, were significantly elevated in S7-D2 (lowest $\log_2$fold change=4.35, *arcC*; highest $\log_2$fold change=6.72, *arcA*) (**Figure 2.5A**). However, *argF* was significantly downregulated ($\log_2$fold change=-1.94) (**Figure 2.5A**). Although the expression levels of *arcB* ($\log_2$fold change=6.16) and *argF* changed in opposite directions in S7-D2, the increase in *arcB* was far larger than the decrease in *argF*, and thus we could safely conclude that overall, more citrulline was converted to ornithine and that more carbamoyl phosphate was produced in S7-D2.

arcR is located immediately upstream of the *arcABDC* genes, and codes for a protein which regulate genes involved in anaerobic metabolism (173). It has also been shown that ArcR activates the expression of the *arc* operon, possibly in conjunction with ArgR (arginine repressor), which is located upstream of the *arcA* gene in the ADI gene cluster (173). In our transcriptomics analysis, *arcR* and *argR* were both significantly upregulated in S7-D2 ($\log_2$fold change=4.67 and 1.08, respectively). Considering all the genes in the ADI cluster along with *argF*, we concluded that the ADI pathway was upregulated in S7-D2 as compared to the parent strain S7. Consistent with the upregulated ADI pathway, **Figure 2.33B** showed that the level of citrulline was significantly increased in S7-D2 during the mid-exponential phase (19.3-fold), although other metabolites in the ADI pathway were not measured in the targeted metabolomics. **Figure 2.33B** also demonstrated that more citrulline was produced in S7 in the stationary phase, resulting in a 4.02-fold increase than the level in S7-D2. This suggests that the upregulation of

the ADI pathway likely only happened in the mid-exponential phase when S7-D2 was actively growing.

In addition to serving as a source of carbamoyl phosphate, citrulline can also be converted to L-arginosuccinate and then back to arginine in the urea cycle through the actions of AgrG (argininosuccinate synthase) and AgrH (argininosuccinate lyase) (**Figure 2.33A**). In our transcriptomics analysis, both genes had positive $\log_2$fold changes but less than 1 (indicative of slight increase in the gene expression in S7-D2), and only the expression level of *agrG* was significantly different between S7 and S7-D2. *agrJ* (glutamate *N*-acetyltransferase), coding for the enzyme AgrJ that converts *N*-acetylornithine to ornithine (**Figure 2.33A**), was slightly decreased in S7-D2 (non-significantly) (**Table 2.8**). Surprisingly, based on the metabolomics results shown in **Figure 2.33B**, the levels of *N*-acetylornithine were significantly elevated in both the mid-exponential phase and stationary phase (49.8-fold and 16.3-fold, respectively). This might be due to pathways upstream of the AgrJ reaction, leading to *N*-acetylornithine formation.

In conclusion, the ADI gene cluster has been shown to allow *S. aureus* to utilize arginine as an energy source under anaerobic conditions (173). Although we did not grow S7 and S7-D2 under anaerobic conditions, it is possible that the improved ability of S7-D2 to convert arginine into energy contributes to its better survival in response to the external stress from antimicrobials such as vancomycin and dalbavancin. However, the mechanisms behind this possibility and the mechanisms of how overexpression of the *vraTSR* regulatory system might lead to the elevated expression of the ADI genes remain unclear and warrant further investigation.

2.2.5. Lipidomics analysis of S7 and S7-D2

Because several genes associated with the FASII fatty acid synthesis pathway were significantly altered (**Table 2.4** and **Figure 2.5A**), we performed lipidomics on both the mid-

exponential (**Table 2.2**) and stationary phase samples of S7 and S7-D2. **Figure 2.34A** showed that the short-chain phosphatidylglycerols (PGs) were significantly increased in S7-D2 (28:0 and 29:0 for stationary phase, with an additional 30:0 for mid-exponential phase), while the long-chain PGs were significantly decreased (34:0, 35:0 and 37:0 for stationary phase, with additional 33:0 and 36:0 for mid-exponential phase). A similar trend was observed for lysyl-PGs (**Figure 2.34B**) at stationary phase: lysyl-PG 28:0 and lysyl-PG 29:0 were significantly increased while lysyl-PG 34:0 and lysyl-PG 35:0 were significantly decreased in S7-D2. However, for the mid-exponential phase, only the short-chain lysyl-PGs (28:0 and 29:0) were significantly increased, although the levels of long-chain lysyl-PGs were not significantly changed. As for the cardiolipins (CLs) (**Figure 2.34C**), the levels were lowered in both mid-exponential phase and stationary phase in S7-D2, which was consistent with the increased membrane rigidity (**Figure 2.4B**). Overall, the phospholipid levels in S7-D2 were decreased as compared to S7 in both phases. This observation was consistent with the decrease in the *fabZ* expression level (**Table 2.4**) and the general trend of decreased levels of lipids in the resistant strains of other genetic backgrounds as observed in previous studies (24, 104, 117–119). It also confirmed our hypothesis from the lipidomics of the JE2 *vraTSR* mutants (section 2.2.1) that *vraT* loss-of-function mutations are insufficient to lead to lipid changes, but gain-of-function point mutations might be. However, the levels of branched-chain lipids were not clearly elucidated and could be achieved by fragmentation of the fatty acid acyl chains with targeted MS/MS experiments (174).

2.2.6. AFN-1252 demonstrated synergy with daptomycin and oritavancin, independent of *vraTSR* regulatory system

We hypothesized that AFN-1252 would decrease the lipid abundance in *S. aureus* while cerulenin would lead to an increase in lipid species with shorter fatty acid chains, with a

corresponding decrease in lipid species with longer fatty acid chains. This hypothesis was based on the targets of AFN-1252 and cerulenin, as AFN-1252 acts on FabI, which catalyzes the formation of the precursors to lipid synthesis, while cerulenin acts on FabF, which catalyzes the elongation of the fatty acid chains (**Figure 2.7**). To test that hypothesis, we grew S7 and S7-D2 in the presence and absence of subinhibitory (half-MIC) concentrations of cerulenin and AFN-1252 and measured the lipidomic changes using HILIC-IM-MS. **Figure 2.35** demonstrated that cerulenin shifted the fatty acid chains of various lipid species to shorter chains, while AFN-1252 decreased the lipid synthesis overall, consistent with our expectations. The exception lay in CLs (**Figure 2.36**) in the presence of AFN-1252, where the fatty acid composition shifted to shorter chains in S7, but overall CL levels increased in S7-D2, suggesting that CL synthase was activated with exposure to AFN-1252 in this strain.

Based on the above lipid profile, the shift of fatty acid chains to shorter lengths and increase of CL levels by AFN-1252 and cerulenin could result in increased membrane fluidity, which might, in turn, contribute to bacterial killing by daptomycin (130–132, 136). Because of the presence of cross-resistance among cell-envelope-targeting antimicrobials (22–24), we aimed to determine whether such lipid metabolism modulation would enhance the antimicrobial susceptibility of daptomycin, as well as vancomycin, daptomycin, and oritavancin. We used the time-kills to assess the synergy between AFN-1252 and those antimicrobials for S7 and S7-D2. For both strains, synergy was observed for AFN-1252 and daptomycin (S7: 2.91$\log_{10}$CFU reduction; S7-D2: 2.30$\log_{10}$CFU reduction; 24-h) and for AFN-1252 and oritavancin (S7: 4.65$\log_{10}$CFU reduction; S7-D2: 3.63$\log_{10}$CFU reduction; 24-h), but not with AFN-1252 and vancomycin or AFN-1252 and dalbavancin (<2$\log_{10}$CFU reduction; 24-h) (**Figure 2.37** and **Figure 2.38**). The synergy was independent of the *vraTSR* regulatory system as S7 and S7-D2

behaved similarly. The synergy between AFN-1252 and daptomycin has been observed before (175), but to the best of our knowledge, this is the first time the synergy between AFN-1252 and oritavancin has been demonstrated. Interestingly, another lipoglycopeptide antimicrobial, dalbavancin, did not exhibit synergy with AFN-1252, suggesting that the mechanisms of action of oritavancin might involve the bacterial membrane as daptomycin does while dalbavancin does so to a lesser extent (20, 176). As a future direction, it would be interesting to determine how the shift to shorter chain length by cerulenin would affect the killing by the cell-envelope-targeting antimicrobials.

2.2.7. Histidine kinase inhibitor demonstrated synergy with vancomycin for S7, but not S7-D2

In addition to lipid synthesis inhibitors, we investigated how histidine kinase inhibitors might modulate the effects of cell-envelope active antimicrobials. Because VraT-specific inhibitor is not yet developed, we tested F1374-0037, which has been shown to bind specifically to VraS and not VraR or some other histidine kinases (124). **Figure 2.39** showed that S7 exhibited synergy between F1374-0037 and vancomycin (2.12$\log_{10}$CFU reduction; 24-h), but not S7-D2 (<2$\log_{10}$CFU reduction; 24-h). One possibility of the variation in killing between S7 and S7-D2 is that the elevated levels of *vraS* due to upregulation of *vraTSR* in S7-D2 might be able to counteract the inhibition by the histidine kinase inhibitor, and thus, the vancomycin killing profile remained the same with or without the inhibitor. However, the difference could also be due to other mechanisms of killing not directly involving binding to *vraS*, since, to the best of our knowledge, how the histidine kinase inhibitors function to kill *S. aureus* has not been determined (124). S7 could be producing fewer VraTSR proteins because it was becoming less viable through other killing mechanisms, especially considering that the N315 *vraS* KO did not exhibit MIC-lowering effects against the cell-envelope-targeting antimicrobials (**Table 2.1**). As a

result, we would need to rule out other possibilities to fully confirm that the upregulation of *vraTSR* contributed to the differences in killing. Future time-kill experiments involving other cell-envelope-targeting antimicrobials and *vraS* loss-of-function mutants, *e.g.* JE2 *vraS* transposon mutant and N315 *vraS* KO, are needed to unveil deeper into the possible mechanisms.

2.3 Discussion

Several observations from our experiments pointed to the crosstalk between cell wall synthesis and lipid metabolism. Firstly, the demonstrated decrease in UNAG (**Figure 2.10**), together with the decrease in the *murA* gene expression (**Table 2.3**), indicated that in S7-D2 less UNAG might be generated in pathways upstream of the reactions catalyzed by the MurA-F enzyme family. This observation also coincided with the observation where the initiation of the FASII pathway was upregulated in S7-D2 (**Table 2.4**), in that acetyl-CoA, a precursor to both the synthesis of fatty acids (34) and the synthesis of NAG and NAM (9) (**Figure 1.3**), might be converted to the intermediates in the FASII fatty acid synthesis pathway to a greater extent than to NAGs and NAMs. Nevertheless, the fatty acid synthesis might still be downregulated due to the decrease in *fabZ* (**Table 2.4**) while the peptidoglycan synthesis might be upregulated due to the increase in other cell wall synthesis-related genes (**Table 2.3**). Isotopic labeling of acetyl-CoA and measurement of the cell wall thickness with transmission electron microscopy (128, 177) is likely to provide more evidence for acetyl-CoA as one connecting point between cell wall synthesis and lipid metabolism in *S. aureus*. Secondly, inactivating mutations in *sgtB* have been shown to allow *S. aureus* to survive in the absence of LTAs (148). In the same study, mutations in *vraT* have also been demonstrated to support the growth of LTA-deficient *S. aureus*, although those mutations did not allow the bacteria to entirely bypass the requirement of LTAs (148).

Considering that *sgtB* significantly increased in S7-D2 (**Table 2.3**), that the overall lipid abundance decreased in S7-D2 (**Figure 2.34**), that SgtB and LTAs are related (148), and that the backbone and the headgroup of LTAs are products of lipid metabolism in *S. aureus* (36, 38, 178), we hypothesize that the amount of LTAs might be increased as a result of *vraTSR* upregulation, which might contribute to the observed antimicrobial resistance. It would be helpful to elucidate the LTA changes in S7-D2 as compared to S7 and the potential roles of *vraT* in LTA synthesis. This could be accomplished by Western blot (148) and/or matrix-assisted laser desorption/ionization mass spectrometry (MALDI-MS) (179).

Modulating the gene levels of the FASII fatty acid synthesis pathway could alter the composition of the synthesized lipids, as implicated by the lipid profile of S7 and S7-D2 with exposure to AFN-1252 and cerulenin (**Figure 2.35** and **Figure 2.36**). Nevertheless, the lipids were not shifted to longer chains in S7-D2 (**Figure 2.34**) despite the significant increase in the *fabF* expression levels (**Table 2.4**), possibly because the extent of the increase in *fabF* was not sufficient to lead to the shift to longer chains. At the same time, the upregulation of the initiation of the FASII fatty acid synthesis pathway caused by the elevated levels of *fabH* and *accBC*, along with the downregulation of the *fabZ* gene, might indicate that 2-hydroxyacyl-ACP accumulated in S7-D2, which might be responsible for the overall decrease in lipid abundance in S7-D2 (**Figure 2.34**).

In our studies of lipid synthesis inhibitors, we observed in the presence of AFN-1252 there was shift among CLs to shorter chain length in S7 and an increase in CL levels in S7-D2 compared to the unexposed strains (**Figure 2.36**). The decrease in chain length, as well as the increase in CLs (136), would decrease the packing of the membrane and thus lead to increased fluidity of the cell membrane. This might contribute to the synergy between AFN-1252 and

daptomycin (**Figure 2.38A**), because daptomycin has been shown to exhibit decreased susceptibility when membranes are either too fluid (130, 132) or too rigid (131) (the so-called "Goldilocks effect" (180)). Additionally, although *S. aureus* does not synthesize unsaturated lipids on its own (181), unsaturated PGs have been observed in *S. aureus* grown in the presence of AFN-1252 (174). The accumulation of the enoyl-ACP intermediate in the FASII fatty acid synthesis pathway as a result of the exposure to AFN-1252 (174) could increase the amount of carbon-carbon double bonds in the bacterial membrane, contributing to increased fluidity and thus the observed synergy (**Figure 2.38A**). It would be of interest to identify the *trans*-2-enoyl-ACP intermediate from the lipidomics studies and compare their relative amounts to uncover the underlying mechanisms in greater depth. Those mechanisms could potentially provide an alternative explanation to why AFN-1252 synergizes with daptomycin than by inhibiting lipid shedding from *S. aureus* (175), since it has been shown that the contribution of lipid shedding to daptomycin tolerance varies (182).

Another observation from the time-kill experiments with AFN-1252 was that oritavancin, but not dalbavancin, synergized with AFN-1252 in the killing of S7 and S7-D2 (**Figure 2.37B** and **Figure 2.38B**). Oritavancin and dalbavancin are both lipoglycopeptide antimicrobials, which are derived from the glycopeptides chloroeremomycin and teicoplanin respectively (20, 183). Oritavancin's mechanism of action (MOA) involves at least 3 known mechanisms: inhibition of transglycosylation, inhibition of transpeptidation, and cell membrane interaction/disruption (176). Dalbavancin exerts its antimicrobial activity through interaction with terminal *D*-alanyl-*D*-alanine residues of peptidoglycan precursors, and its lipophilic side chain has been implicated in the dimerization of dalbavancin and anchoring it to lipid II in the cell membrane (20). This anchoring strengthens adherence to the *D*-alanyl-*D*-alanine target site and allows for enhanced

activity compared to vancomycin and teicoplanin (20). Our observation of the differential killing by oritavancin and dalbavancin in the presence of AFN-1252 suggested that oritavancin might function more similarly to daptomycin than to vancomycin and this greater similarity to daptomycin is implied by the above reporting on the membrane disruption/depolarization being one MOA.

In the transcriptomics analysis, we determined that two of the five *pbp* genes in *S. aureus*, *pbp2* and *pbp4*, significantly increased in the expression levels in S7-D2 as compared to S7 (**Table 2.3**). However, the MIC of nafcillin, a β-lactam antimicrobial that binds to PBPs non-specifically (184, 185), did not change for S7-D2 as compared to S7 (16 μg/mL for both strains). It is possible that the degree to which the two *pbp*s were elevated was not sufficient to bring about changes in nafcillin MICs. It would be interesting to measure the MICs of other β-lactams, especially those that specifically target PBP2 (*e.g.* ceftriaxone (185)) and PBP4 (*e.g.* cefoxitin (185, 186)), to determine if the elevated *pbp* levels would result in increased resistance to β-lactam antimicrobials. Furthermore, β-lactam seesaw effect has been observed in many previous studies (22, 23, 187, 188), where the susceptibility to β-lactam in MRSA increases as the resistance to vancomycin or daptomycin increases. By measuring more β-lactam MICs, we could potentially gain insights into the role of the increased PBPs caused by *vraTSR* upregulation on the emergence of β-lactam seesaw effect.

In the above discussions and the transcriptomics, metabolomics and lipidomics results elaborated on in Section 2.2, we showed that increasing VraT activity increases antimicrobial resistance and plays crucial roles in modulating transcriptomic and metabolic changes. Furthermore, the presence of the *arlSR* and *saeSR* regulatory systems in functional annotation cluster 2 (**Figure 2.8**) suggested the existence of crosstalk among different regulatory systems in

S. aureus, as observed in previous studies (50, 60, 116), which further necessitates the need for a better understanding of VraT and the VraTSR system. However, while the structures of VraS (PDB ID 4GT8) and VraR (PDB IDs 2RNJ (189), 4GVP (190), 4IF4 (190), and 7VE4-7VE6 (191)) have been resolved to various degrees, the structure of VraT has not been clarified and only its transmembrane domains have been predicted based on the structure of LiaF in *Bacillus subtilis* (87). Further elucidating the structure of VraT *via* biophysical methods is critical and imperative based on our results.

2.4 Experimental Procedure

2.4.1. Susceptibility Testing and PAP

The susceptibility to vancomycin, daptomycin, and dalbavancin was evaluated by broth microdilution in accordance with CLSI guidelines (10). PAP was performed by plating overnight bacterial growth culture (approximately $1x10^8$ CFU/mL) on the brain heart infusion agar (BHIA, Difco, Detroit, MI) plates containing various concentrations of vancomycin and daptomycin and incubating the plates at 37°C for 48 h. The CFU/mL was then quantified from the BHIA plates and evaluated as function of the drug concentrations (12).

2.4.2. Construction of N315 *vraS* KO

The N315 *vraS* KO was constructed using the *p*IMAY plasmid (127). The primers used in the construction are listed in **Table 2.9** and were ordered from Integrated DNA Technologies, Inc. (Coralville, Iowa). Briefly, the homology arms upstream and downstream of the *vraS* gene were amplified using polymerase chain reaction (PCR). The homology arms were joined into one piece through the splicing by overlap extension PCR (SOE-PCR) and cloned into the *p*CR®2.1-TOPO® vector (Invitrogen, Thermo Fisher Scientific, Waltham, MA). Restriction enzymes KpnI (NEB, Ipswich, MA) and SacI (NEB, Ipswich, MA) were used to piece the homology arms into

the *p*IMAY plasmid, which was then electroporated into *S. aureus* N315 strain. Bacterial growth underwent a series of temperature-sensitive steps for homologous recombination, as detailed in (127). The resulting colonies were screened by PCR and Sanger sequencing (primers: vraSup_left and vraSdown_right in **Table 2.9**) to confirm successful KO of the *vraS* gene.

2.4.3. Growth Characterization and Membrane Fluidity Measurement

A 0.5-McFarland bacterial suspension was prepared from overnight growth on tryptic soy agar (TSA, Becton, Dickinson and Company, Franklin Lakes, NJ) and was diluted 100-fold. 50 µL of the diluted suspension was inoculated into 200 µL TSB (Becton, Dickinson and Company, Franklin Lakes, NJ) in a 96-well clear flat-bottom microplate. The optical density at 600 nm (OD_{600}) was read every 10 min for 26 h on the BioTek Synergy H1 microplate reader (Agilent, Santa Clara, CA). The microplate was shaken continuously at a frequency of 180 cpm (6 mm) at 37°C in the double-orbital mode. Each bacterial strain was measured in pentaplicate. Membrane fluidity was measured as previously described (134).

2.4.4. Biofilm Quantification and Osmotic Tolerance Characterization

Biofilm formation was quantified by the well-documented crystal violet assay (161). The osmotic pressure tolerance was characterized by measuring the growth curve, as described in Section 2.4.3, for 30 h under different concentrations of maltodextrin (0 mg/mL, 10 mg/mL, 25 mg/mL, 50 mg/mL, 75 mg/mL, and 100 mg/mL) (dextrose equivalent 4.0-7.0; Sigma-Aldrich, St. Louis, MO). All bacteria were grown in five replicates. The OD_{600} of maltodextrin standards was also measured over the 30-h period in triplicate. The area under the curve (AUC) was calculated in GraphPad Prism (GraphPad Software, Boston, MA). The growth rate at the mid-exponential phase was calculated by simple linear regression in GraphPad Prism over a 2-h time period, as tabled in **Table 2.2**.

2.4.5. Transcriptomics Sample Preparation and Analysis

Bacteria were grown in 5 mL TSB at 37°C to mid-exponential phase (6.5 h for S7 and 8.5 h for S7-D2). The endpoint OD_{600} for the mid-exponential phase was confirmed on the BioTek Synergy H1 microplate reader by sampling 250 µL of the bacterial suspension (**Table 2.2**). Bacteria were pelleted, resuspended in DNA/RNA Shield™ (Zymo Research, CA), and sent to Novogene Corporation Inc. (Sacremento, CA) for total RNA isolation and sequencing. Data processing was performed on Linux (hisat2 (192), SAMtools sort (193) and featureCounts (194)), with R (DESeq2 (195)), and with the Database for Annotation, Visualization and Integrated Discovery (DAVID) (158). Each strain was grown in quadruplicate.

2.4.6. Metabolomics Sample Preparation and Analysis

Bacteria were grown in 5 mL TSB at 37°C to mid-exponential phase (6.5 h for S7 and 10 h for S7-D2) and stationary phase (24 h). The endpoint OD_{600} for the mid-exponential phase was confirmed on the BioTek Synergy H1 microplate reader by sampling 250 µL of the bacterial suspension (**Table 2.2**). Targeted metabolomics was conducted by Dr. Haiwei Gu's group at Arizona State University. Untargeted metabolomics was performed on a Waters Synapt G2-XS ion mobility-QTOF mass spectrometer (Waters Corp.,Milford, MA). From the untargeted metabolomics, the total ion abundance was calculated for each sample based on the positive mode data by summing up the raw abundances of all ions identified in each sample (denoted as S_n, where n represents each individual sample). The maximum value of S_n was identified (denoted as maxS), and a normalization factor was calculated by the ratio of maxS to S_n. The abundance of each metabolite identified in the targeted metabolomics was multiplied by the normalization factor to account for any total ion current (TIC) differences among the samples.

Finally, pathway analysis was conducted using MetaboAnalyst (162) based on the normalized data. Each condition was performed in quadruplicate.

2.4.7. Lipidomics Sample Preparation and Analysis

Bacteria were grown in 5 mL TSB at 37°C to mid-exponential phase (6.5 h for S7 and 10 h for S7-D2) and stationary phase (24 h for JE2 *vraTSR* mutants, S7 and S7-D2, and S7 and S7-D2 grown with or without AFN-1252 or cerulenin). The endpoint OD_{600} for the mid-exponential phase was confirmed on the BioTek Synergy H1 microplate reader by sampling 250 µL of the bacterial suspension (**Table 2.2**). AFN-1252 was dosed at 0.0078 µg/mL for S7 and 0.0039 µg/mL for S7-D2, and cerulenin was dosed at 8 µg/mL for S7 and 1 µg/mL for S7-D2. All the concentrations used were half of the respective minimum inhibitory concentrations (MICs).

For all conditions, bacteria were pelleted and washed twice with sterile water. Lipid extraction, hydrophilic interaction liquid chromatography-ion mobility-mass spectrometry (HILIC-IM-MS), and data analysis were performed as previously described (104). Briefly, lipid was extracted using the Bligh and Dyer method (196–198). HILIC-IM-MS was conducted on the Waters Synapt G2-XS ion mobility-QTOF mass spectrometer equipped with an electrospray ionization (ESI) source. Progenesis QI (Nonlinear Dynamics, Waters Corp.,Milford, MA) was used for data alignment, peak detection (limited to the chromatographic region from 0.4 to 9.0 min), and normalization. The software selected the reference sample for alignment from the pooled quality control samples and normalized the data to all compounds to correct for TIC differences. Analysis of variance (ANOVA; $p \leq 0.05$) was used to filter the resulting features, and student's *t*-tests were performed by a two-tailed distribution and equal variance for comparison between two samples (104). Each condition was analyzed in triplicate.

2.4.8. Static Time-kill Assay

A 0.5-McFarland bacterial suspension was prepared from overnight growth on TSA and was diluted 100-fold. 50 µL of the diluted suspension was inoculated into 200 µL total volume of MHB50 or MHB supplemented with 0002% PS80 in a 24-well clear flat-bottom plate. For oritavancin, 15 mL Falcon tubes was used instead of 24-well clear flat-bottom plates. Antimicrobials (half-MIC) and inhibitors (2xMIC) were dosed depending on the conditions. The concentrations are listed in **Table 2.10**. Samples were taken at designated time points, serially diluted, and spiral-plated on TSA plates to evaluate the bacterial growth over time. All conditions were performed in duplicate.

Figures

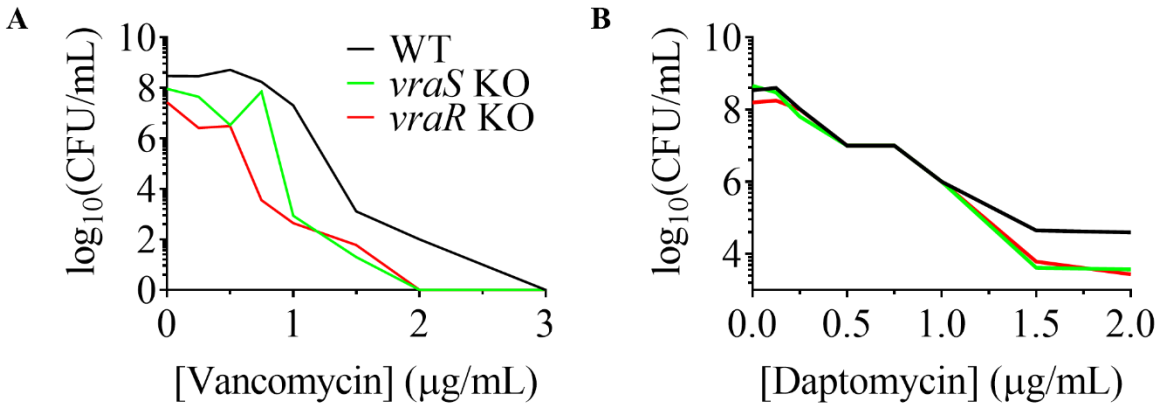

Figure 2.1 Population analysis profiling against varied concentrations of **A)** vancomycin and **B)** daptomycin of the WT USA300 JE2 strain and the *vraS* and *vraR* transposon mutants.

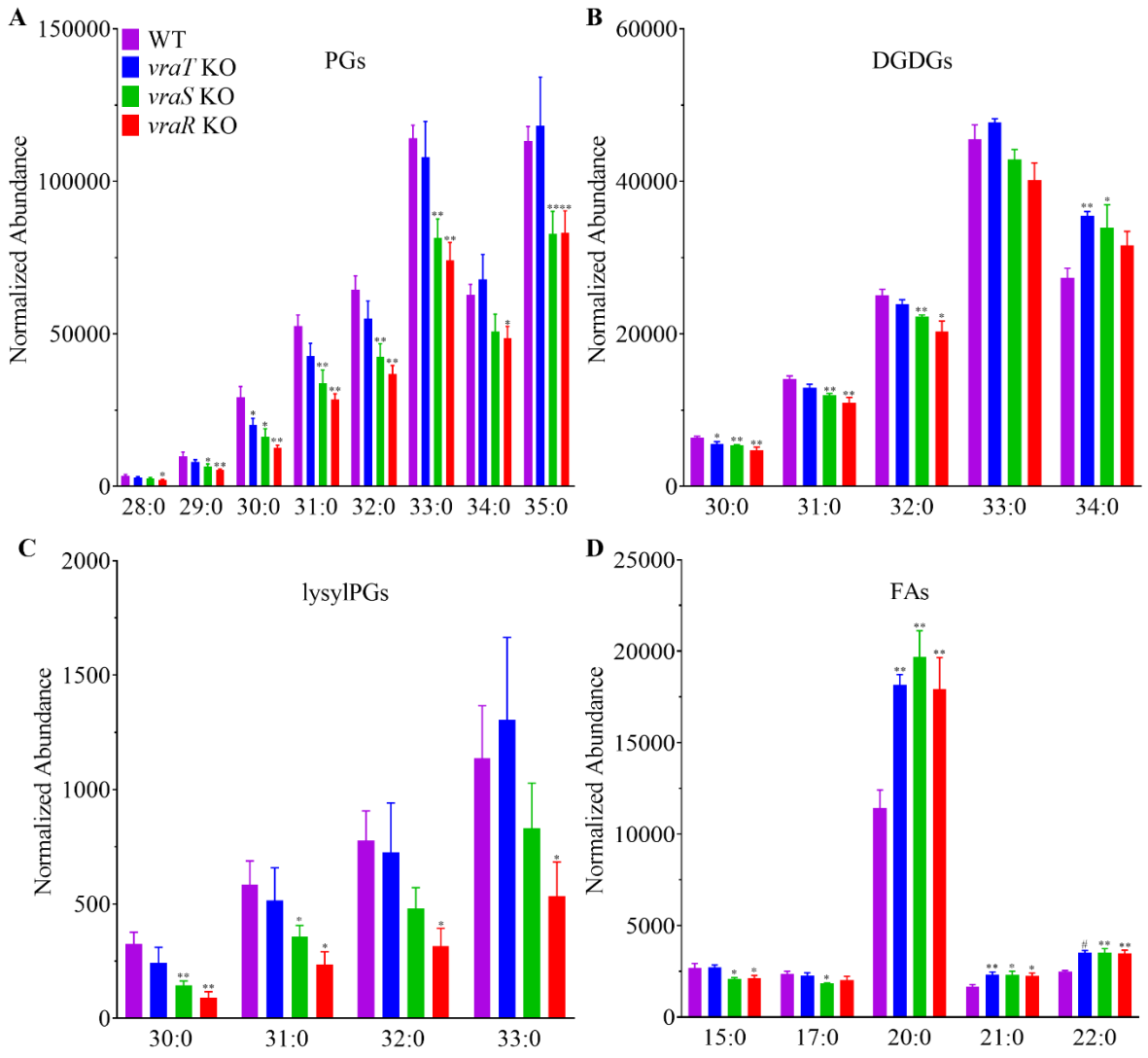

Figure 2.2 The phosphatidylglycerols (PGs; **A)**, diglucosyl-diacylglycerols (DGDGs; **B)**, lysyl-phosphatidylglycerols (lysyl-PGs; **C)** and fatty acids (FAs; **D)** profile of the WT USA300 JE2 strain and the *vraT*, *vraS* and *vraR* transposon mutants. Individual lipid species are represented as the number of carbons: the degree of unsaturation in the fatty acid chains. $^{\#}p<0.001$; $^{**}0.001<p<0.01$; $^{*}0.01<p<0.05$ (Student's *t*-test, two-tailed, equal variance). $N=3$.

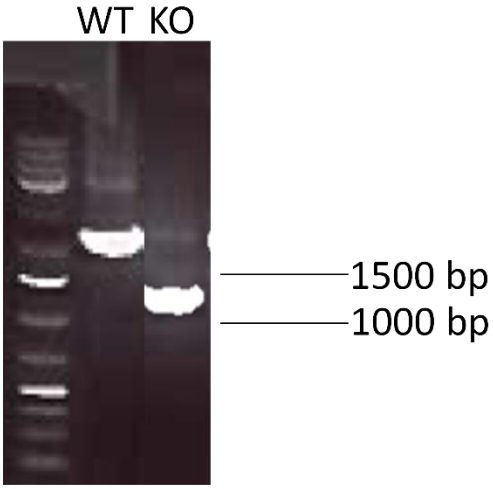

Figure 2.3 Electrophoresis gel image confirmed that *vraS* KO was successfully generated in *S. aureus* N315. The polymerase chain reaction (PCR) product of the *vraS* KO is expected to have 1,340 bp.

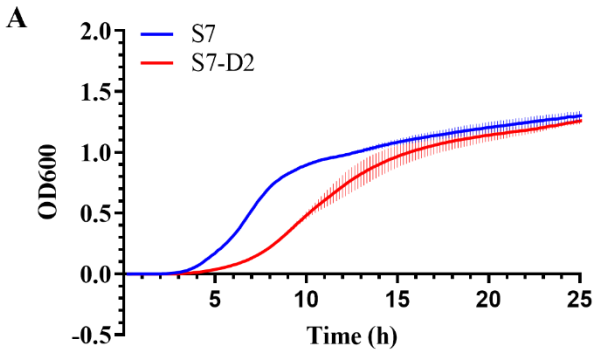

	S7	S7-D2
Slope (std. error)	0.2048 (0.001817)	0.1329[#] (0.003522)
Y-intercept (std. error)	-0.9142 (0.01275)	-0.8487 (0.03173)
R^2	0.9951	0.9576
Time interval	6 h – 8 h	8 h – 10 h

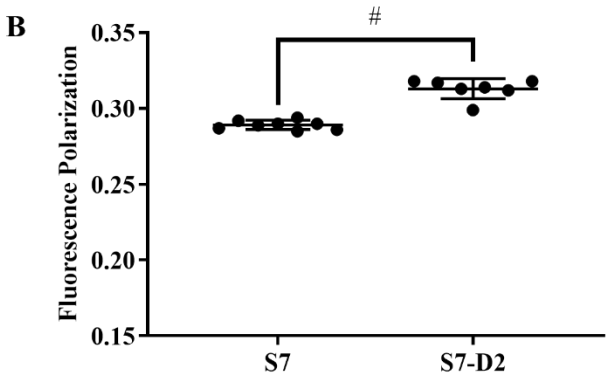

Figure 2.4 Phenotypic characterization of S7 and S7-D2. **A**) The growth curve of S7 and S7-D2, measured by the BioTek Synergy H1 platereader for 24 h at 37°C in TSB media. *N*=5. Linear regression results of the mid-exponential phase are listed. Time interval: the time period from the linear regression was performed. Std. error: standard error. **B**) The membrane fluidity measurements of S7 and S7-D2 at stationary phase using the TMA-DPH fluorescent probe. *N*=8. [#]$p<0.001$ (Student's *t*-test, unpaired, two-tailed, equal variance; y-intercept not tested).

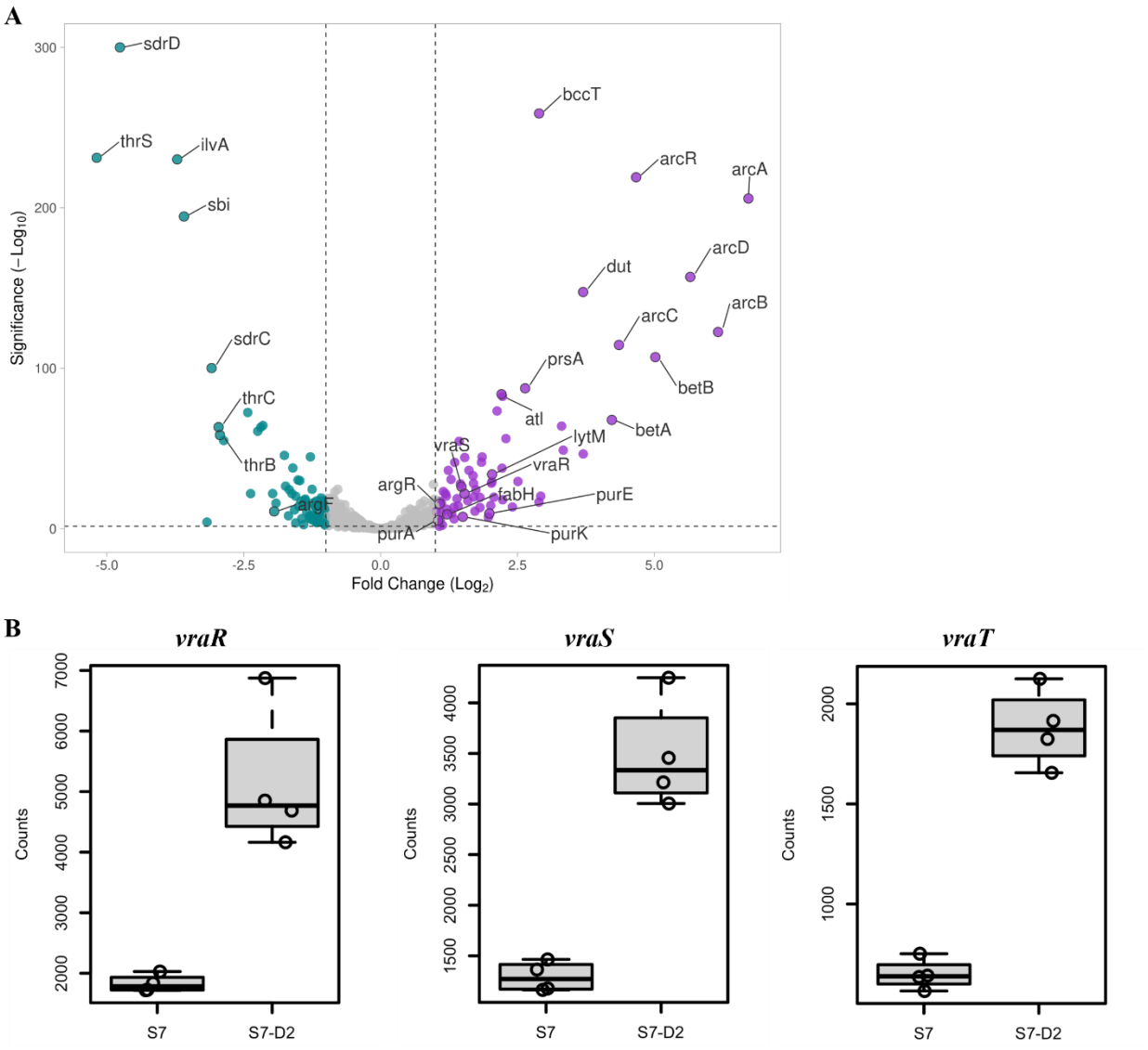

	vraR	*vraS*	*vraT*
Fold change (log_2)	1.47	1.41	1.52
Adjusted *p* value (Benjamini)	5.79E-20	1.67E-23	8.20E-33

Figure 2.5 Transcriptomics results comparing S7-D2 with S7 (fold change=S7-D2/S7). *N*=4. **A**) Volcano plot of the differentially expressed genes (DEGs) from the annotated analysis with reference genome USA300-FPR3757. Cutoff for log_2fold change and $-log_{10}p$: ±1 and 1.5. Labeled genes: top 15 hits ranked by Manhattan distance from the origin and 10 genes of interest. **B**) the counts, log_2fold changes, and adjusted *p* values of *vraR*, *vraS*, and *vraT* from the unannotated analysis with the same reference genome.

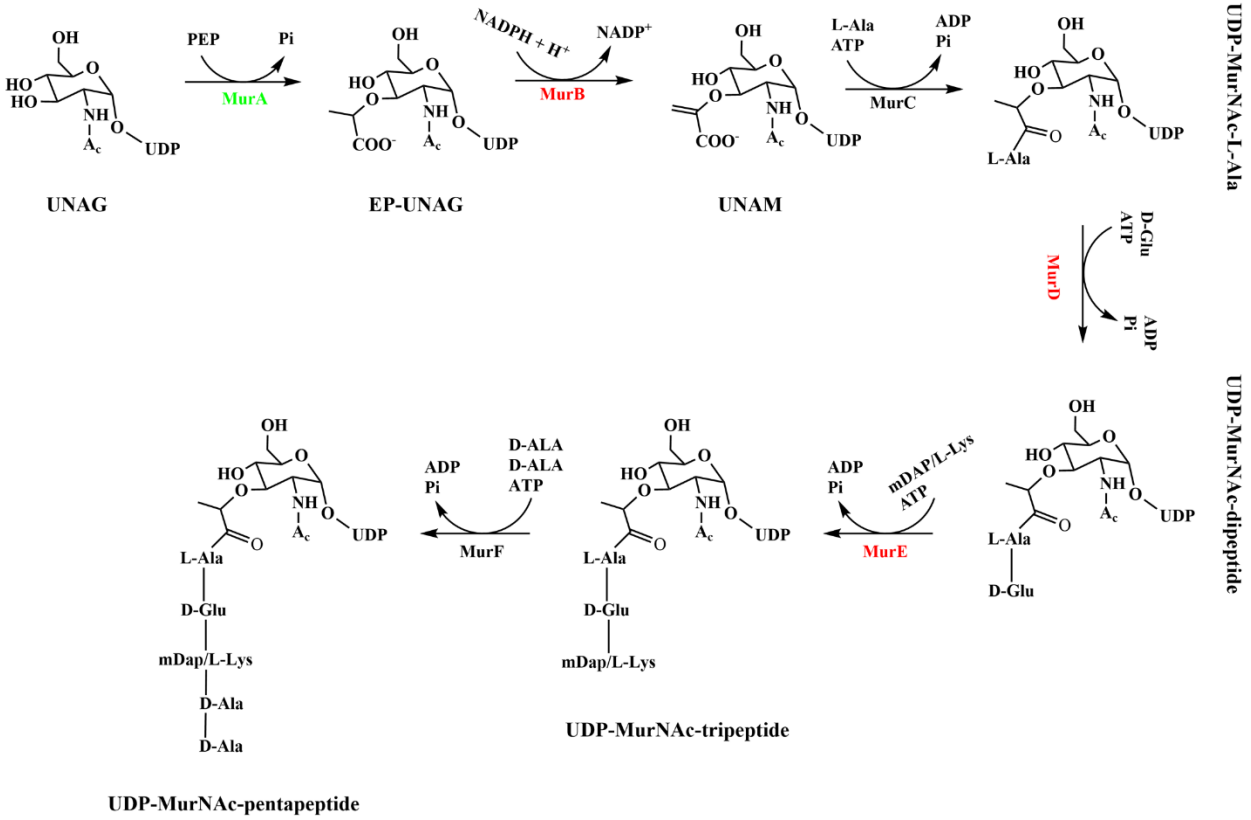

Figure 2.6 Schematic of the reactions catalyzed by the MurA-F enzyme family. Adapted from **(154)**. Red: upregulated; Green: downregulated; Black: unchanged.

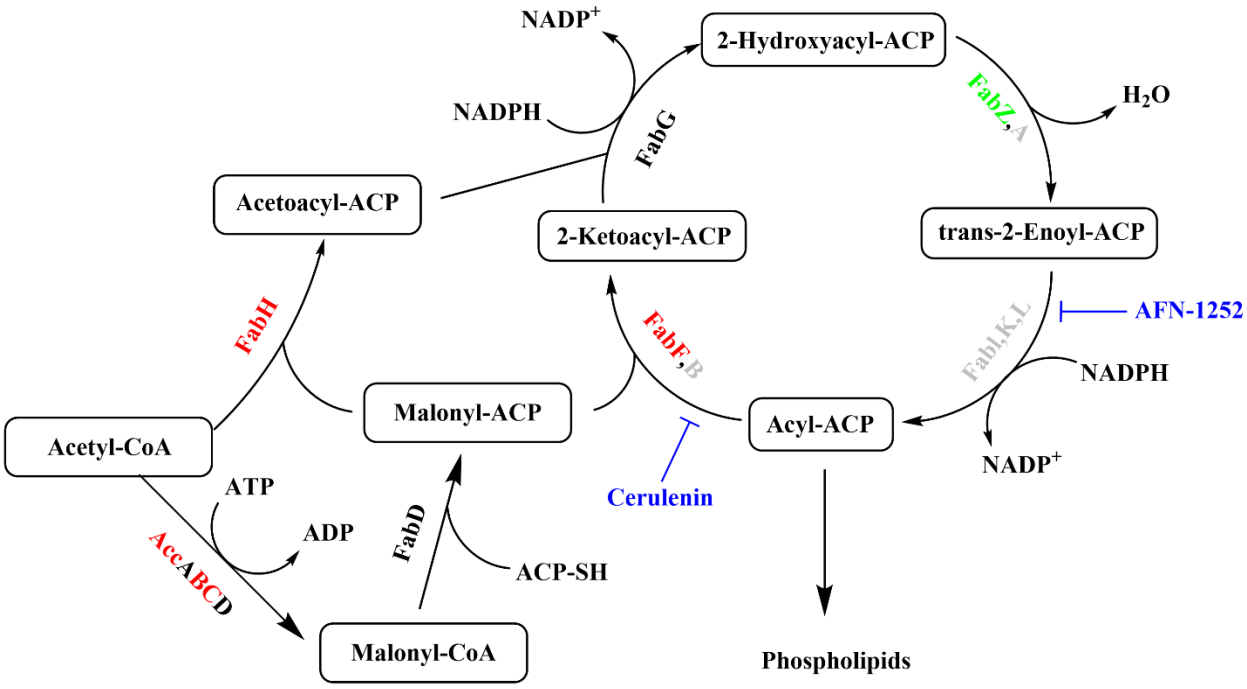

Figure 2.7 Schematic of the FASII fatty acid synthesis pathway. AFN-1252 inhibits FabI, and cerulenin inhibits FabF. Red: upregulated; Green: downregulated; Black: unchanged; Gray: unannotated. Adapted and reprinted with permission from **(123)**. Copyright 2011 Elsevier Ltd.

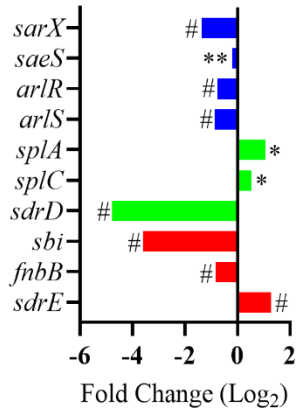

sdrE	Adhesin of unknown specificity, similar to bone sialoprotein-binding protein Bbp
fnbB	Fibronectin binding protein
sbi	IgG-binding protein
sdrD	Adhesin of unknown specificity
splC	Serine protease
splA	Serine protease
arlS	Histidine kinase of *arlSR*
arlR	Response regulator of *arlSR*
saeS	Histidine kinase of *saeSR*
sarX	Hypothetical protein

Figure 2.8 Individual genes involved in the functional annotation clusters, their $\log_2$fold changes and the proteins they encode (naming based on annotations in the genome USA300-FPR3757 **(199)**). Red: both clusters; Green: annotation cluster 1; Blue: annotation cluster 2. $^{\#}$adjusted $p<0.001$; **0.001<adjusted $p<0.01$; *0.01<adjusted $p<0.05$.

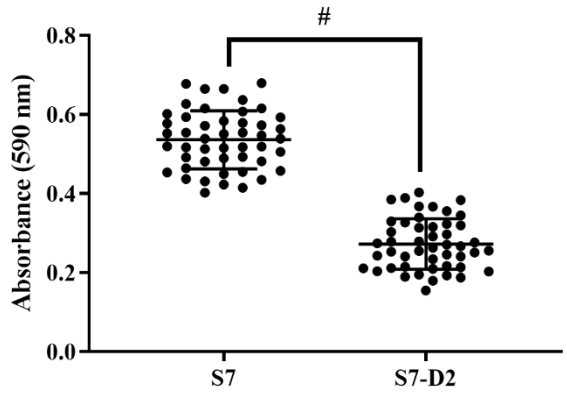

Figure 2.9 Biofilm formation of S7 and S7-D2 after 24 h growth, quantified by the crystal violet method. $^{\#}p<0.001$ (Student's *t*-test, unpaired, two-tailed, equal variance). $N=48$.

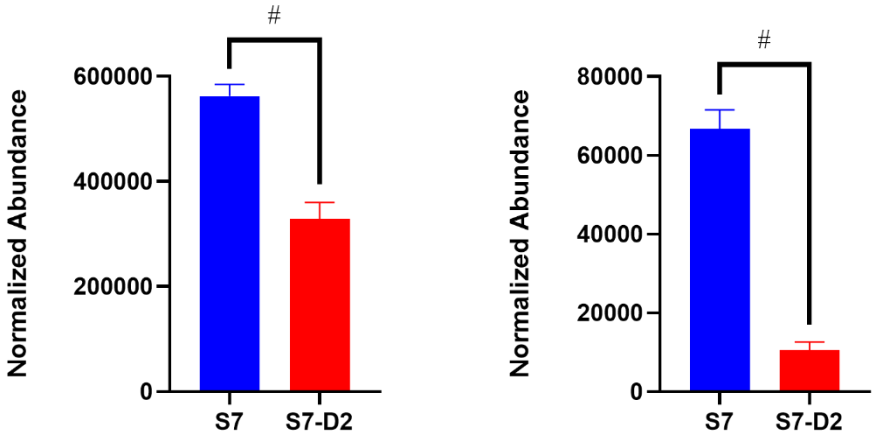

Figure 2.10 UDP-N-acetyl-α-*D*-glucosamine (UNAG) changes comparing S7 and S7-D2 during the mid-exponential phase (left) and the stationary phase (right). $^{\#}p<0.001$(Student's *t*-test, unpaired, two-tailed, equal variance). *N*=4.

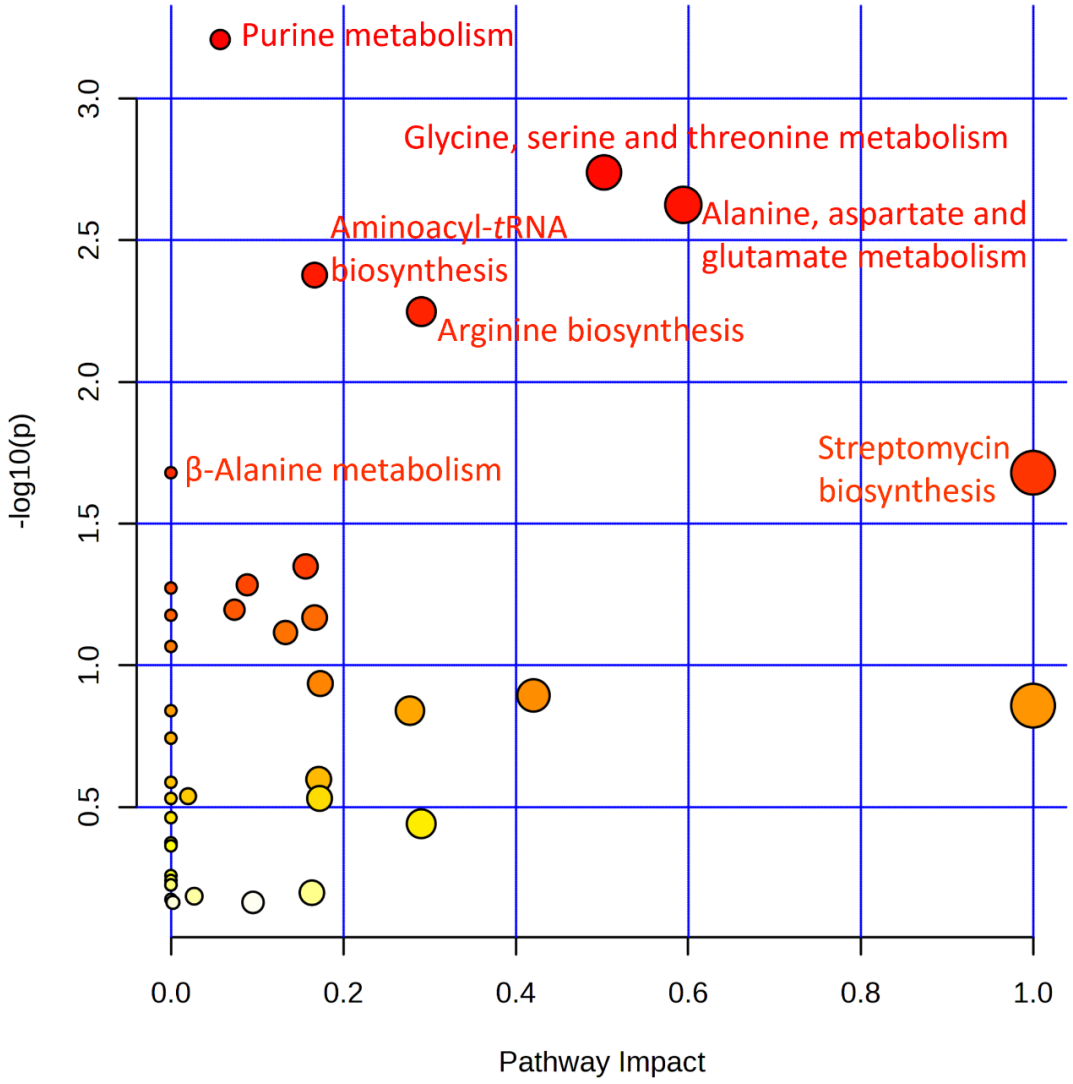

	Total	Expected	Hits	Raw p	-log10(p)	Holm adjust	FDR	Impact
Purine metabolism	54	2.62	9	6.19E-04	3.21E+00	4.64E-02	4.64E-02	0.06
Glycine, serine and threonine metabolism	29	1.41	6	1.82E-03	2.74E+00	1.35E-01	5.93E-02	0.5
Alanine, aspartate and glutamate metabolism	21	1.02	5	2.37E-03	2.62E+00	1.73E-01	5.93E-02	0.59
Aminoacyl-tRNA biosynthesis	45	2.18	7	4.20E-03	2.38E+00	3.02E-01	7.87E-02	0.17
Arginine biosynthesis	16	0.78	4	5.65E-03	2.25E+00	4.01E-01	8.47E-02	0.29
beta-Alanine metabolism	5	0.24	2	2.09E-02	1.68E+00	1.00E+00	2.24E-01	0
Streptomycin biosynthesis	5	0.24	2	2.09E-02	1.68E+00	1.00E+00	2.24E-01	1

Figure 2.11 Pathway enrichment results from MetaboAnalyst **(162)** of the targeted metabolomics of S7 and S7-D2 during the mid-exponential phase. The top pathways are labeled and summarized.

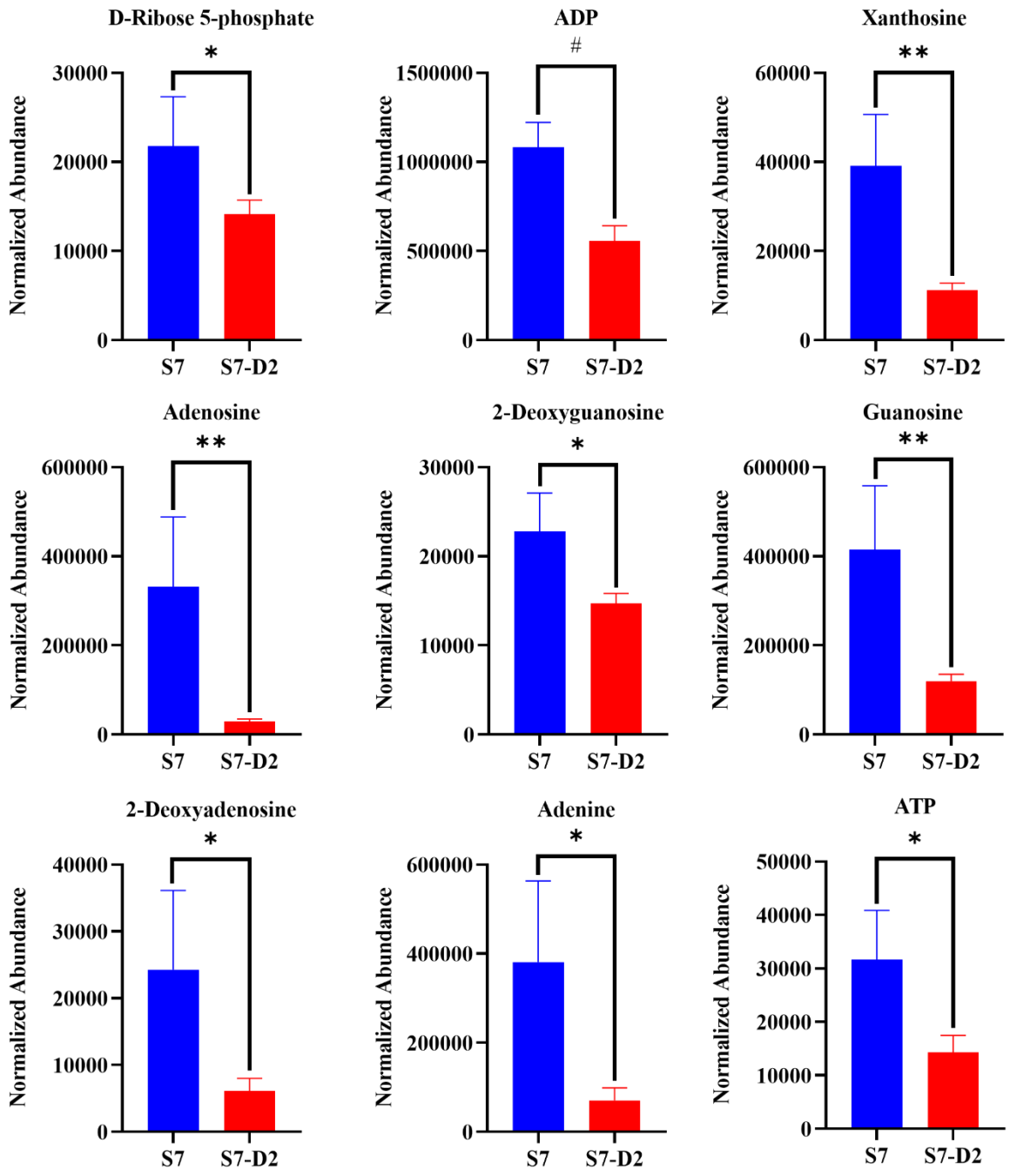

Figure 2.12 Individual metabolite changes comparing S7 and S7-D2 in the purine metabolism pathway (KEGG: SAU00230 **(163)**) during the mid-exponential phase. $^{\#}p<0.001$; $^{**}0.001<p<0.01$; $^{*}0.01<p<0.05$ (Student's *t*-test, unpaired, two-tailed, equal variance). $N=4$.

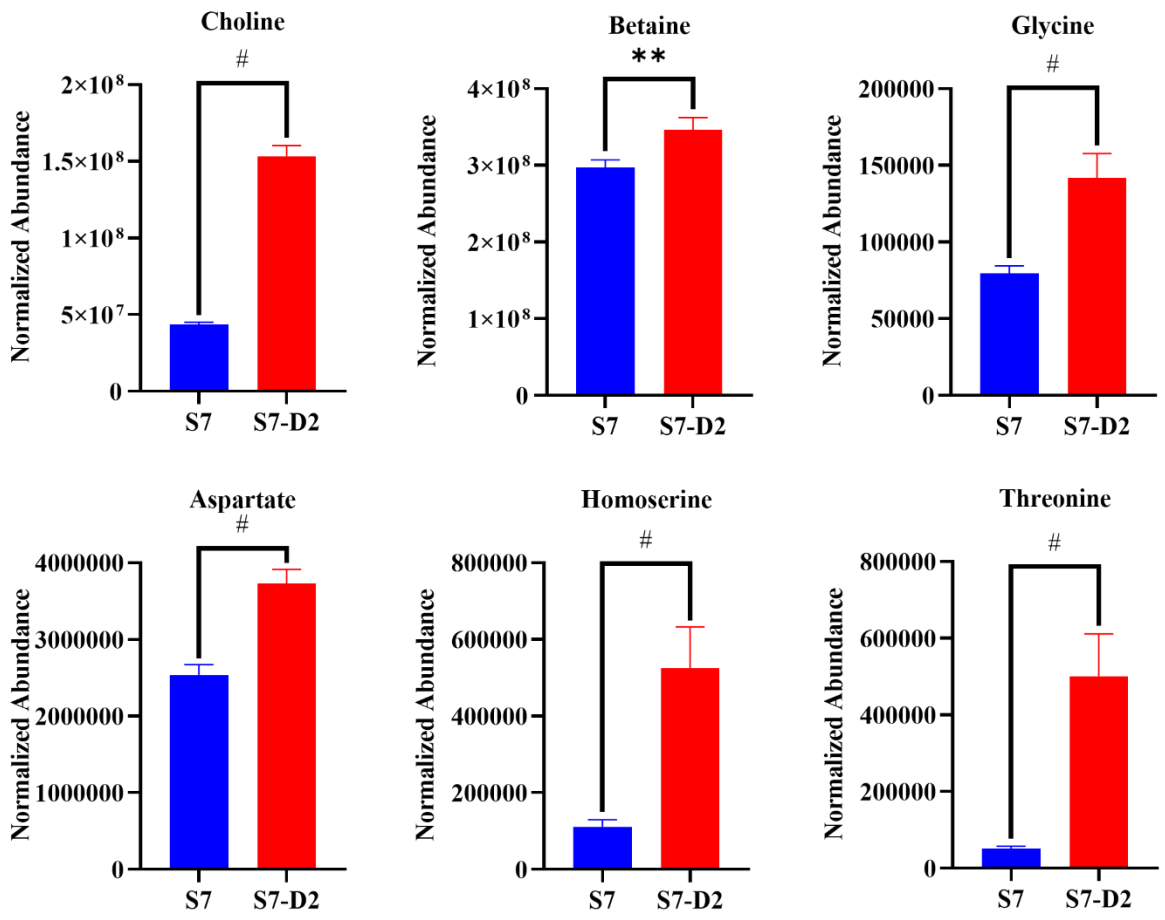

Figure 2.13 Individual metabolite changes comparing S7 and S7-D2 in the glycine, serine and threonine metabolism pathway (KEGG: SAU00260 **(163)**) during the mid-exponential phase. $^{\#}p<0.001$; $^{**}0.001<p<0.01$ (Student's *t*-test, unpaired, two-tailed, equal variance). $N=4$.

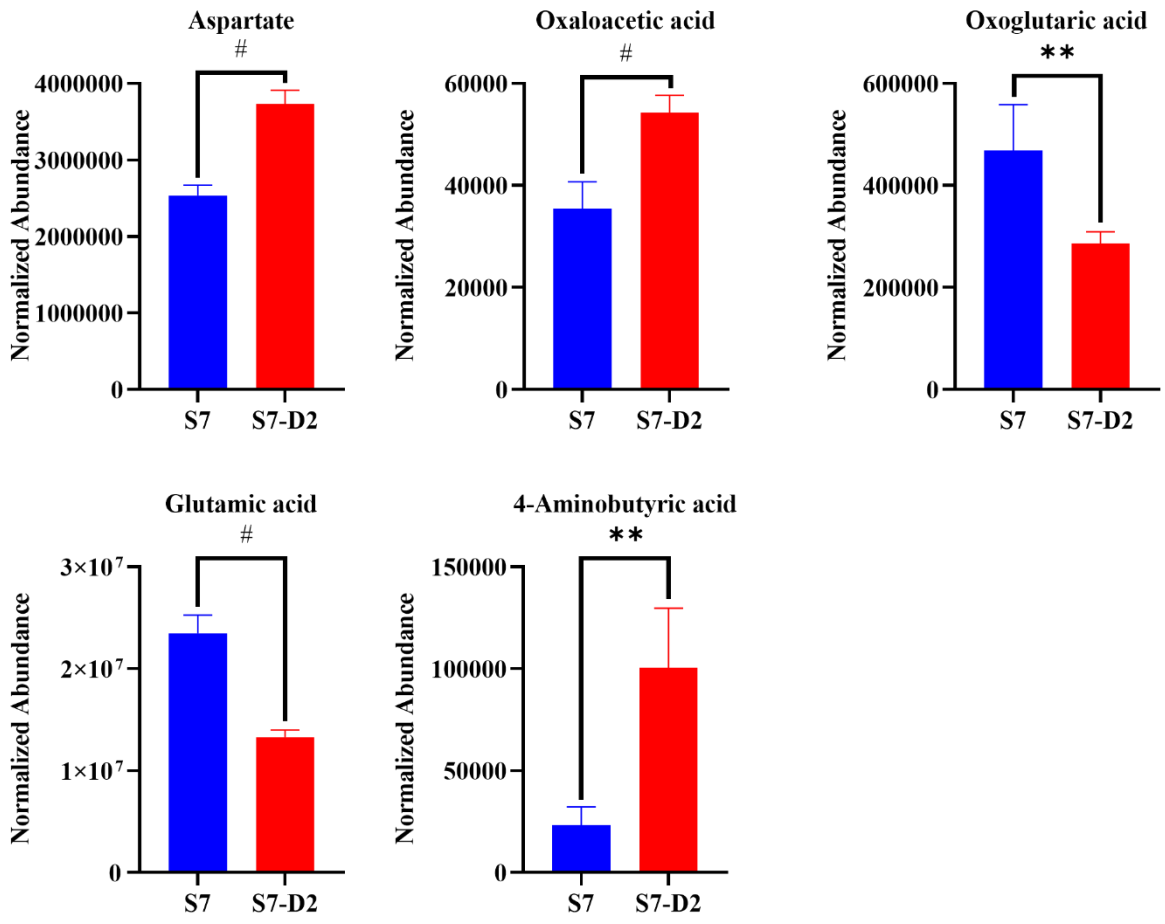

Figure 2.14 Individual metabolite changes comparing S7 and S7-D2 in the alanine, aspartate and glutamate metabolism (KEGG: SAU00250 **(163)**) during the mid-exponential phase. $^{\#}p<0.001$; $^{**}0.001<p<0.01$ (Student's *t*-test, unpaired, two-tailed, equal variance). $N=4$.

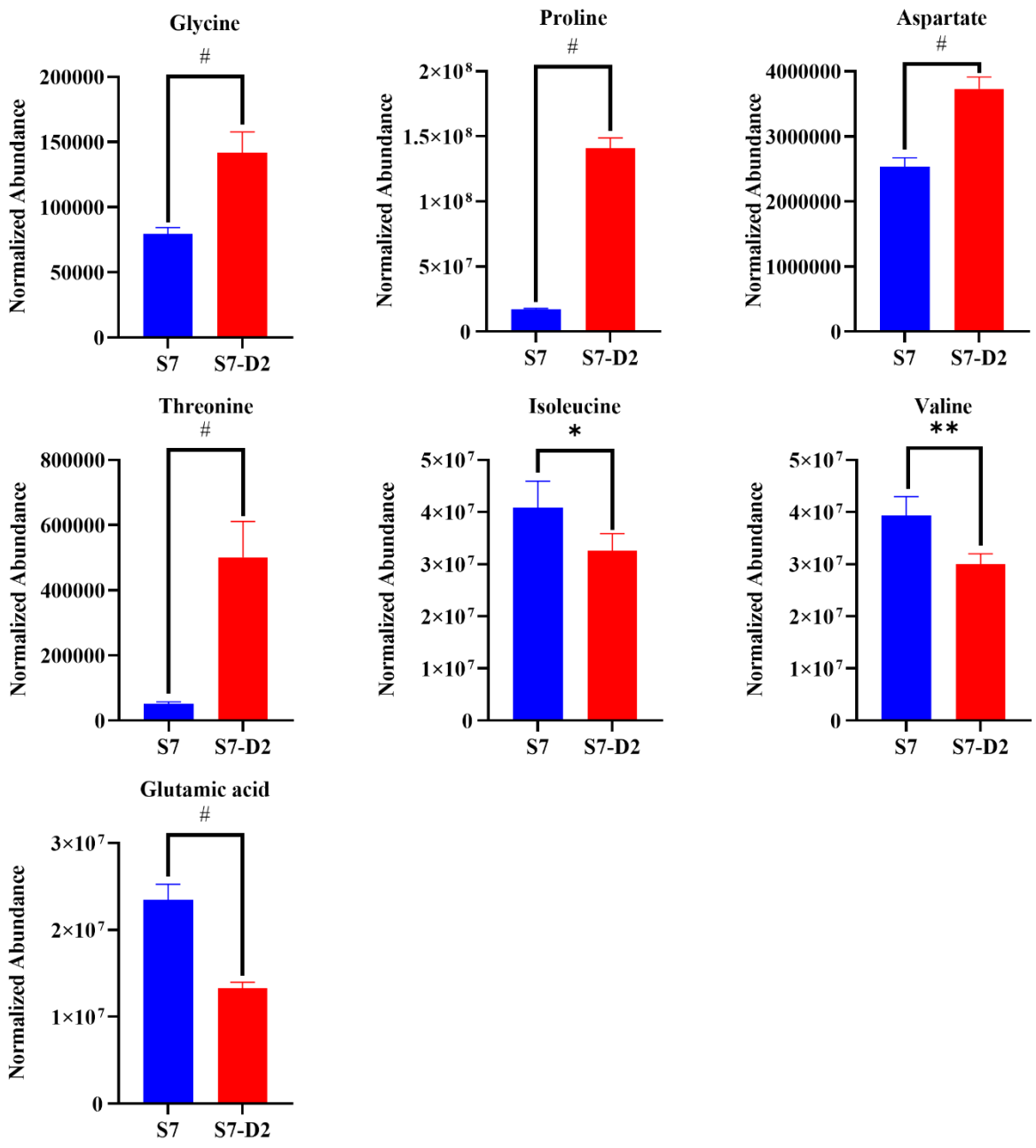

Figure 2.15 Individual metabolite changes comparing S7 and S7-D2 in the aminoacyl-*t*RNA biosynthesis pathway (KEGG: SAU00970 **(163)**) during the mid-exponential phase. $^{\#}p<0.001$; $^{**}0.001<p<0.01$; $^{*}0.01<p<0.05$ (Student's *t*-test, unpaired, two-tailed, equal variance). $N=4$.

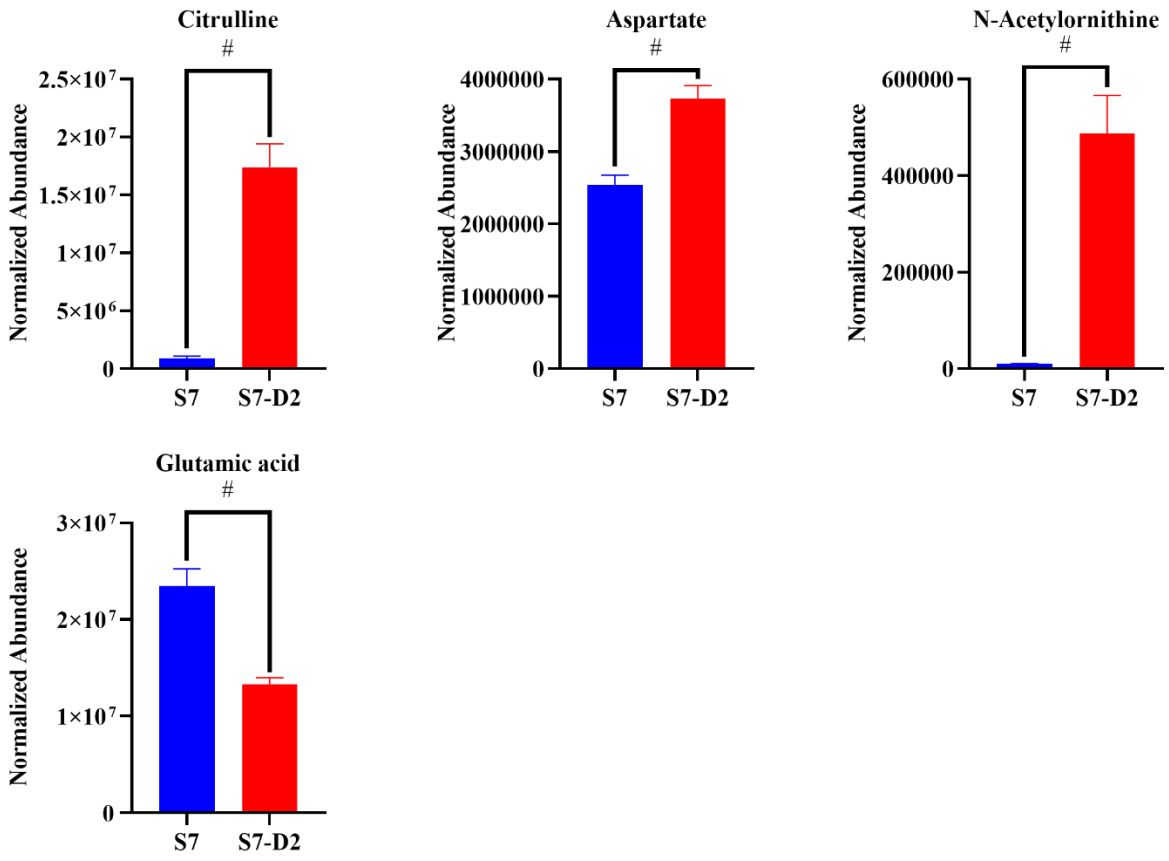

Figure 2.16 Individual metabolite changes comparing S7 and S7-D2 in the arginine biosynthesis pathway (KEGG: SAU00220 **(163)**) during the mid-exponential phase. $^{\#}p<0.001$ (Student's *t*-test, unpaired, two-tailed, equal variance). $N=4$.

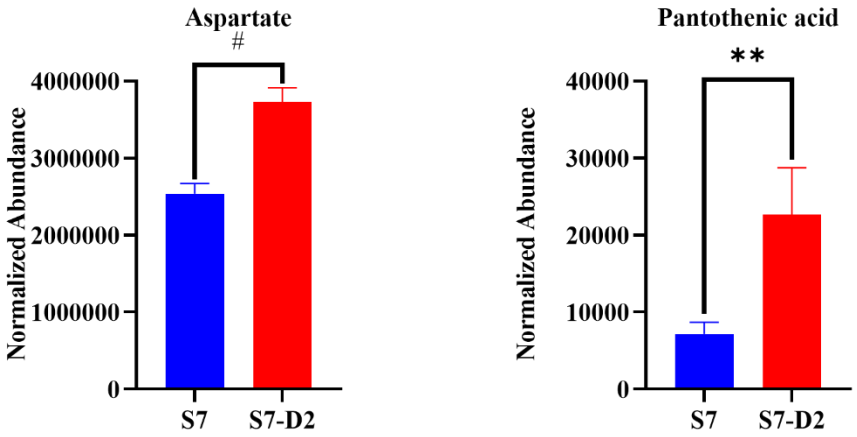

Figure 2.17 Individual metabolite changes comparing S7 and S7-D2 in β-alanine metabolism pathway (KEGG: SAU00410 **(163)**) during the mid-exponential phase. $^{\#}p<0.001$; $^{**}0.001<p<0.01$ (Student's *t*-test, unpaired, two-tailed, equal variance). $N=4$.

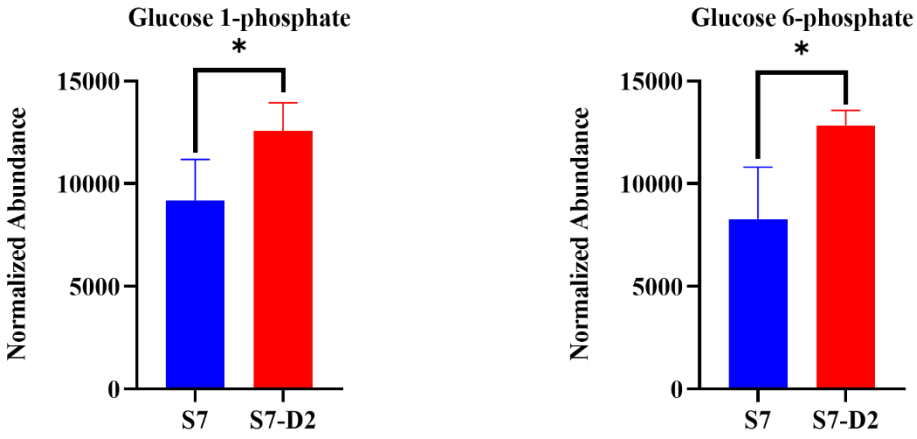

Figure 2.18 Individual metabolite changes comparing S7 and S7-D2 in the streptomycin biosynthesis pathway (KEGG: SAU00521 **(163)**) during the mid-exponential phase. $^{*}0.01<p<0.05$ (Student's *t*-test, unpaired, two-tailed, equal variance). $N=4$.

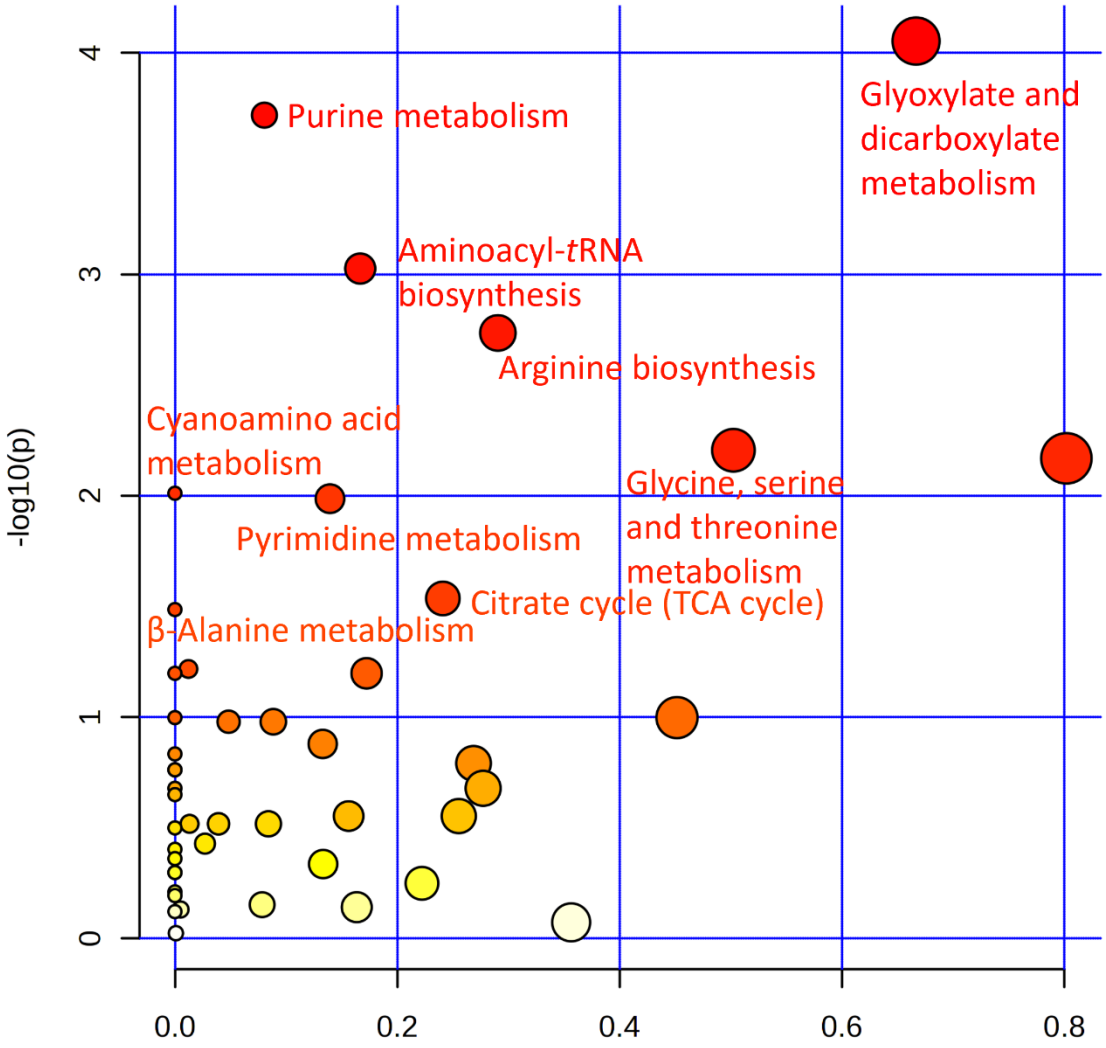

	Total	Expected	Hits	Raw p	-log10(p)	Holm adjust	FDR	Impact
Glyoxylate and dicarboxylate metabolism	20	1.23	7	8.84E-05	4.05E+00	6.63E-03	6.63E-03	0.67
Purine metabolism	54	3.31	11	1.91E-04	3.72E+00	1.41E-02	7.16E-03	0.08
Aminoacyl-tRNA biosynthesis	45	2.76	9	9.42E-04	3.03E+00	6.88E-02	2.36E-02	0.17
Arginine biosynthesis	16	0.98	5	1.84E-03	2.74E+00	1.33E-01	3.45E-02	0.29
Glycine, serine and threonine metabolism	29	1.78	6	6.23E-03	2.21E+00	4.43E-01	8.48E-02	0.5
Alanine, aspartate and glutamate metabolism	21	1.29	5	6.78E-03	2.17E+00	4.75E-01	8.48E-02	0.8
Cyanoamino acid metabolism	8	0.49	3	9.75E-03	2.01E+00	6.73E-01	9.67E-02	0
Pyrimidine metabolism	32	1.96	6	1.03E-02	1.99E+00	7.02E-01	9.67E-02	0.14
Citrate cycle (TCA cycle)	20	1.23	4	2.91E-02	1.54E+00	1.00E+00	2.43E-01	0.24
beta-Alanine metabolism	5	0.31	2	3.27E-02	1.49E+00	1.00E+00	2.45E-01	0

Figure 2.19 Pathway enrichment results from MetaboAnalyst **(162)** of the targeted metabolomics of S7 and S7-D2 during the stationary phase. The top pathways are labeled and summarized.

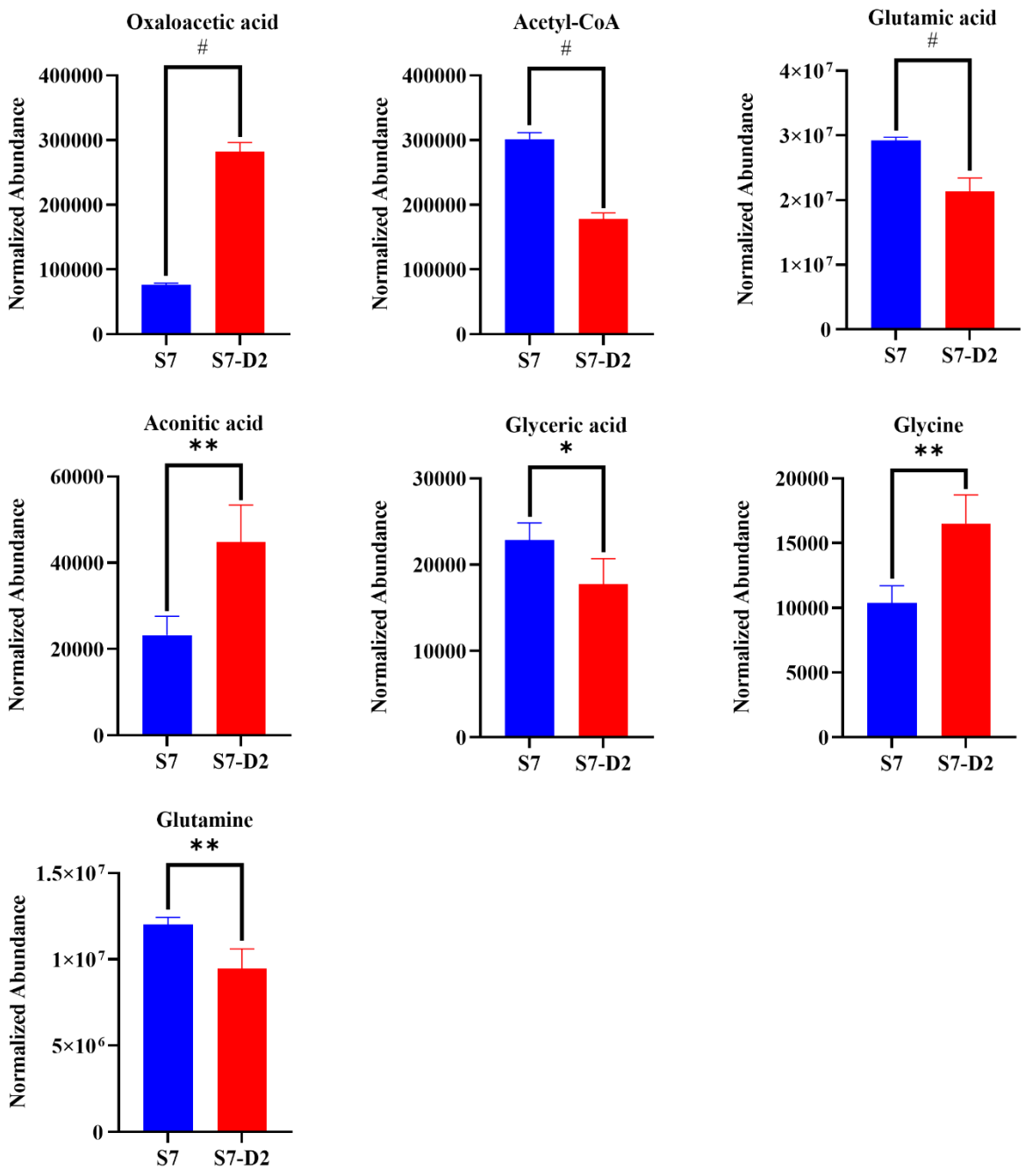

Figure 2.20 Individual metabolite changes comparing S7 and S7-D2 in the glyoxylate and dicarboxylate metabolism pathway (KEGG: SAU00630 **(163)**) during the stationary phase. $^{\#}p<0.001$; $^{**}0.001<p<0.01$; $^{*}0.01<p<0.05$ (Student's *t*-test, unpaired, two-tailed, equal variance). $N=4$.

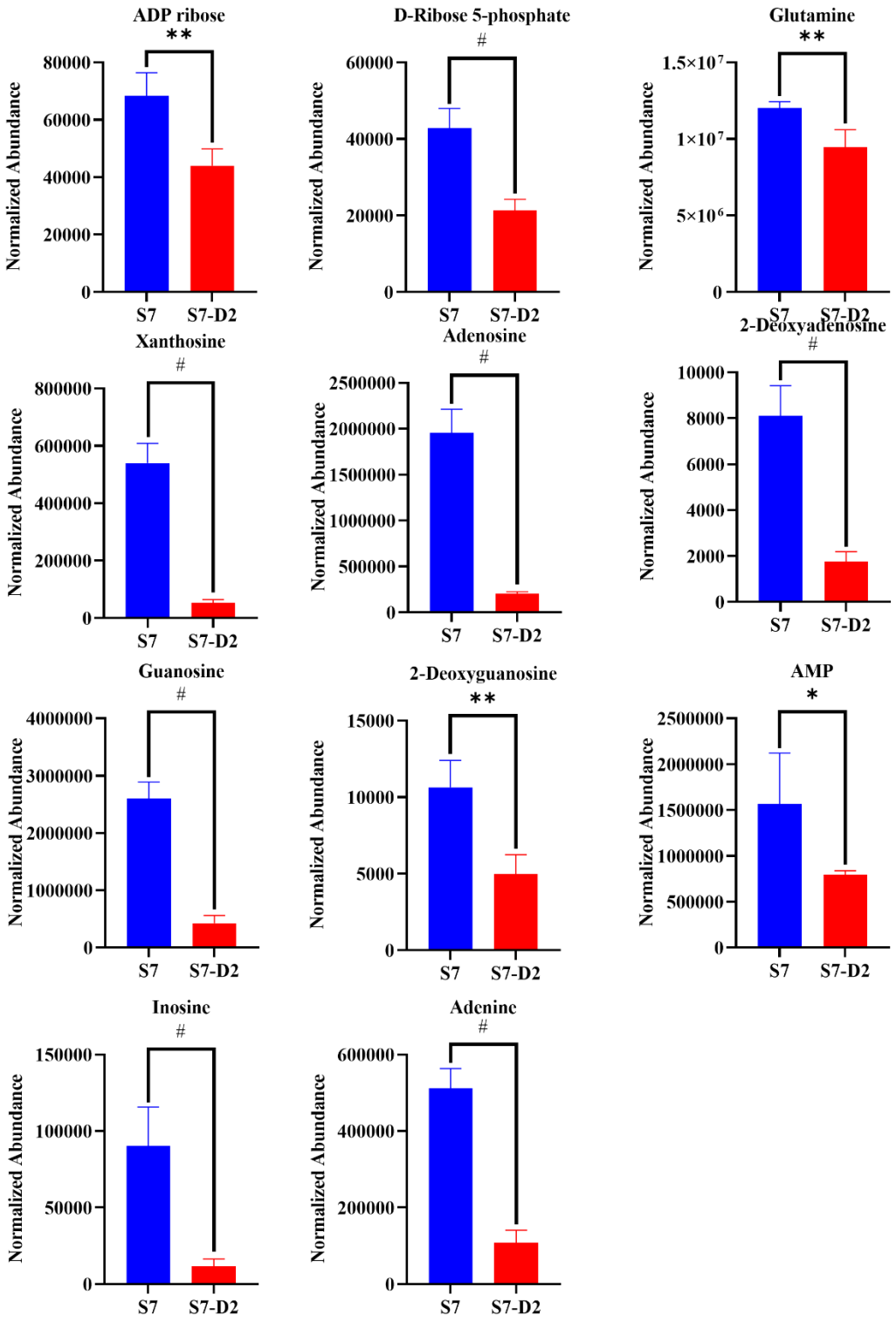

Figure 2.21 Individual metabolite changes comparing S7 and S7-D2 in the purine metabolism pathway (KEGG: SAU00230 **(163)**) during the stationary phase. $^{\#}p<0.001$; $^{**}0.001<p<0.01$; $^{*}0.01<p<0.05$ (Student's *t*-test, unpaired, two-tailed, equal variance). $N=4$.

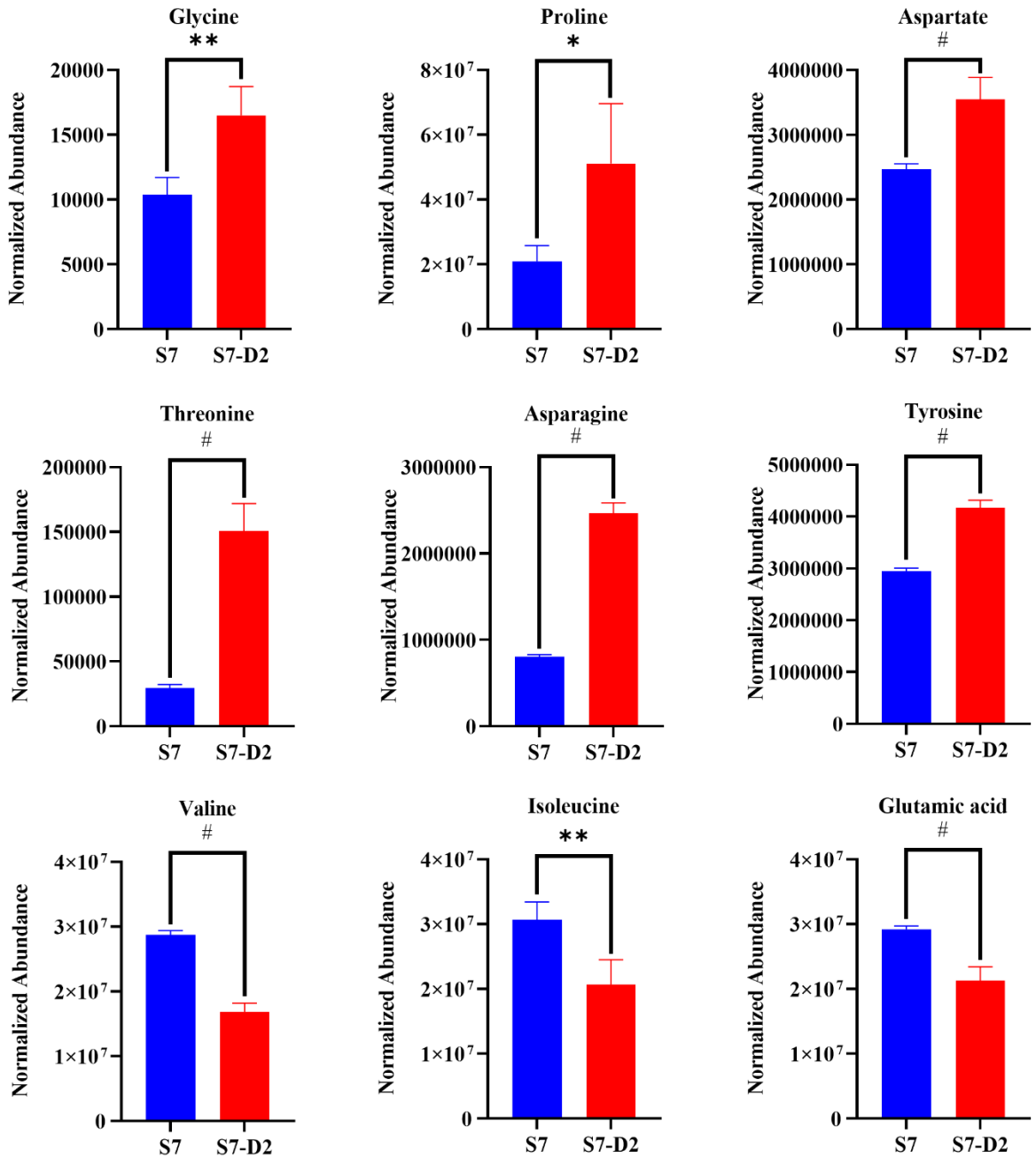

Figure 2.22 Individual metabolite changes comparing S7 and S7-D2 in the aminoacyl-*t*RNA biosynthesis pathway (KEGG: SAU00970 **(163)**) during the stationary phase. $^{\#}p<0.001$; $^{**}0.001<p<0.01$; $^{*}0.01<p<0.05$ (Student's *t*-test, unpaired, two-tailed, equal variance). $N=4$.

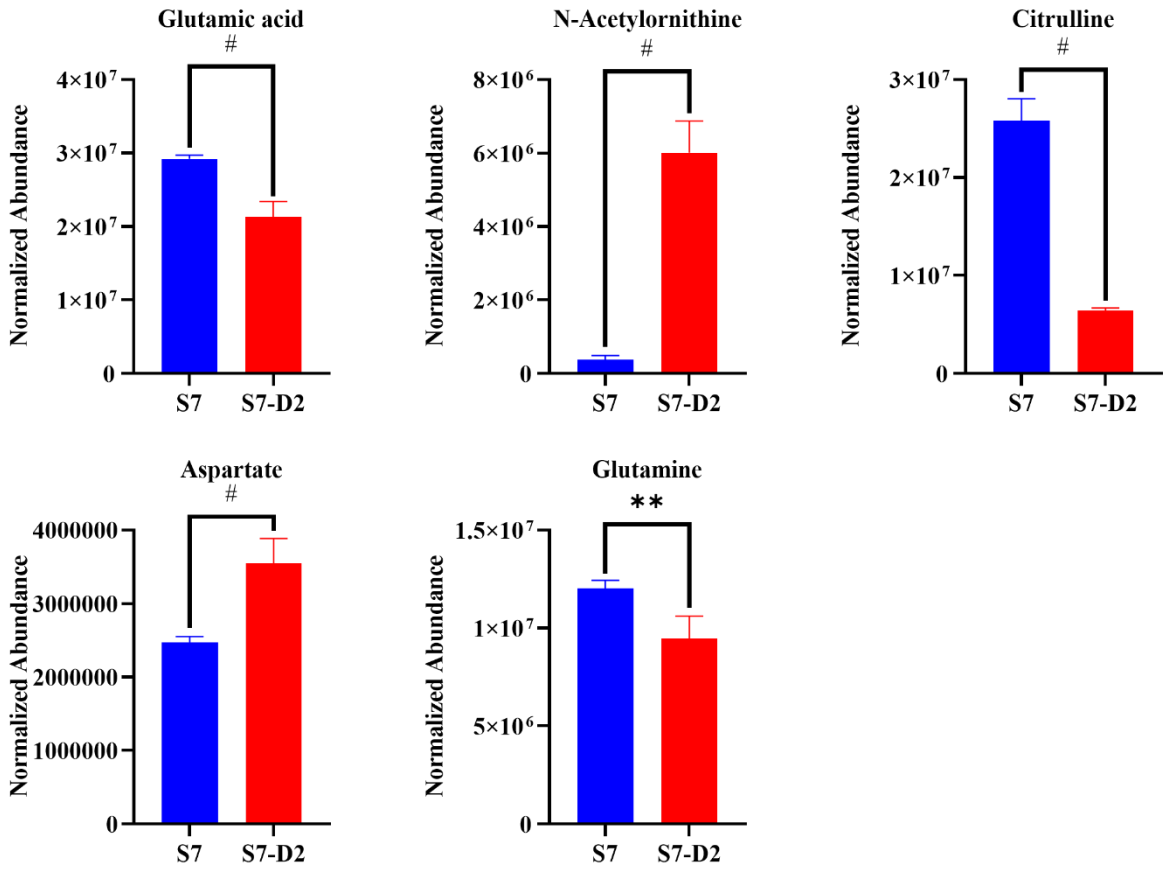

Figure 2.23 Individual metabolite changes comparing S7 and S7-D2 in the arginine biosynthesis pathway (KEGG: SAU00220 **(163)**) during the stationary phase. $^{\#}p<0.001$; $^{**}0.001<p<0.01$ (Student's *t*-test, unpaired, two-tailed, equal variance). $N=4$.

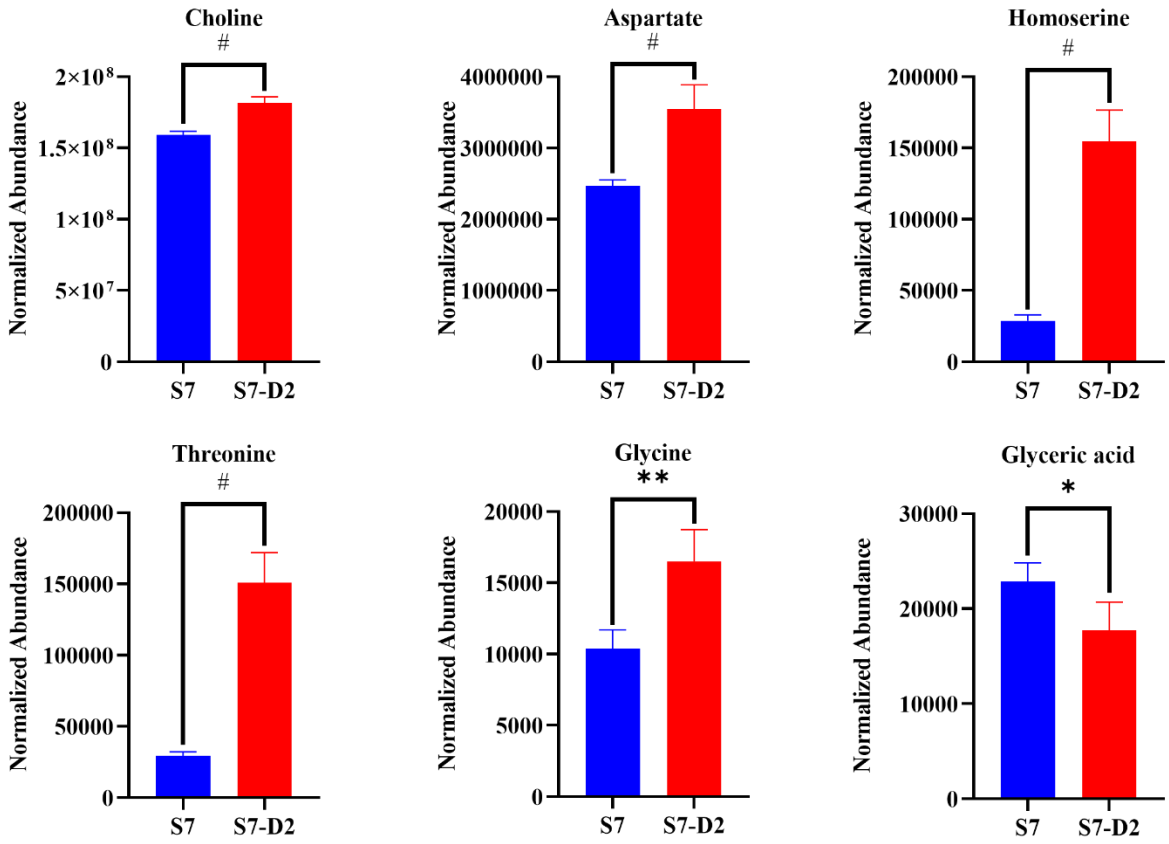

Figure 2.24 Individual metabolite changes comparing S7 and S7-D2 in the glycine, serine and threonine metabolism pathway (KEGG: SAU00260 **(163)**) during the stationary phase. $^{\#}p<0.001$; $^{**}0.001<p<0.01$; $^{*}0.01<p<0.05$ (Student's *t*-test, unpaired, two-tailed, equal variance). $N=4$.

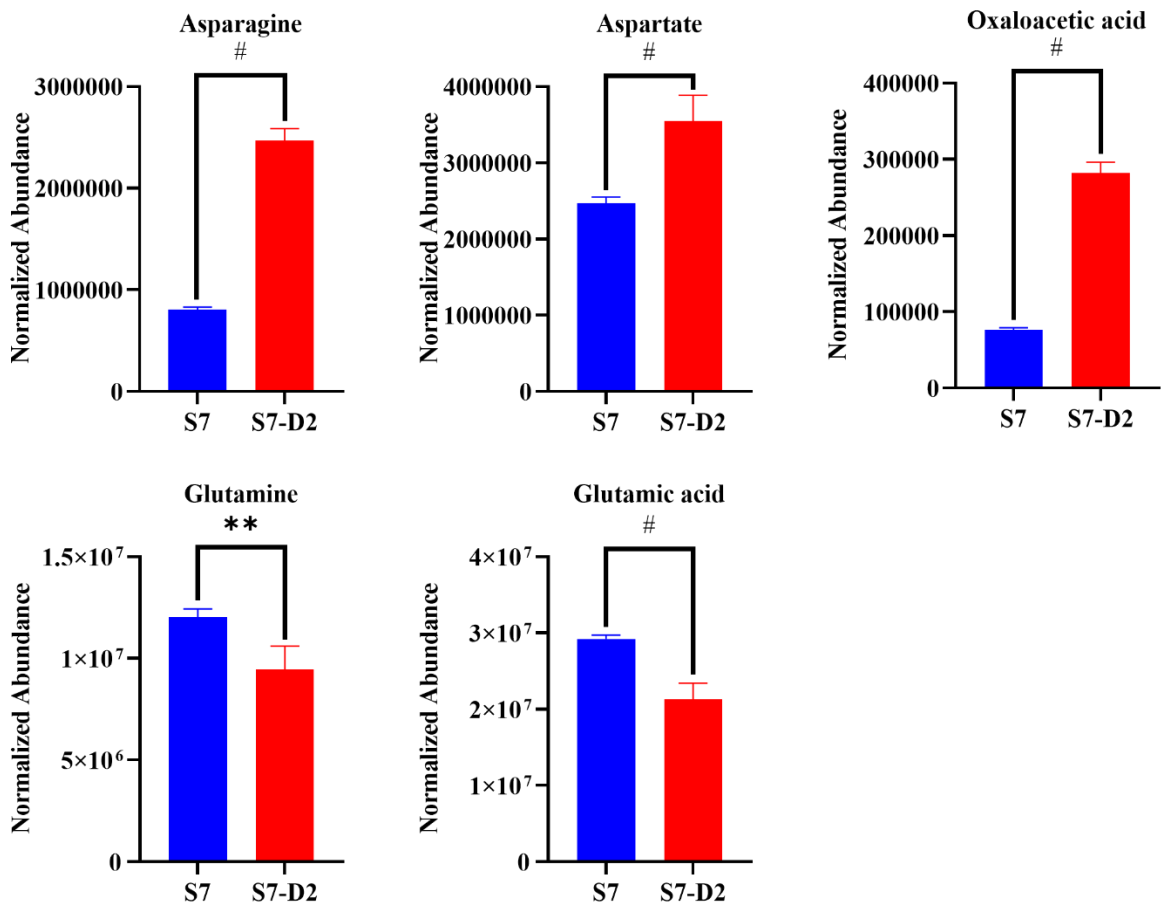

Figure 2.25 Individual metabolite changes comparing S7 and S7-D2 in the alanine, aspartate and glutamate metabolism (KEGG: SAU00250 **(163)**) during the stationary phase. $^{\#}p<0.001$; $^{**}0.001<p<0.01$ (Student's *t*-test, unpaired, two-tailed, equal variance). $N=4$.

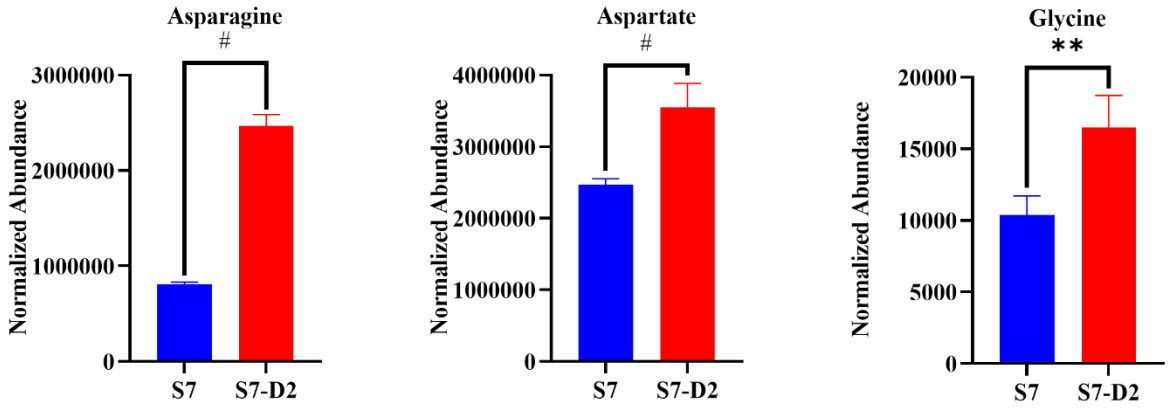

Figure 2.26 Individual metabolite changes comparing S7 and S7-D2 in the cyanoamino acid metabolism (KEGG: SAU00460 **(163)**) during the stationary phase. $^{\#}p<0.001$; $^{**}0.001<p<0.01$ (Student's *t*-test, unpaired, two-tailed, equal variance). $N=4$.

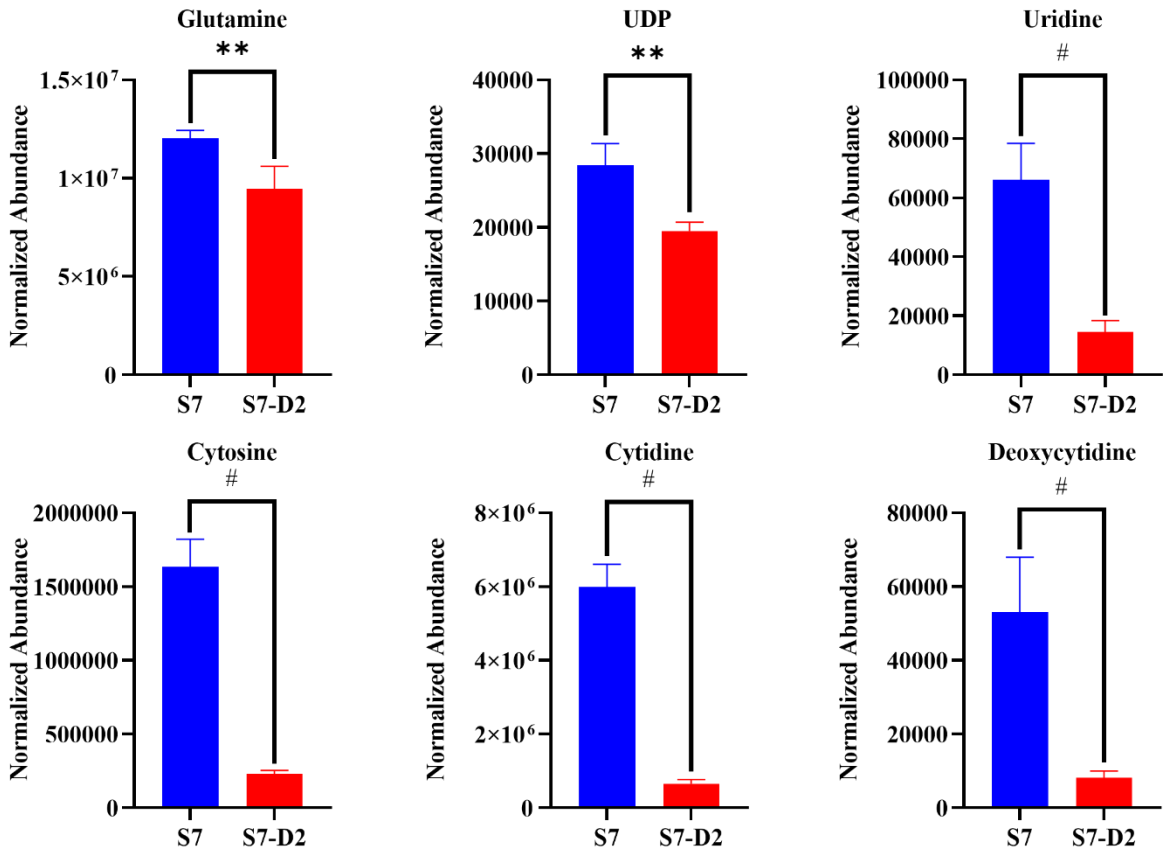

Figure 2.27 Individual metabolite changes comparing S7 and S7-D2 in the pyrimidine metabolism (KEGG: SAU00240 **(163)**) during the stationary phase. $^{\#}p<0.001$; $^{**}0.001<p<0.01$ (Student's *t*-test, unpaired, two-tailed, equal variance). $N=4$.

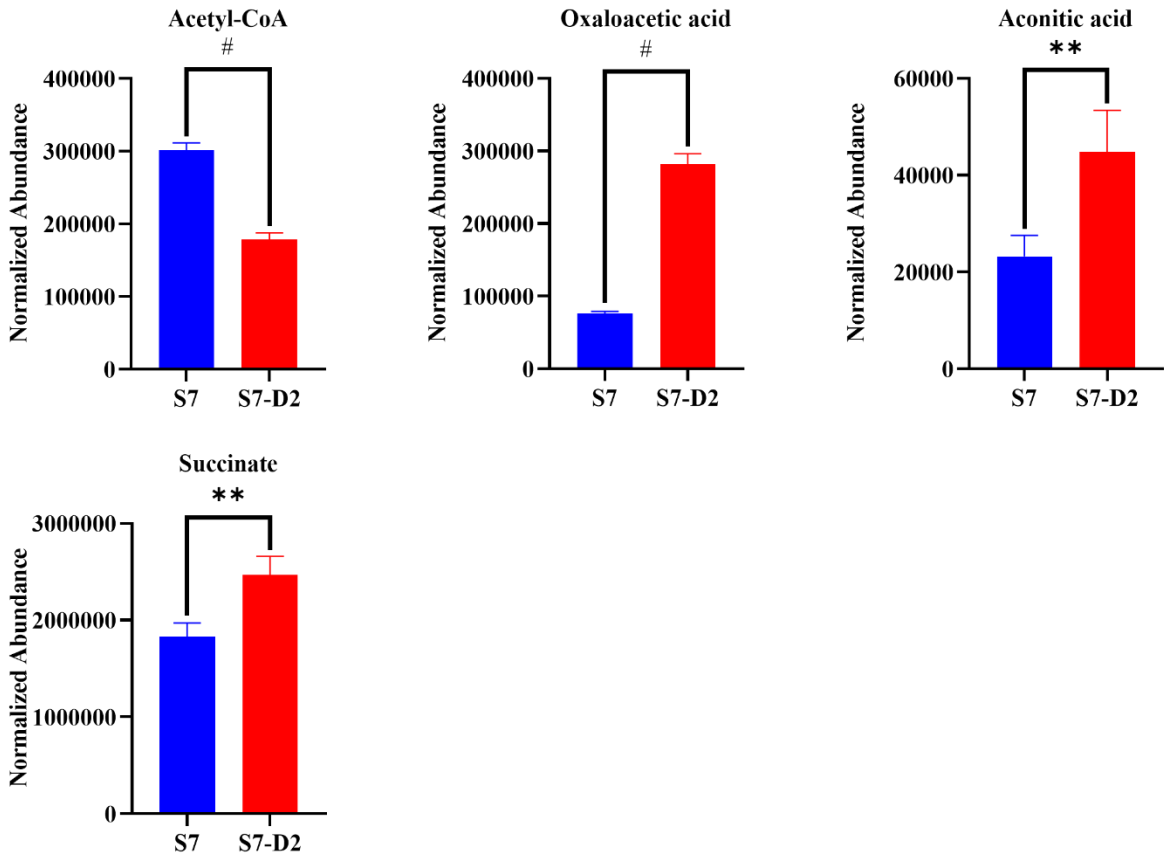

Figure 2.28 Individual metabolite changes comparing S7 and S7-D2 in the TCA cyle (KEGG: SAU00020 **(163)**) during the stationary phase. $^{\#}p<0.001$; $^{**}0.001<p<0.01$ (Student's *t*-test, unpaired, two-tailed, equal variance). $N=4$.

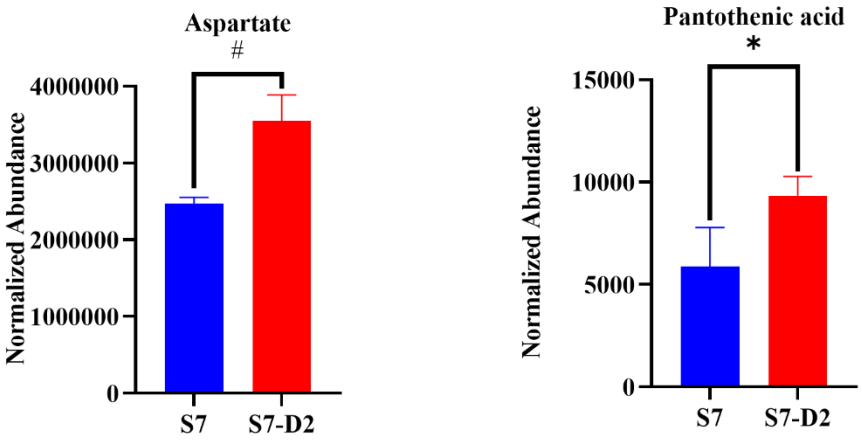

Figure 2.29 Individual metabolite changes comparing S7 and S7-D2 in β-alanine metabolism pathway (KEGG: SAU00410 **(163)**) during the stationary phase. $^{\#}p<0.001$; $^{*}0.01<p<0.05$ (Student's *t*-test, unpaired, two-tailed, equal variance). $N=4$.

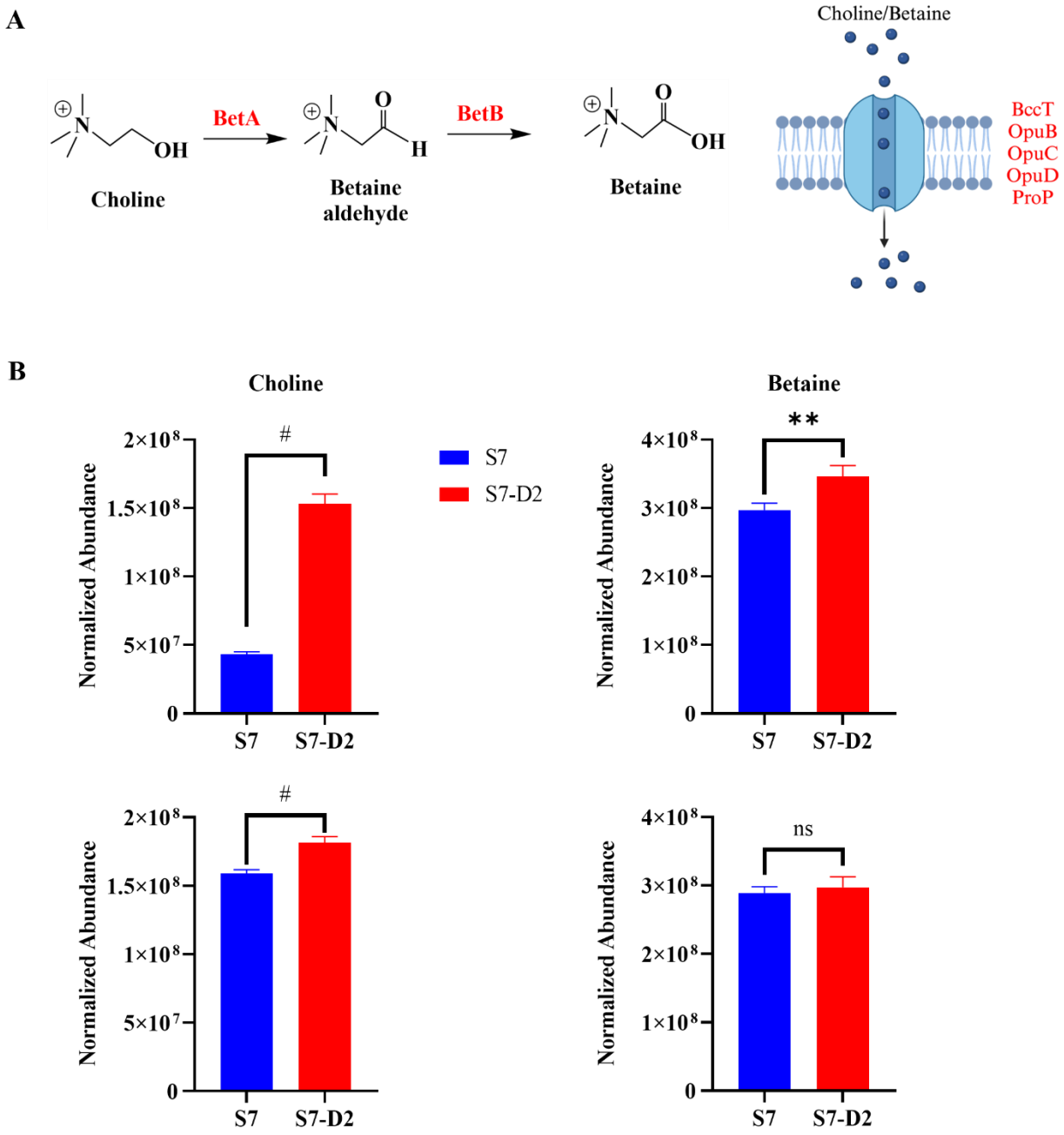

Figure 2.30 A) Schematic of the betaine biosynthesis pathway from choline to betaine *via* the action of BetA and BetB. Choline and betaine can also be transported into the bacteria *via* various choline/betaine transporters. **B)** Choline and betaine changes comparing S7 and S7-D2. Top panel: mid-exponential phase; bottom panel: stationary phase. $^{\#}p<0.001$; $^{**}0.001<p<0.01$; ns: non-significant (Student's *t*-test, unpaired, two-tailed, equal variance). *N*=4. Choline/betaine transporter illustration created with BioRender.com.

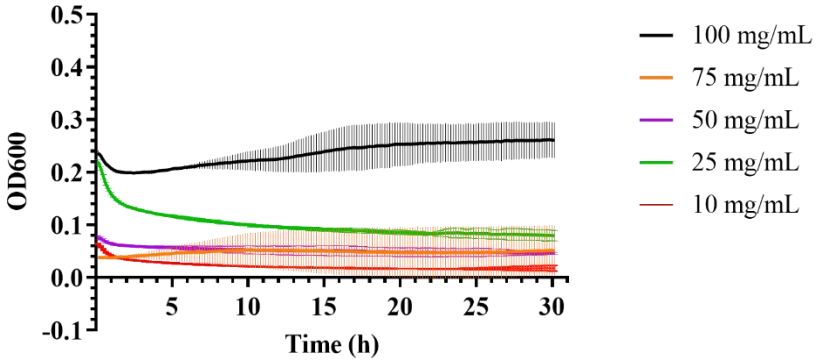

Figure 2.31 The OD_{600} of different concentrations of maltodextrin over the 30-h growth period, measured by the BioTek Synergy H1 platereader at 37°C in TSB media. *N*=3.

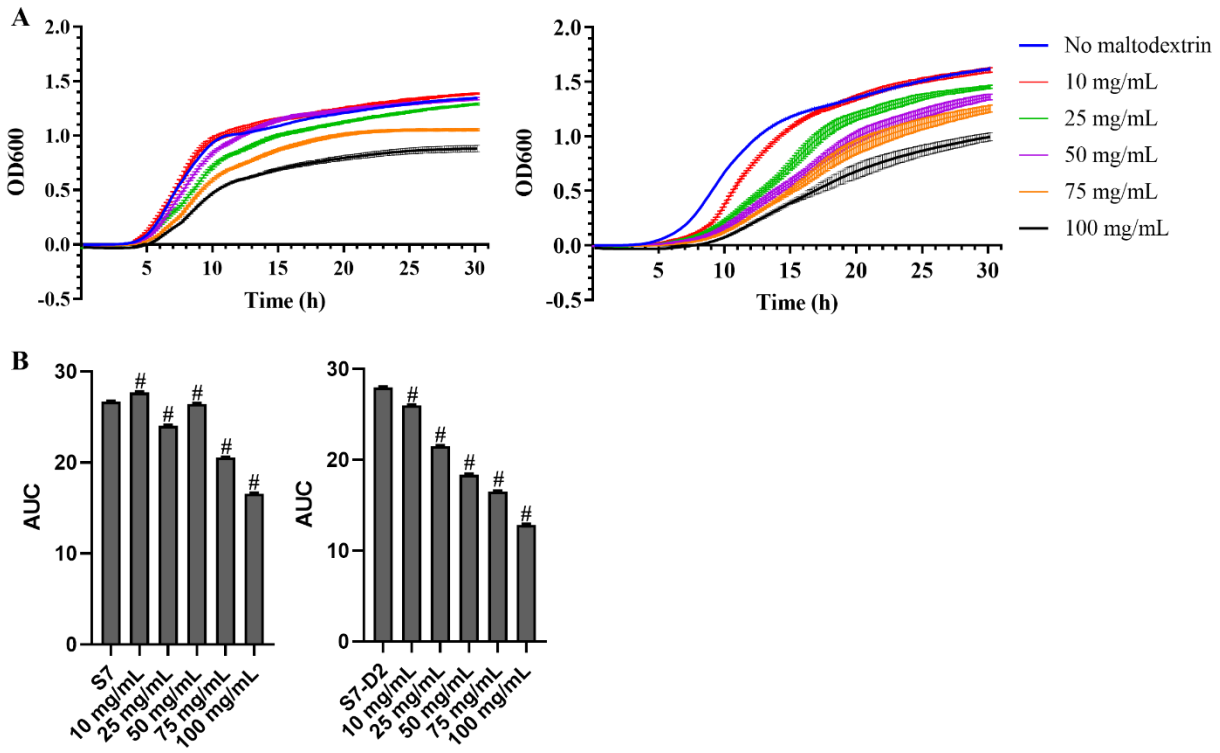

AUC (Maltodextrin) / AUC (No Maltodextrin)					
Maltodextrin Concentration	10 mg/mL	25 mg/mL	50 mg/mL	75 mg/mL	100 mg/mL
S7	103.7%	90.0%	99.1%	76.9%	62.1%
S7-D2	93.0%	76.9%	65.7%	59.0%	45.9%

Figure 2.32 Quantification of the total growth over the 30-h period of S7 and S7-D2 under different maltodextrin concentrations. **A)** The growth curve measured by the BioTek Synergy H1 platereader at 37°C in TSB media. *N*=5. Left: S7; Right: S7-D2. **B)** Calculations of the area under the curve (AUC) based on the growth curve in **A**. Absolute values and ratios are shown. Ratios were calculated relative to the AUC of the bacteria alone. $^{\#}p<0.001$ (Student's *t*-test, unpaired, two-tailed, equal variance).

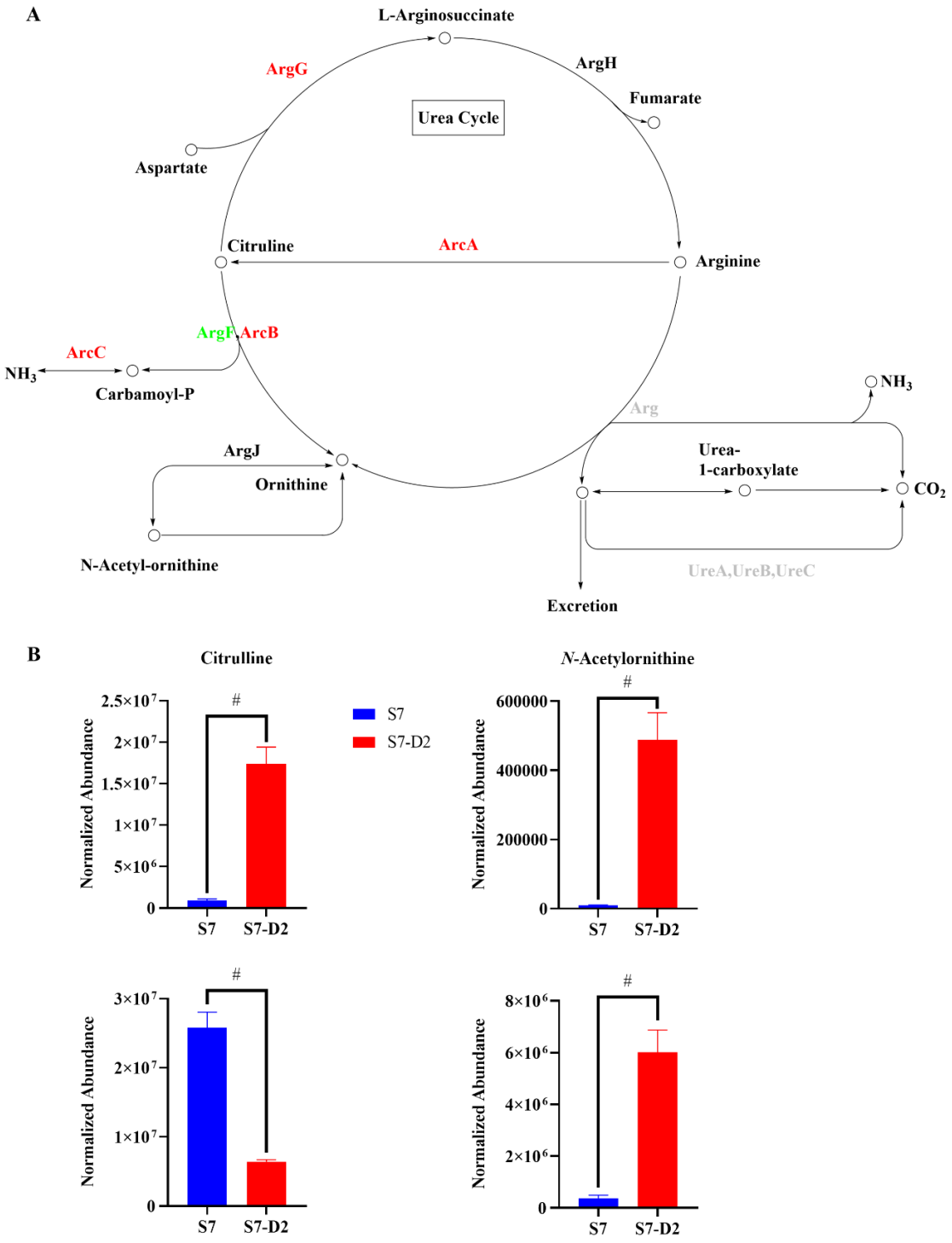

Figure 2.33 A) Schematic of the arginine deiminase (ADI) pathway coupled with the urea cycle (KEGG pathway SAU00220). Adapted and reprinted with permission from (163). Copyright 1995-2024 Kanehisa Laboratories. **B**) Citrulline and *N*-acetylornithine changes comparing S7 and S7-D2. Top panel: mid-exponential phase; bottom panel: stationary phase. # $p<0.001$(Student's *t*-test, unpaired, two-tailed, equal variance). $N=4$. Red: upregulated; Green: downregulated; Black: unchanged; Gray: unannotated or unchecked.

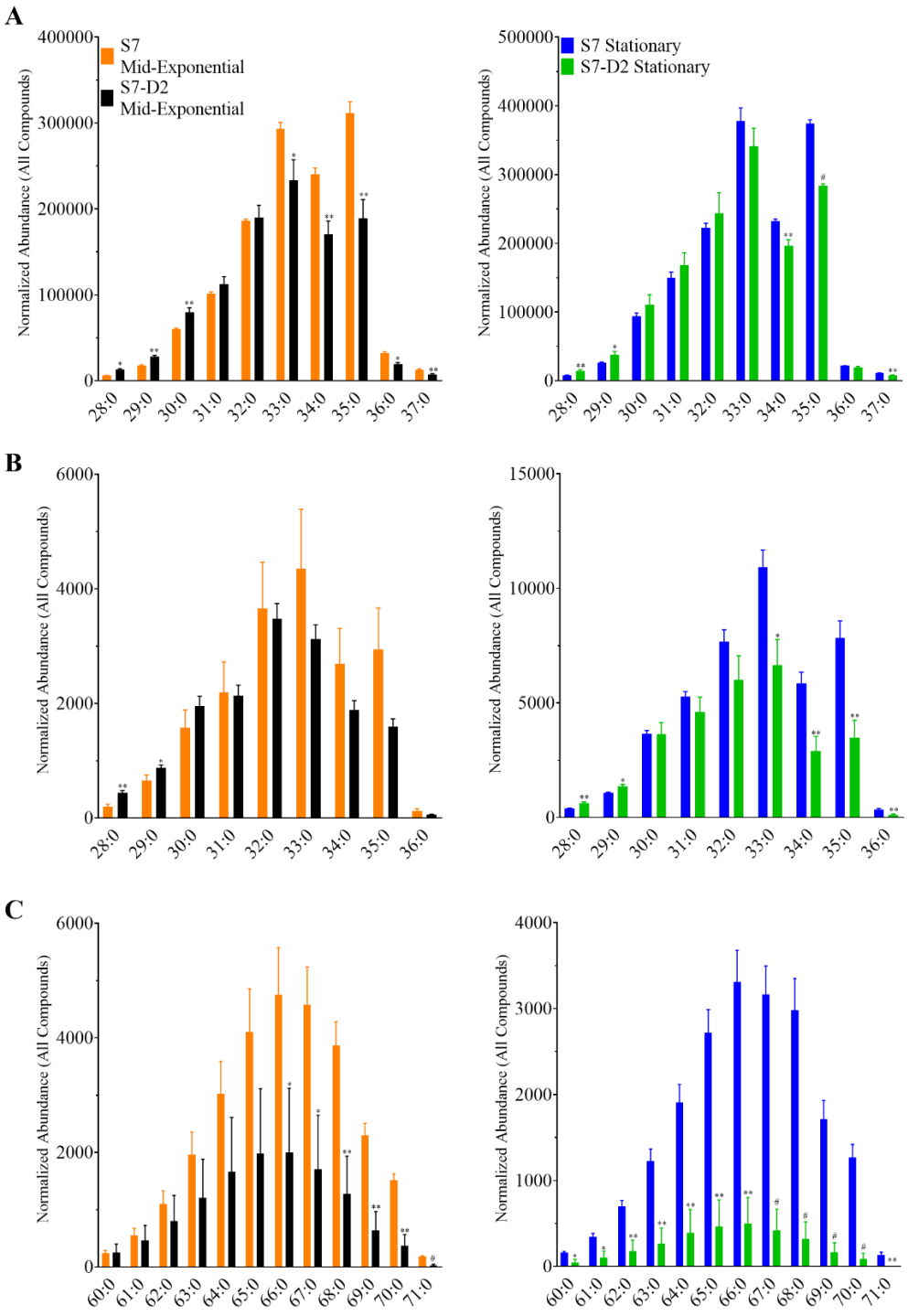

Figure 2.34 The phosphatidylglycerols (PGs; **A)**, lysyl-phosphatidylglycerols (lysyl-PGs; **B)**, and cardiolipins (CLs; **C)** profile of the parent S7 and the S7-D2 strains during the mid-exponential phase (left) and the stationary phase (right). Individual lipid species are represented as the number of carbons: the degree of unsaturation in the fatty acid chains. $^{\#}p<0.001$; $^{**}0.001<p<0.01$; $^{*}0.01<p<0.05$ (Student's *t*-test, two-tailed, equal variance). $N=3$.

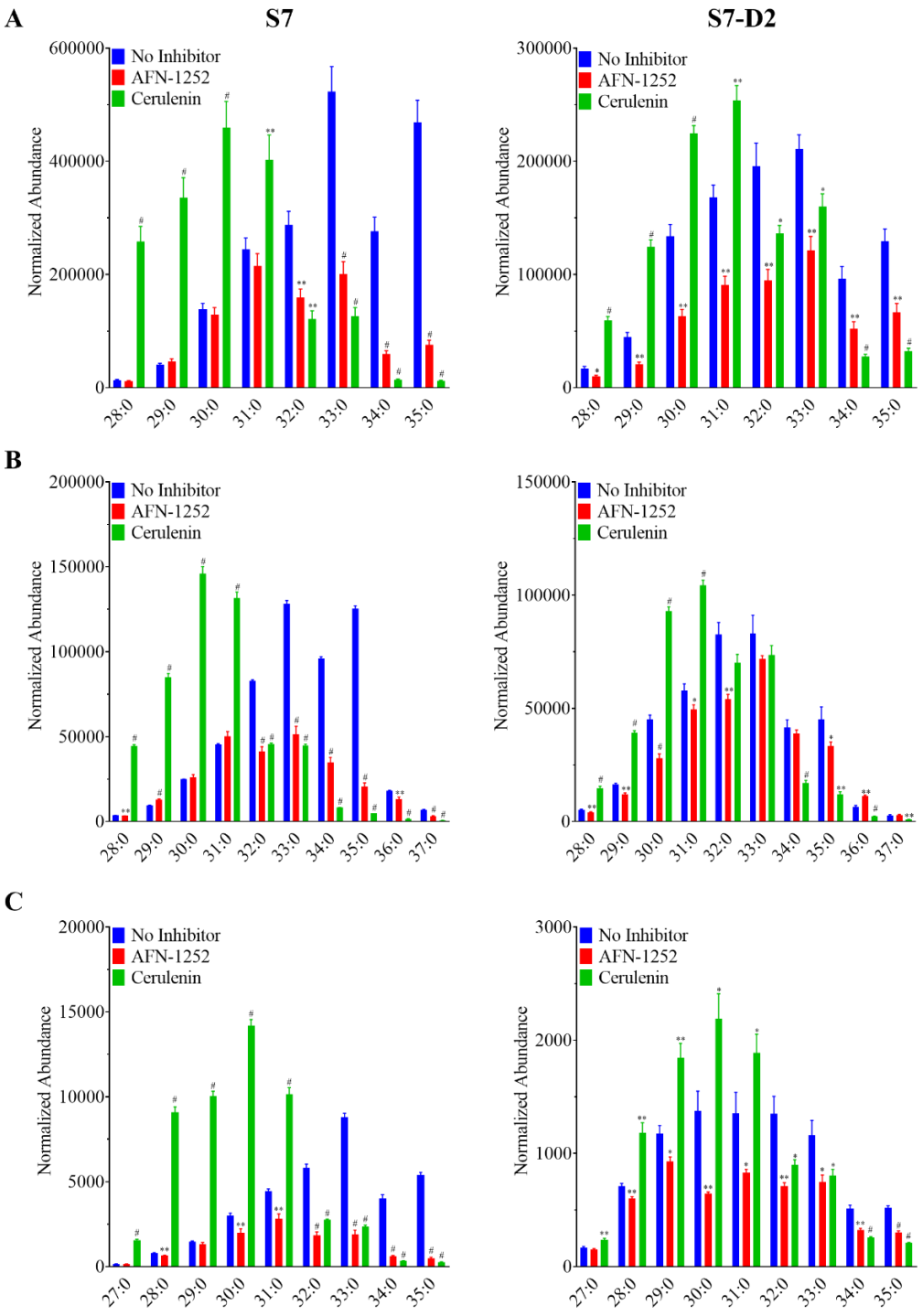

Figure 2.35 The phosphatidylglycerols (PGs; A), diglucosyl-diacylglycerols (DGDGs; B), and lysyl-phosphatidylglycerols (lysylPGs; C) profile of the parent S7 (left) and the S7-D2 (right) strains with or without exposure to half-MIC concentration of AFN-1252 or cerulenin. All samples were grown to the stationary phase. Individual lipid species are represented as the number of carbons: the degree of unsaturation in the fatty acid chains. $^{\#}p<0.001$; $^{**}0.001<p<0.01$; $^{*}0.01<p<0.05$ (Student's *t*-test, two-tailed, equal variance). $N=3$.

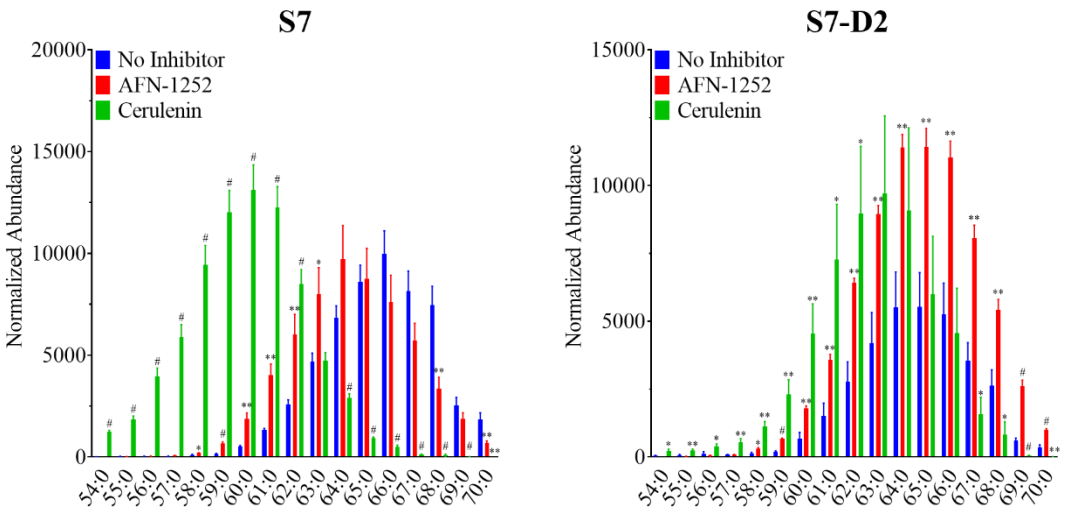

Figure 2.36 The cardiolipins (CLs) profile of the parent S7 (left) and the S7-D2 (right) strains with or without exposure to half-MIC concentration of AFN-1252 or cerulenin. All samples were grown to the stationary phase. Individual lipid species are represented as the number of carbons: the degree of unsaturation in the fatty acid chains. $^{\#}p<0.001$; $^{**}0.001<p<0.01$; $^{*}0.01<p<0.05$ (Student's *t*-test, two-tailed, equal variance). $N=3$.

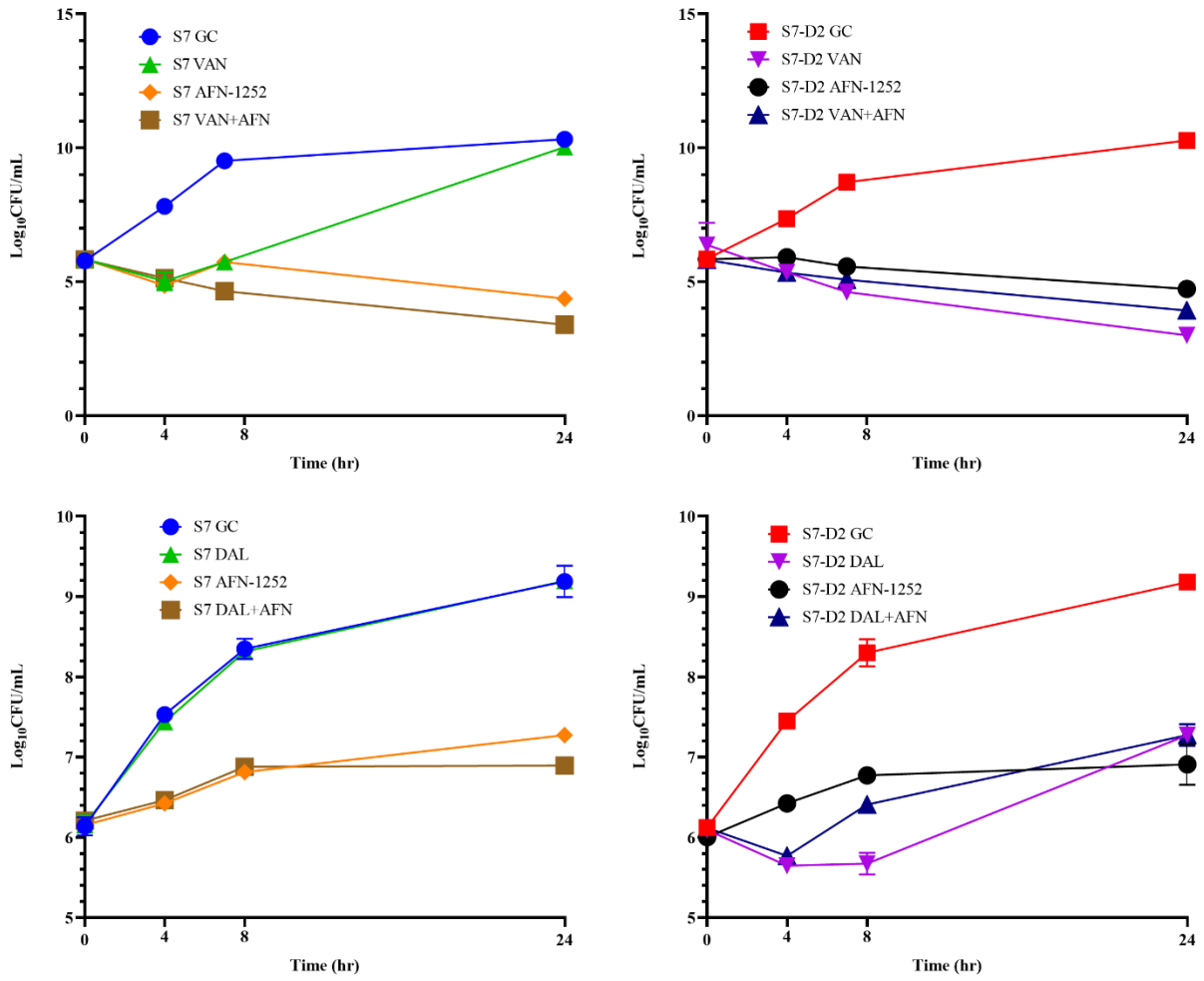

Figure 2.37 The time-kills of S7 (left) and S7-D2 (right) with AFN-1252 (2xMIC) and half-MIC of **A)** vancomycin or **B)** dalbavancin. *N*=2.

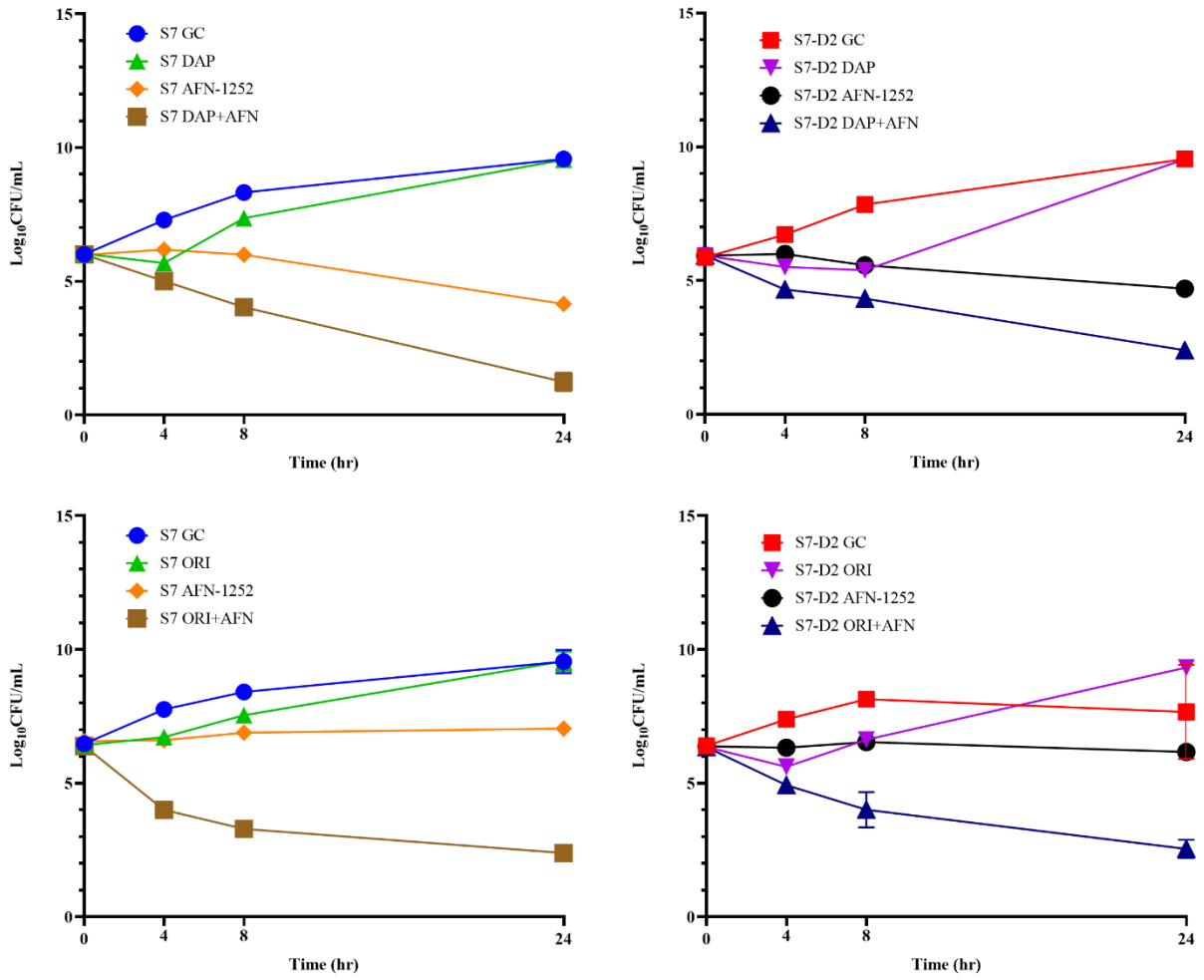

Figure 2.38 The time-kills of S7 (left) and S7-D2 (right) with AFN-1252 (2xMIC) and half-MIC of **A)** daptomycin or **B)** oritavancin. *N*=2.

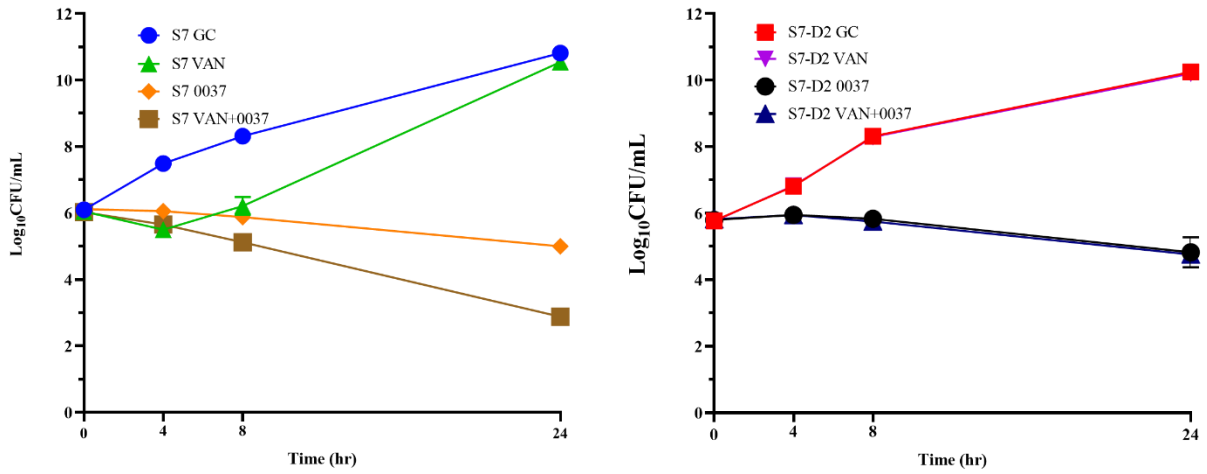

Figure 2.39 The time-kills of S7 (left) and S7-D2 (right) with F1374-0037 (2xMIC) and half-MIC of vancomycin. *N*=2.

Tables

Table 2.1 Susceptibility profile of the USA300 JE2 strains and the N315 strain pair. The MICs were measured by the broth microdilution method.

Minimum inhibitory concentration (μg/mL)			
JE2 strains	Vancomycin	Daptomycin	Dalbavancin
WT	1	0.5	0.0078
vraT::Tn	0.5	0.125	<0.0039
vraS::Tn	0.5~1	0.25~0.5	<0.00195
vraR::Tn	0.5~1	0.25	<0.00195
N315 strains	Vancomycin	Daptomycin	Dalbavancin
WT	0.5	0.125	0.0039
vraS KO	0.5	0.125	<0.0078

Table 2.2 The growth time and end-point OD_{600} of the S7 and S7-D2 mid-exponential phase samples for multi-omics analysis. Transcriptomics and metabolomics: quadruplicates; lipidomics: triplicates.

	S7					S7-D2				
	Time	OD_{600}				Time	OD_{600}			
Transcriptomics	6.5 h	0.539	0.588	0.664	0.634	8.5 h	0.583	0.585	0.577	0.487
Metabolomics	6.5 h	0.73	0.785	0.743	0.77	10 h	0.734	0.776	0.737	0.805
Lipidomics	6.5 h	0.604	0.598		0.553	10 h	0.611	0.603		0.679

Table 2.3 The log_2fold changes and adjusted *p*-values of a selection of genes involved in cell wall synthesis. The proteins they encode are also listed (naming based on annotations in the genome USA300-FPR3757 **(199)**).

	Protein	Fold change (log_2)	Adjusted *p*-value (Benjamini)
pbp1	Penicillin-binding protein 1	0.225	0.0865
pbp2	Penicillin-binding protein 2	0.965	2.57E-28
pbp3	Penicillin-binding protein 3	0.0327	0.772
pbp4	Penicillin-binding protein 4	0.300	0.0381
sgtA	Transglycosylase	0.156	0.271
sgtB	Glycosyltransferase	1.18	1.41E-22
murA	UDP-*N*-acetylglucosamine 1-carboxyvinyltransferase	-0.415	2.06E-5
murB	UDP-*N*-acetylenolpyruvoylglucosamine reductase	0.426	9.22E-4
murC	UDP-*N*-acetylmuramate--*L*-alanine ligase	-0.0575	0.603
murD	UDP-*N*-acetylmuramoyl-*L*-alanyl-*D*-glutamate synthetase	0.220	0.0140
murE	UDP-*N*-acetylmuramoylalanyl-*D*-glutamate--*L*-lysine ligase	0.253	0.0425
murF	UDP-*N*-acetylmuramoyl-tripeptide--*D*-alanyl-*D*-alanine ligase	0.238	0.123
murG	Undecaptrenyldiphospho-muramoylpentapeptide β-*N*-acetylglucosaminyltransferase	0.221	0.0352

Table 2.4 The log_2fold changes and adjusted *p*-values of a selection of genes involved in the FASII fatty acid synthesis pathway. The proteins they encode are also listed (naming based on annotations in the genome USA300-FPR3757 **(199)**).

	Protein	Fold change (log_2)	Adjusted *p*-value (Benjamini)
fabH	3-oxoacyl-(acyl carrier protein) synthase III	1.21	1.19E-9
fabD	Malonyl CoA-acyl carrier protein transacylase	0.102	0,576
fabF	3-oxoacyl-(acyl carrier protein) synthase II	0.939	5.32E-9
fabG	3-oxoacyl-(acyl carrier protein) reductase	0.234	0.231
fabZ	(3R)-hydroxymyristoyl-ACP dehydratase	-0.910	1.05E-19
accA	Acetyl-CoA carboxylase carboxyltransferase subunit α	0.149	0.178
accB	Acetyl-CoA carboxylase, biotin carboxyl carrier protein	0.859	2.24E-10
accC	Acetyl-CoA carboxylase biotin carboxylase subunit	0.797	5.53E-18
accD	Acetyl-CoA carboxylase subunit β	0.242	0.0718

Table 2.5 Functional annotation clustering results from DAVID, listing only the categories with adjusted p <0.05. Annotation cluster 1: cell adhesion; annotation cluster 2: virulence.

Annotation cluster 1				Enrichment score: 1.46			
Category	Term	Count	%	*p*-value	Fold enrichment	Adjusted *p*-value (Benjamini)	FDR
GOTERM_CC_DIRECT	GO:0005576~extracellular region	6	1.60	0.00700	4.24	0.0350	0.0350
UP_KW_CELLULAR_COMPONENT	KW-0964~Secreted	6	1.60	0.00966	3.92	0.0483	0.0483
Annotation cluster 2				Enrichment score: 1.28			
Category	Term	Count	%	*p*-value	Fold enrichment	Adjusted *p*-value (Benjamini)	FDR
UP_KW_BIOLOGICAL_PROCESS	KW-0843~Virulence	7	1.87	0.00196	4.24	0.0275	0.0255

Table 2.6 The $\log_2$fold changes and adjusted *p*-values of various choline/betaine transporters.

	opuC(a)	*opuC(b)*	*opuC(c)*	*opuC(d)*	*opuD*
Fold change ($\log_2$)	0.508	0.0155	-0.309	-0.406	-0.597
Adjusted *p*-value (Benjamini)	0.0339	0.936	0.0397	0.0321	0.000302

Table 2.7 Linear regression results of the mid-exponential phase based on the growth curves in **Figure 2.32 A**. The slope, y-intercept and R^2 are listed. A percentage of the slope (0 mg/mL) was calculated. Time interval: the time period from the linear regression was performed. Std. error: standard error. [#] $p<0.001$ (Student's *t*-test, unpaired, two-tailed, equal variance; y-intercept not tested).

Maltodextrin Concentration	0 mg/mL	10 mg/mL	25 mg/mL	50 mg/mL	75 mg/mL	100 mg/mL
			S7			
Slope (std. error)	0.2033 (0.002895)	0.2041 (0.006346)	0.1413[#] (0.002553)	0.1787[#] (0.002339)	0.1385[#] (0.001526)	0.1104[#] (0.001413)
Y-intercept (std. error)	-0.9758 (0.02030)	-0.9625 (0.05083)	-0.7056 (0.02045)	-0.8920 (0.01873)	-0.7733 (0.0122)	-0.6305 (0.01132)
R^2	0.9874	0.9426	0.9799	0.9893	0.9924	0.9898
Slope % of 0 mg/mL	-	100.4%	69.50%	87.90%	68.13%	54.30%
Time interval	6 h – 8 h			7 h – 9 h		
			S7-D2			
Slope (std. error)	0.1771 (0.002881)	0.1792 (0.002597)	0.09903[#] (0.005194)	0.08320[#] (0.005435)	0.07687[#] (0.001440)	0.06493[#] (0.002233)
Y-intercept (std. error)	-1.101 (0.02595)	-1.412 (0.02858)	-0.7750 (0.06753)	-0.6686 (0.07066)	-0.6600 (0.01872)	-0.5821 (0.02904)
R^2	0.9836	0.9869	0.8523	0.7881	0.9784	0.9306
Slope % of 0 mg/mL	-	101.2%	55.92%	46.98%	43.40%	36.66%
Time interval	8 h – 10 h	10 h – 12 h		12 h – 14 h		

Table 2.8 The $\log_2$fold changes and adjusted *p*-values of some genes in the arginine deiminase pathway and the urea cycle not included in **Figure 2.33A**.

	argF	*argJ*	*argG*	*argH*
Fold change ($\log_2$)	-1.94	-0.280	0.582	0.171
Adjusted *p*-value (Benjamini)	1.66E-11	0.110	0.00787	0.240

Table 2.9 List of primers used in the construction of the N315 *vraS* KO.

Primer	Sequence
vraSup_left	GGTACCGCATAGAAAGGCGGCGAAAC
vraSup_right	CCACAAACAATACTTTAATCGTCATCGATAAATCACCTCTACGTCTCC
vraSdown_left	TCGGAGACGTAGAGGTGATTTATCGATGACGATTAAAGTATTGTTTGTGG
vraSdown_right	GAGCTCGGAATGCATAGATGACAGCT

Table 2.10 Concentrations of the antimicrobials and inhibitors used in the time-kill assay.

	Concentration (μg/mL)	
	S7	S7-D2
Vancomycin	0.5 (half-MIC)	2 (half-MIC)
Daptomycin	0.25 (half-MIC)	0.5 (half-MIC)
Dalbavancin	0.0078 (half-MIC)	0.5 (half-MIC)
Oritavancin	0.0156 (half-MIC)	0.0625 (half-MIC)
AFN-1252	0.0312 (double-MIC)	0.0156 (double-MIC)
F1374-0037	0.5 (double-MIC)	0.5 (double-MIC)

Chapter 3 Varied Contribution of Phospholipid Shedding From Membrane to Daptomycin Tolerance in *Staphylococcus aureus*

Portions of this chapter have been adapted and reproduced with permission from:

Shen T, Hines KM, Ashford NK, Werth BJ, Xu L. 2021. Varied Contribution of Phospholipid Shedding From Membrane to Daptomycin Tolerance in *Staphylococcus aureus*. Front Mol Biosci 8:679949.

3.1 Introduction

Daptomycin is a lipopeptide antimicrobial that consists of a cyclic polypeptide with 13 amino acids and a decanoyl fatty acyl tail that plays an important role in the management of invasive infections caused by methicillin-resistant *Staphylococcus aureus* (MRSA). Its mechanism of action involves direct interaction with the negatively charged membrane lipids, phosphatidylglycerols (PGs), leading to loss of membrane potential and cell death (180, 200–202). As such, most studies on daptomycin resistance point to development of mutations in genes that control membrane lipid metabolism and/or lead to changes in surface charge, membrane fluidity, or both, such as *mprF*, *cls*, *pgsA*, and the *dlt* operon, which reduces binding of daptomycin to the cell membrane or prevents disruption of the membrane by daptomycin (103–106, 108, 203–207). Mutations in two-component regulatory systems that regulate cell wall and cell membrane metabolism, such as *vraSR* and *walKR* (94, 97, 185), have also been shown to contribute to daptomycin resistance. We previously applied a novel multi-dimensional lipidomic method to characterizing the detailed lipid profile changes associated with MRSA strains that have developed resistance to daptomycin and found overall greatly decreased levels of PGs in a resistant strain with mutations in both *pgsA* and *mprF* (104) and greatly elevated levels of lysyl-phosphatidylglycerols (lysylPGs) and cardiolipins (CLs) in a strain with only an *mprF* mutation

(24). Thus, altering lipid metabolism is an important route for bacteria to acquire resistance to daptomycin.

In recent years, inactivation of daptomycin by phospholipids released by *S. aureus* upon daptomycin exposure was proposed as a novel mechanism of daptomycin tolerance (110). The authors found that this effect may be antagonized by the production of amphipathic peptides called phenol soluble modulins (PSMs), which bind released phospholipids and thus prevent inactivation of daptomycin (110, 208). PSM production is regulated by the accessory gene regulator (Agr) system, which is encoded by a four-gene operon (*agrBDCA*) and a regulatory RNA gene (RNAIII) (209). Pader *et al.* suggested that the loss of the Agr quorum-sensing system enhances *S. aureus* survival during daptomycin exposure since PSMs are not released, and thus there is no competition for daptomycin sequestration by the shed lipids. However, the detailed composition of membrane lipids and shed lipids by *S. aureus* strains with variable Agr activity in response to daptomycin exposure has not been elucidated and the effect of lipid shedding on daptomycin activity has not been examined under clinically relevant kinetic drug exposures. In this work, we assessed the impact of Agr function on daptomycin activity and lipid metabolism in several genetic backgrounds and in static time-kills and *in vitro* pharmacokinetic/pharmacodynamic (PK/PD) models to better understand the contribution of lipid shedding to daptomycin tolerance.

3.2 Results

3.2.1. Not All Agr-Deficiency Slowed Down the Killing of *Staphylococcus aureus* by Daptomycin

We compared the survival of *agr* wild-type and *agr*-defective *S. aureus* under daptomycin exposure using three series of isogenic strain pairs (**Table 3.1**): SH1000, SH1001

(full *agr* KO), and SH1000- (H174L mutation in AgrA); USA300 LAC and USA300 LAC Δ*agrA*; and JE2 transposon mutants in *agrA*, *agrB*, and *agrC* (110, 125, 210, 211). Some of these strains have been well characterized previously (110, 210, 211), and we also confirmed the Agr function of SH1001 and the transposon mutants of *agrA*, *agrB*, or *agrC* by examining their hemolytic activity (**Figure 3.1**). The daptomycin minimum inhibitory concentration (MIC) was 0.25–0.5 µg/ml for all strains (**Table 3.1**). Daptomycin time-kill curves for each strain series are illustrated in **Figure 3.2A–D**. The wild-type SH1000 survived similarly or better than the *agr* KO strain SH1001, under both high and low aeration for 24 h. SH1000 and SH1001 in **Figure 3.2A** were grown under lower aeration than in **Figure 3.2C**. The higher aeration allowed both strains to re-grow to a higher and similar CFU/mL at 24 h, although the aeration conditions did not impact the general trend of daptomycin killing of wild-type vs. *agr* KO strains. However, **Figure 3.2C** also showed that the *agr* mutant SH1000- survived better than SH1000 and SH1001 for 8 h, with 1.7- and 1.4-$\log_{10}$ CFU/ml improved survival, respectively, at the 8 h timepoint. In USA300 LAC background the *agr*-KO strain survived better than the wild-type for 8 h, with 1.5-$\log_{10}$ CFU/ ml improved survival at the 8 h timepoint (**Figure 3.2D**). However, JE2 strains demonstrated similar growth among the wild-type and the *agr* mutant for 24 h (**Figure 3.2B**). Overall, SH1000- and USA300 LAC Δ*agrA* displayed a similar trend as observed previously (110), but the *agr*-KO SH1001 and transposon *agr*-mutant strains did not display improved survival relative to their matching wild-type strains when exposed to 20 µg/ml daptomycin.

3.2.2. Lipid Profiles Released by *Staphylococcus aureus* Upon Daptomycin Exposure Did Not Correlate With Agr Genotypes and Killing Profiles by Daptomycin

SH1000, SH1001 and SH1000- were grown for 6 h in static time-kills in the presence and absence of 20 µg/ml of daptomycin, and comprehensive lipidomics were carried out on the cell

pellets and the broth to profile the membrane lipids and shed lipids. Average dry pellet weights +/− standard deviations of all strains are shown in **Table 3.2**. The relative abundance of all lipid species including free fatty acids (FAs), diglucosyl-diacylglycerol (DGDGs), PGs, lysylPGs, and CLs were measured and normalized to all compounds. A heatmap depicting the relative abundance of each lipid is shown in **Figure 3.3** (see **Figure 3.4** for the bar graphs of the relative abundance). All three strains released lipids, regardless of daptomycin exposure, but the levels of shed lipids were higher in the presence of daptomycin. Specifically, the levels of shed PGs were higher with daptomycin exposure than without for all three strains. The Agr-defective strains, SH1001 and SH1000-, shed more PGs than the wild-type SH1000 strain under daptomycin exposure (see **Table 3.3** for the complete list of *p* values using Student's *t*-test). The levels of shed lysylPGs followed a similar trend, except the undetected minor species lysylPG 36:0. CLs were also shed more with daptomycin exposure than without. However, the wild-type SH1000 strain released the largest amount of CLs than SH1001 and SH1000-. FAs and DGDGs were shed only slightly more with daptomycin exposure than without for all three strains, suggesting that PGs, lysylPGs, and CLs are the major lipid classes released in response to daptomycin.

Comparing the levels of shed lipids with the levels of membrane lipids in cell pellets, we found that low levels of shed lipids correlated with high level of membrane lipids, and *vice versa*, regardless of daptomycin exposure, especially for FAs, DGDGs, PGs, and lysylPGs. The same trend was observed for shed and membrane CLs when the three strains were grown under daptomycin exposure. However, when the three strains were grown without daptomycin, the levels of both shed and membrane CLs were relatively low, suggesting CLs might be synthesized and shed specifically in response to daptomycin exposure.

Overall, daptomycin exposure induced more lipids released into the broth, with PGs, lysylPGs, and CLs being the major classes, but the *agr* mutants SH1001 and SH1000- showed similar profile of released lipids, suggesting that the released lipids do not account for their differential killing profiles (**Figure 3.2C**).

3.2.3. Killing Profile in a Pharmacokinetic/ Pharmacodynamic Model of Daptomycin Exposure Did Not Correlate With Agr Genotypes

The changes in bacterial densities over time during clinically meaningful kinetic exposures to daptomycin in the PK/PD model are illustrated in **Figure 3.5A**. To our surprise, the wild-type SH1000 appear to survive better than the *agr* mutant SH1000- up to 24 h although the difference was not statistically significant (Student's *t*-test, two-tailed, equal variance). Furthermore, both grew similarly after the second dose of daptomycin administered at 24 h. These data suggest that lack of Agr function does not provide meaningful advantage to the bacteria under conditions that replicate clinically relevant daptomycin exposures.

The released lipids in the effluent were evaluated at 4–5 h, when the greatest differences in survival were observed, and at 28–29 h, when the wild-type and the *agr* mutant grew back to similar CFU/ml. DGDGs, PGs, lysylPGs and CLs were identified from the lipidomics analysis, as shown in **Figure 3.5B–E** (see **Table 3.4** for the complete list of *p* values using Student's *t*-test), among which PGs were the most abundant. Both strains released more lipids at 4–5 h than at 28–29 h, and SH1000 released more than SH1000- at 4–5 h, which seems to correlate with the better survival of the SH1000 strain.

3.3 Discussion

Inactivation of daptomycin by shed lipids of *S. aureus* is an intriguing potential mechanism for daptomycin tolerance. However, after examining the time-kill profiles of *agr*

mutant and wild-type strains in three different genetic backgrounds, not all *agr* mutant strains displayed improved survival relative to their isogenic control strains (**Figure 3.2**), suggesting that the protection afforded by defective Agr and thus lack of secreted PSMs is not universal. Lipidomic profiling of SH1001 (loss of Agr function due to an *agrA* mutation) (210) and SH1000- (full *agr*-KO) (211) showed that both strains released similar lipid profiles to the media (**Figure 3.3**) even though their time-kill profiles dramatically differed with only SH1000- displaying better survival than SH1000 (**Figure 3.2C**). Furthermore, although SH1001 released more PGs and lysylPGs, but less CLs, than the wild-type SH1000, SH1000 survived better or similarly relative to SH1001 depending on the aeration conditions (**Figure 3.2**). These observations suggest that the amount of released lipids does not correlate with the survival of *S. aureus* in the presence of daptomycin.

Comprehensive lipid profiling suggests that phospholipids, including PGs, lysylPGs, and CLs, are preferentially released by *S. aureus* relative to DGDGs and FFAs in response to daptomycin exposure. Furthermore, the lipids released to the media appear to account for relative reductions in the residual membrane lipids in the cell pellets, except CLs. The preferential release of some lipid classes suggests an active releasing process. In particular, daptomycin exposure also upregulates both the synthesis and the release of CLs. This is intriguing as gain-of-function mutation in *cls2*, which encodes cardiolipin synthase, has been associated with daptomycin resistance (207).

In the comprehensive lipidomics analysis of the static time-kills, the average dry pellet weight of the *agr* mutants SH1000- and SH1001 was overall higher than their isogenic wild-type SH1000 with daptomycin exposure (**Table 3.2**), which is seemingly contradictory to the survival profile (**Figure 3.2C**). However, many factors might contribute to the pellet weight, such as the

degree of protein synthesis and aggregation of bacterial cells. Additionally, the lipid profile was normalized to all compounds, and hence the differences in pellet weight is unlikely to confound our results.

S. aureus and many other bacteria are known to release membrane lipids as extracellular vesicles into their surrounding environment. These released vesicles are composed of lipids, varieties of proteins, polysaccharides, and nucleic acids, and thus may contribute to a variety of biological functions including delivery of intracellular contents for quorum sensing or delivery of virulence factors to host cells (212, 213). PSMs were found to promote the biogenesis of extracellular vesicles by disrupting cytoplasmic membrane (213). *S. aureus* with *psmα*-KO was found to produce significantly less and smaller extracellular vesicles than wild-type. Other factors, such as peptidoglycan cross-linking and autolysis enzymes, also affect the formation of extracellular vesicles. Therefore, it is possible that alternative factors other than PSMs in the extracellular vesicles released by *S. aureus* could contribute to the survival of the bacteria under daptomycin pressure. Elucidation of such factors could shed light on the discrepancy that some *agr* mutant strains resulted in improved survival against daptomycin while others did not.

3.4 Experimental Procedure

3.4.1. Susceptibility Testing and Agr Functionality Testing

The susceptibility to daptomycin was evaluated by broth microdilution in accordance with CLSI guidelines. The Agr functionality was tested on BBL™ Trypticase™ soy agar with 5% sheep blood (TSA II; Becton, Dickinson and Company, Franklin Lakes, NJ, United States) as previously described (214). Briefly, a 0.5- McFarland suspension of RN4220 was streaked in a line down the center of the agar plate dividing the plate into two halves, and the test strains were

streaked from the edge of the agar plate to the center line of RN4220. Hemolysis was examined after overnight incubation at 37°C.

3.4.2. Static Time-Kill Assay

Overnight cultures of each strain were inoculated into tryptic soy broth (TSB, Remel Lenexa, KS, United States) supplemented with 50 μg/ml of elemental calcium and 20 μg/ml of daptomycin (Merck, Kenilworth, NJ, United States) to ~10^8 CFU/ml in 50 ml conical tubes, incubated at 37°C with shaking. Samples were taken at 0, 2, 4, 6, 8, and 24 h, serially diluted and spiral plated on tryptic soy agar (TSA; Becton, Dickinson and Company, Franklin Lakes, NJ, United States) plates to evaluate the bacterial growth over time with exposure to daptomycin. Experiments were performed under lower aeration (30 ml of culture in 50 ml tube shaken at 85 rpm; SH1000 and SH1001, JE2 and JE2 *Δagr*) and higher aeration (9 ml of culture in 50 ml tube shaken at 180 rpm; SH1000, SH1001, and SH1000-, USA300 LAC and USA300 LAC *ΔagrA*) conditions, the latter of which were more consistent with the methods by (110). All experiments were performed in duplicate.

3.4.3. Lipid Profiling of Static Time-kill of SH1000, SH1001, and SH1000-

Overnight cultures of SH1000, SH1001, and SH1000- were inoculated into TSB containing 50 μg/ml of elemental calcium to ~10^8 CFU/ml in 50 ml conical tubes, with or without exposure to daptomycin (20 μg/ml) and incubated at 37°C and 180 rpm with a total media culture of 9 ml. Each strain was grown in triplicate for 6 h and pelleted by centrifugation, with 5 ml of the supernatant saved for lipid profiling of the broth. The pellets and the broth were dried in a SpeedVac vacuum concentrator (Thermo Fisher Savant, Waltham, MA, United States), the pellets weighed, and both stored at −80°C until analysis. Lipid extraction, hydrophilic interaction liquid chromatography-ion mobility-mass spectrometry (HILIC-IM-MS), and data

analysis were performed as previously described (24, 104), using a Waters Synapt G2- Si ion mobility-QTOF mass spectrometer (Waters Corp., Milford, MA, United States) equipped with an electrospray ionization (ESI) source.

3.4.4. *In Vitro* Pharmacokinetic/ Pharmacodynamic Model and Lipid Profiling

A one-compartment glass model was used to test the impact of a simulated daptomycin exposure on the survival and lipid shedding profile of SH1000 and SH1000-, as previously described (185, 215). The model apparatus was prefilled with cation adjusted Mueller-Hinton-II broth (MHB; Becton, Dickinson and Company, Franklin Lakes, NJ, United States) supplemented with 50 µg/ml of elemental calcium, and fresh medium was continuously added and removed from the compartment along with the drug *via* a reciprocating syringe pump network (New Era Pump Systems Inc.), set to simulate the average plasma half-life of daptomycin (8 h). The starting inoculum was ~8 $\log_{10}$ CFU/ml. Daptomycin was administered at 0 and 24 h as a bolus injection to achieve the average peak free-drug concentration (C_{max}) associated with a 10 mg/kg/day dose (11.3 mg/L) (216). All models were performed in duplicate and run continuously for 48 h. All effluent (21.6 ml/h per replicate) was collected from 4 to 5 h and 28–29 h and centrifuged to remove cells. The supernatant was divided into four technical replicates, and subjected to lipid profiling as described above.

Figures

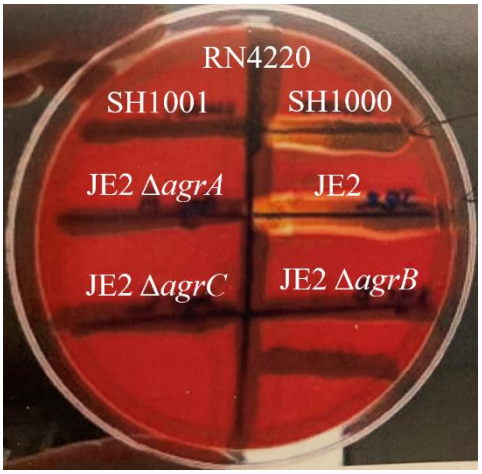

Figure 3.1 Hemolytic activity of SH1001 and the transposon mutants of *agrA*, *agrB* and *agrC*.

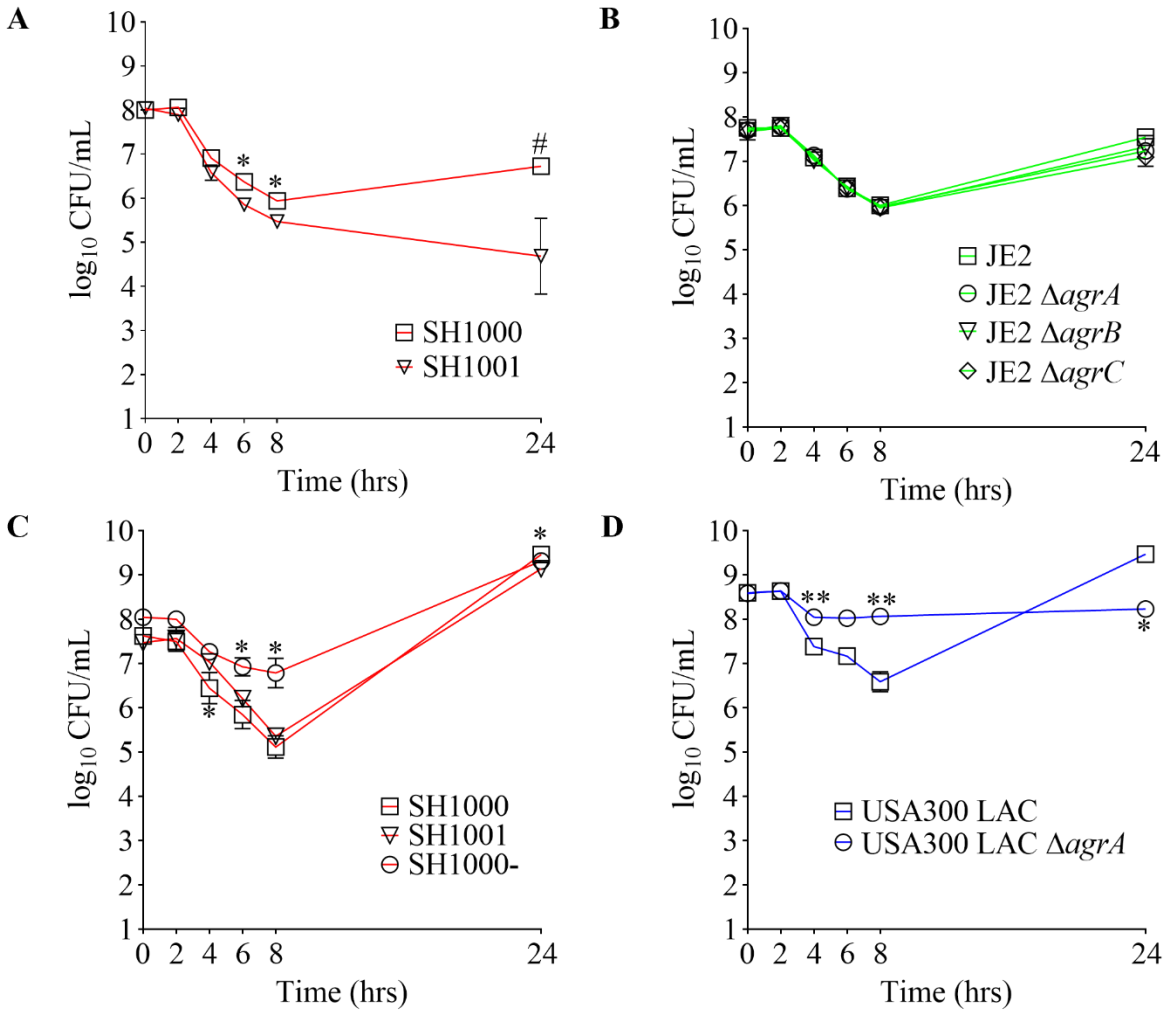

Figure 3.2 The daptomycin time kill profile of **A**) SH1000 and SH1001 pair under lower aeration; **B**) JE2 transposon series under lower aeration; **C**) SH1000, SH1001 and SH1000- series under higher aeration; and **D**) USA300 LAC pair under higher aeration. $^{\#}p<0.001$; $^{**}0.001<p<0.01$; $^{*}0.01<p<0.05$ (based on the percent survival at each timepoint, relative to the wild-type, Student's *t*-test, two-tailed, equal variance).

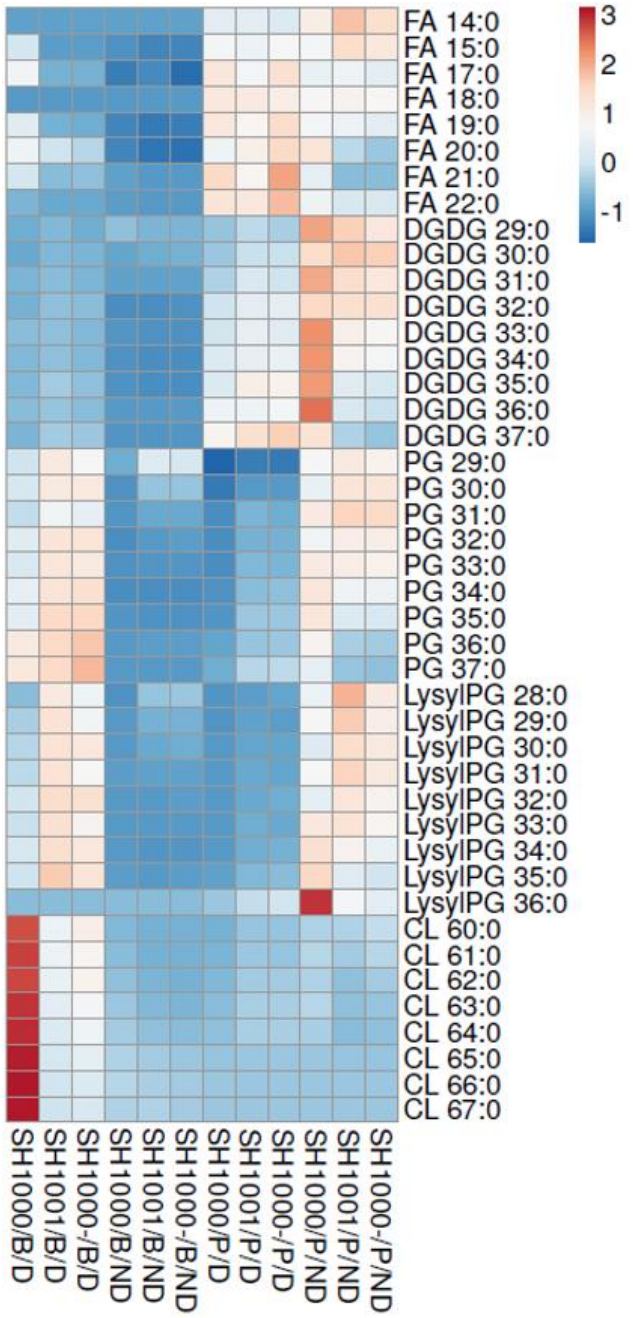

Figure 3.3 Heatmap of the lipid profile in the broth (B) and the bacterial pellet (P) of the time-kill of SH1000, SH1001 and SH1000-, with (D) or without (ND) daptomycin exposure (row-centered; unit variance scaling applied to rows). Individual lipid species are represented as the number of carbons: the degree of unsaturation in the fatty acid chains. FA: free fatty acid; DGDG: diglucosyl-diacylglycerol; PG: phosphatidylglycerol; LysylPG: lysyl-phosphatidylglycerol; CL: cardiolipin. *N*=3 per group. See **Table 3.3** for *p* values from Student's *t*-test analysis.

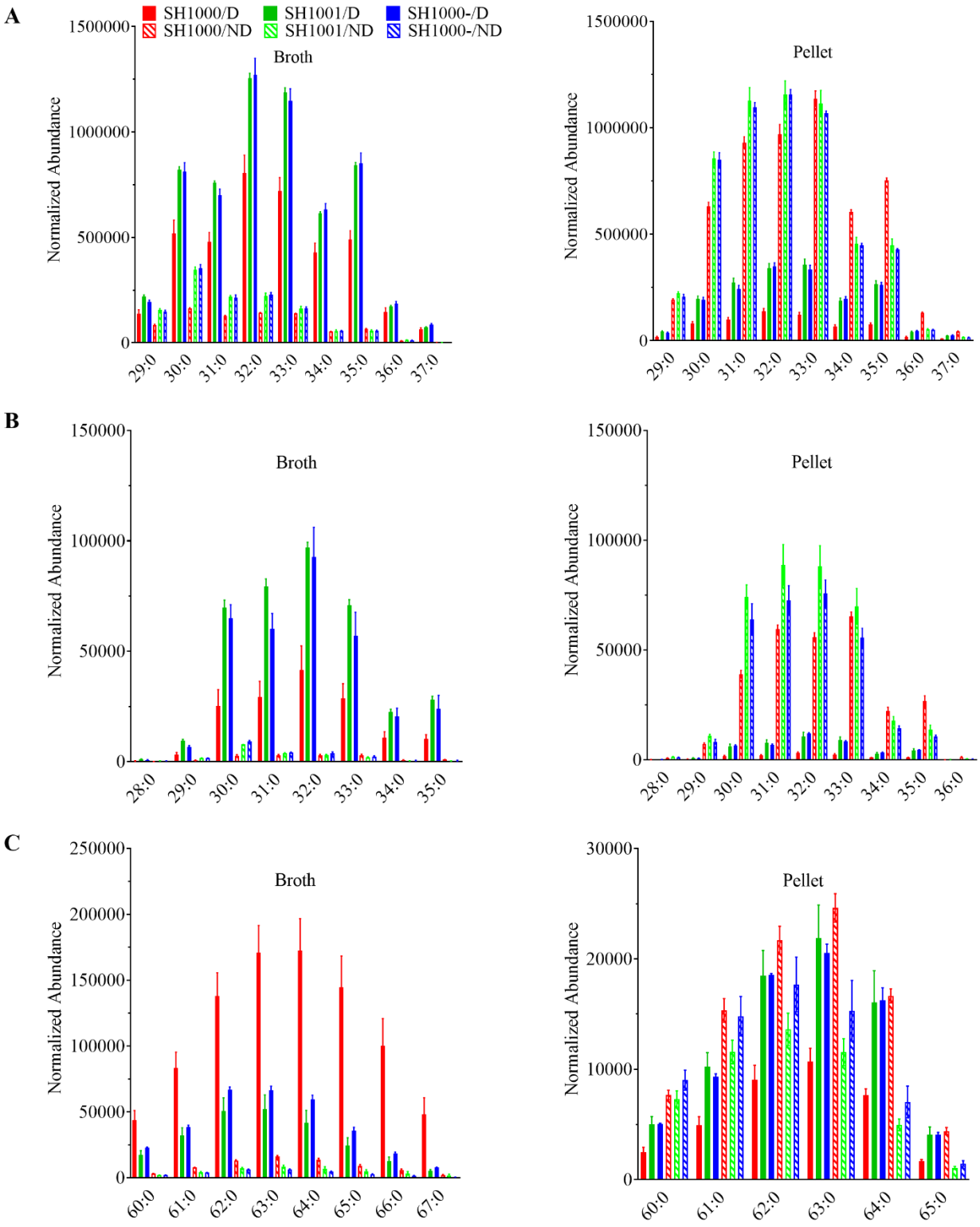

Figure 3.4 The phophatidylglycerols (**A**), lysyl-phosphatidylglycerols (**B**) and cardiolipins (**C**) profiles in the broth (left) and the bacterial pellet (right) of the time-kill of SH1000, SH1001 and SH1000-, with (D) or without (ND) daptomycin exposure. Individual lipid species are represented as the number of carbons: the degree of unsaturation in the fatty acid chains.

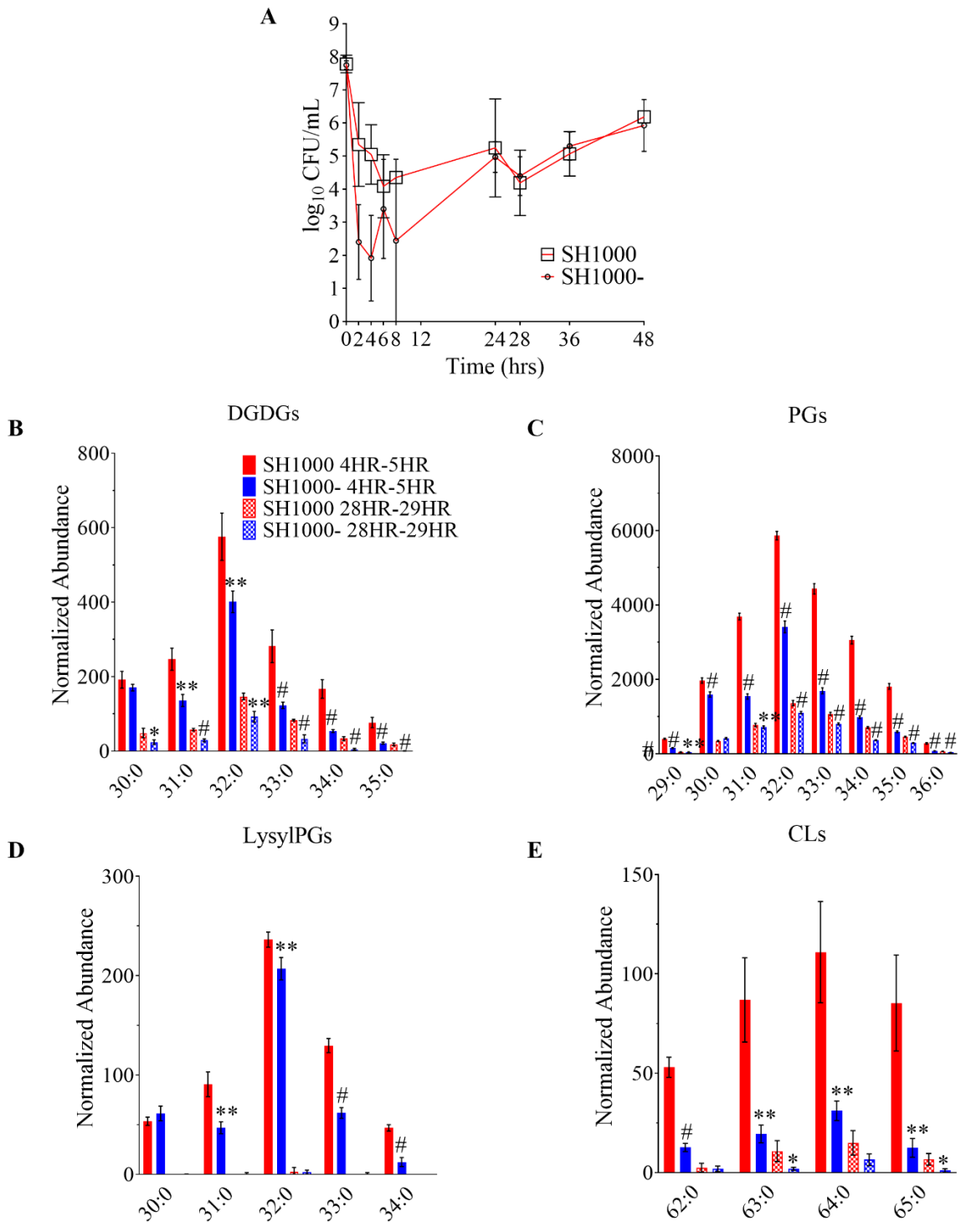

Figure 3.5 The survival profile (**A**) and lipid profile during 4HR-5HR and 28HR-29HR (**B-E**) of SH1000 and SH1000- in the pharmacokinetics/pharmacodynamics (PK/PD) model of daptomycin exposure. Individual lipid species are represented as the number of carbons: the degree of unsaturation in the fatty acid chains. DGDGs: diglucosyl-diacylglycerols; PGs: phosphatidylglycerols; LysylPGs: lysyl-phosphatidylglycerols; CLs: cardiolipins. $^{\#}p<0.001$; $^{**}0.001<p<0.01$; $^{*}0.01<p<0.05$ (Student's *t*-test, two-tailed, equal variance).

Tables

Table 3.1 The three series of isogenic *S. aureus* strain pairs of *agr* wild-type and *agr*-defective used in this study and their daptomycin minimum inhibitory concentration (MIC).

Parent	**MIC (µg/mL)**	**Mutant**	**MIC (µg/mL)**	**Mutation**	**Source**
SH1000	0.25	SH1001	0.25	Full *agr* KO	Dr. Alexander Horswill
		SH1000-	0.5	H174L mutation in AgrA	Dr. Andrew Edwards
USA300 LAC	0.5	USA300 LAC Δ*agrA*	0.5	Full *agrA* KO	
JE2	0.25	JE2 *agrA*::Tn	0.25	Transposon mutants	Nebraska transposon mutant library
		JE2 *agrB*::Tn	0.25		
		JE2 *agrC*::Tn	0.5		

Table 3.2 Average dry pellet weights +/- standard deviations of all strains for the comprehensive lipidomics analysis of the static time-kills of SH1000, SH1001 and SH1000-. *N*=3.

Experimental Group	Average Dry Pellet Weights (mg) ± Standard Deviations (mg)
SH1000, NO DAP	15.1 ± 0.5
SH1001, NO DAP	14.8 ± 0.3
SH1000-, NO DAP	14.6 ± 0.3
SH1000, DAP	3.1 ± 0.4
SH1001, DAP	7.2 ± 0.4
SH1000-, DAP	6.1 ± 0.1

Table 3.3 Student's *t*-test analysis of the lipids of SH1001 or SH1000- compared to SH1000 in the broth (B) or the bacterial pellet (P) of the time-kill of SH1000, SH1001 and SH1000-, with (D) or without (ND) daptomycin exposure (two-tailed, equal variance). $p<0.001$ is highlighted in red, $0.001<p<0.01$ in blue, and $0.01<p<0.05$ in green. "-" dictates that no corresponding lipid was detected in all three strains under the condition. FA: free fatty acid; DGDG: diglucosyl-diacylglycerol; PG: phosphatidylglycerol; LysylPG: lysyl-phosphatidylglycerol; CL: cardiolipin.

	p Values							
Lipids	SH1001/B/D	SH1000-/B/D	SH1001/B/ND	SH1000-/B/ND	SH1001/P/D	SH1000-/P/D	SH1001/P/ND	SH1000-/P/ND
FA 14:0	-	-	-	-	0.927	0.158	0.0166	0.0172
FA 15:0	0.000588	0.00163	0.0539	0.0174	0.325	0.761	0.0181	0.00483
FA 17:0	0.00453	0.00700	0.444	0.283	0.0725	0.647	0.733	0.373
FA 18:0	-	-	-	-	0.863	0.446	0.473	0.882
FA 19:0	0.0171	0.0174	0.105	0.252	0.216	0.319	0.435	0.0515
FA 20:0	0.0337	0.0638	0.000102	0.000430	0.0592	0.0344	0.00150	0.000411
FA 21:0	0.0438	0.0968	0.0137	0.0162	0.0749	0.277	0.00359	0.00390
FA 22:0	0.0153	0.159	0.0365	0.0204	0.649	0.0849	0.0180	0.0323
DGDG 29:0	0.0463	0.327	0.141	0.150	0.0126	0.104	0.000543	0.00707
DGDG 30:0	0.0186	0.00831	0.184	0.0227	0.00560	0.0108	0.00712	0.403
DGDG 31:0	0.0556	0.996	0.409	0.392	0.00285	0.0292	0.00127	0.00444
DGDG 32:0	0.0366	0.0286	0.873	0.150	0.0237	0.0210	0.106	0.280
DGDG 33:0	0.171	0.417	0.00169	0.00217	0.00727	0.0320	0.000145	0.000229
DGDG 34:0	0.0601	0.169	0.000495	0.000388	0.0606	0.0557	1.65E-05	0.000152
DGDG 35:0	0.00825	0.0259	0.000434	0.000401	0.00118	0.00196	1.82E-06	5.16E-06
DGDG 36:0	0.0707	0.512	0.000734	0.000202	0.929	0.542	0.000127	0.000103
DGDG 37:0	0.00522	0.00874	-	-	0.00453	0.000925	0.000537	0.000356
PG 29:0	0.00501	0.0214	9.33E-05	0.000349	0.000992	0.00160	0.00339	0.157
PG 30:0	0.00266	0.00504	5.17E-05	0.000117	0.000453	0.000311	0.000921	0.00112
PG 31:0	0.00104	0.00425	5.18E-05	0.000577	0.000338	0.000324	0.0136	0.00245
PG 32:0	0.00198	0.00448	0.00118	0.000484	0.000347	0.000156	0.0301	0.00636
PG 33:0	0.000552	0.00215	0.0408	0.00685	0.000287	0.000167	0.671	0.0599
PG 34:0	0.00436	0.00554	0.567	0.151	0.000327	0.000182	0.00275	0.000115
PG 35:0	0.000303	0.00140	0.0371	0.00302	0.000117	6.22E-05	0.000171	2.00E-06
PG 36:0	0.148	0.0599	0.0146	0.00793	0.000744	0.000361	1.92E-05	1.90E-05
PG 37:0	0.0999	0.0273	0.0484	0.00847	0.000217	0.000162	4.57E-05	2.06E-05
LysylPG 28:0	0.00268	0.00853	0.000851	0.000369	0.122	0.0427	0.00264	0.177
LysylPG 29:0	0.00162	0.00989	0.000953	0.000768	0.00194	0.000322	0.00417	0.291
LysylPG 30:0	0.00148	0.00438	0.000182	0.000155	0.00461	7.71E-05	0.000984	0.00875
LysylPG 31:0	0.000873	0.0115	0.0578	0.0327	0.00380	0.000129	0.0120	0.0541
LysylPG 32:0	0.00218	0.0140	0.500	0.125	0.00585	8.67E-06	0.00910	0.0122
LysylPG 33:0	0.000985	0.0324	0.0682	0.230	0.00396	0.000111	0.480	0.0458
LysylPG 34:0	0.00511	0.0438	0.0242	0.0810	0.00465	0.000117	0.0790	0.00636
LysylPG 35:0	0.000628	0.0423	0.00973	0.0518	0.00370	5.22E-05	0.00387	0.000716
LysylPG 36:0	-	-	-	-	0.00580	8.21E-05	0.00411	0.00218
CL 60:0	0.00960	0.0164	0.000385	0.000128	0.0123	0.00117	0.582	0.129
CL 61:0	0.00501	0.00567	0.000315	5.41E-05	0.00666	0.00158	0.0247	0.744
CL 62:0	0.00363	0.00478	0.000998	0.000136	0.00709	0.000519	0.00415	0.112
CL 63:0	0.00196	0.00208	0.00183	0.000117	0.00789	0.000625	0.000474	0.0121
CL 64:0	0.00202	0.00277	0.00632	0.000405	0.0150	0.000651	0.0000374	0.000973
CL 65:0	0.00218	0.00286	0.0182	0.000484	0.00762	0.000166	0.000150	0.000482
CL 66:0	0.00407	0.00506	0.0613	0.000562	-	-	-	-
CL 67:0	0.00833	0.0103	0.679	0.00302	-	-	-	-

Table 3.4 Student's *t*-test analysis of the lipids of SH1001 compared to SH1000- in the broth (B) or the bacterial pellet (P) of the time-kill of SH1000, SH1001 and SH1000-, with (D) or without (ND) daptomycin exposure (two-tailed, equal variance). $0.001<p<0.01$ is highlighted in blue, and $0.01<p<0.05$ in green. "-" dictates that no corresponding lipid was detected in all three strains under the condition. FA: free fatty acid; DGDG: diglucosyl-diacylglycerol; PG: phosphatidylglycerol; LysylPG: lysyl-phosphatidylglycerol; CL: cardiolipin.

	p Values			
Lipids	B/D	B/ND	P/D	P/ND
FA 14:0	-	-	0.168	0.138
FA 15:0	0.887	0.894	0.130	0.175
FA 17:0	0.780	0.0207	0.0651	0.158
FA 18:0	-	-	0.584	0.243
FA 19:0	0.810	0.290	0.0973	0.329
FA 20:0	0.561	0.0614	0.131	0.203
FA 21:0	0.838	0.441	0.0277	0.931
FA 22:0	0.7976	0.923	0.0411	0.588
DGDG 29:0	0.0599	0.776	0.0510	0.0575
DGDG 30:0	0.232	0.0202	0.729	0.705
DGDG 31:0	0.0280	0.958	0.0234	0.116
DGDG 32:0	0.311	0.0592	0.560	0.849
DGDG 33:0	0.0291	0.122	0.109	0.140
DGDG 34:0	0.116	0.377	0.695	0.143
DGDG 35:0	0.0347	0.207	0.488	0.0434
DGDG 36:0	0.0692	0.374	0.366	0.0108
DGDG 37:0	0.158	-	0.0283	0.0241
PG 29:0	0.0307	0.223	0.141	0.122
PG 30:0	0.815	0.635	0.750	0.890
PG 31:0	0.0481	0.784	0.156	0.529
PG 32:0	0.779	0.686	0.708	0.984
PG 33:0	0.392	0.906	0.380	0.357
PG 34:0	0.454	0.918	0.518	0.731
PG 35:0	0.867	0.670	0.784	0.410
PG 36:0	0.152	0.519	0.220	0.340
PG 37:0	0.0591	0.646	0.139	0.484
LysylPG 28:0	0.0574	0.420	0.0709	0.0673
LysylPG 29:0	0.0107	0.700	0.327	0.0486
LysylPG 30:0	0.376	0.00698	0.605	0.184
LysylPG 31:0	0.0237	0.260	0.373	0.115
LysylPG 32:0	0.682	0.162	0.336	0.196
LysylPG 33:0	0.143	0.329	0.629	0.0941
LysylPG 34:0	0.502	0.606	0.278	0.0892
LysylPG 35:0	0.406	0.410	0.852	0.0861
LysylPG 36:0	-	-	0.0388	0.0362
CL 60:0	0.0638	0.281	0.978	0.107
CL 61:0	0.193	0.117	0.353	0.0918
CL 62:0	0.0873	0.233	0.970	0.116
CL 63:0	0.144	0.0773	0.569	0.151
CL 64:0	0.0637	0.105	0.931	0.127
CL 65:0	0.0675	0.121	0.972	0.124
CL 66:0	0.0643	0.134	-	-
CL 67:0	0.0290	0.128	-	-

Chapter 4 Conclusions and Future Directions

Portions of this chapter have been adapted and reproduced with permission from:

Shen T, Hines KM, Ashford NK, Werth BJ, Xu L. 2021. Varied Contribution of Phospholipid Shedding From Membrane to Daptomycin Tolerance in *Staphylococcus aureus*. Front Mol Biosci 8:679949.

In this dissertation, we explored two different regulatory systems in *Staphylococcus aureus*, VraTSR and AgrBDCA, and examined how they related to resistance to cell-envelope-targeting antimicrobials and lipid metabolism. More specifically, we approached the VraTSR system in Chapter 2 with a multi-omics study, combined with various phenotypic characterization experiments. In Chapter 3, we looked at *S. aureus* strains with different Agr mutations and correlated lipid shedding with their daptomycin tolerance in time-kill experiments as well as in *vitro* pharmacokinetic/pharmacodynamic (PK/PD) modeling.

In Chapter 2, we started with *S. aureus* strains with loss-of-function mutations in *vraTSR* and demonstrated that those strains were, in general, more susceptible to vancomycin, daptomycin and dalbavancin compared to their parent strains. Yet, contrary to our expectations, increased levels were observed in only limited lipid species in the *vraTSR* loss-of-function mutants by lipidomics. We then focused on the S7 and S7-D2 *S. aureus* strain pair for the remainder of this Chapter. This strain pair presumably harbors a gain-of-function mutation in *vraT*, which was confirmed by the transcriptomics analysis. In the transcriptomics study, we also found significantly altered genes in the mutant strain, which were associated with cell wall metabolism, fatty acid synthesis, amino acid synthesis, and stress response. The cell wall synthesis genes, *pbp*, *sgt*, and *mur* genes, were overall increased in S7-D2. On the other hand, the

alterations in fatty acid synthesis gene expression pointed to a decrease in lipid abundance in S7-D2, consistent with the lipidomics results and previous observations that an overall decrease in lipid abundance correlated with decreased susceptibility to cell-envelope-targeting antimicrobials.

Multiple experiments to characterize the phenotypes of S7 and S7-D2 were also detailed in Chapter 2. For example, S7-D2 has a growth defect, typical of strains exhibiting vancomycin resistance. This was indicated by the metabolomics data, where the levels of metabolites in the purine and pyrimidine pathways decreased. Furthermore, S7-D2 showed decreased membrane fluidity, probably due to decreased levels of branched-chain lipids and cardiolipins (CLs). The former was implicated by the decreased levels of amino acids valine and isoleucine in the metabolomics, and the latter was demonstrated in the lipidomics. Finally, the transcriptomics data indicated decreased capability of adhesion and virulence by S7-D2, the former of which was confirmed by less biofilm formation.

Several aspects of the omics results warrant further investigation. For instance, we can use targeted MS/MS to investigate the branched-chain lipid levels, which was hypothesized to decrease in S7-D2 based on fluidity and branched-chain amino acids. We can also use transmission electron microscopy to study the cell wall thickness, given the increased expression of cell wall synthesis genes. In addition, the upregulation of the betaine biosynthesis pathway suggested increased osmotic pressure tolerance in S7-D2, but growth with exposure to the osmotic agent maltodextrin showed otherwise, which justified the need to test other agents, *e.g.* salt. Another potential field for further investigation is the arginine deiminase pathway (ADI), of which the genes were upregulated in the mutant strain to a large extent; yet there has not been much direct evidence relating ADI to the VraTSR system and antimicrobial resistance. Lastly,

crosstalk between the cell wall and the cell membrane was implicated from the omics data in two aspects: acetyl-CoA and lipoteichoic acid (LTA). We can track the fate of acetyl-CoA with isotopic labeling to uncover if it is devoted more to the fatty acid synthesis than the peptidoglycan synthesis and perform Western blot and matrix-assisted laser desorption/ionization mass spectrometry (MALDI-MS) to reveal the correlation if increased resistance correlated with increased LTA levels.

Furthermore, in Chapter 2, we demonstrated promising results by modulating resistance to cell-envelope-targeting antimicrobials with small molecule inhibitors. The synergy between AFN-1252 and daptomycin and oritavancin was independent of the *vraTSR* system and could be explained by the shift of CL chain length, increase in CL levels, and possible increase in trans-2-enoyl-ACP intermediates. The intermediate increase needs to be verified from the lipidomics studies as a future step. Future time-kill experiments also need to be conducted for cerulenin, as synergy is similarly expected for this inhibitor as for AFN-1252 due to the observed shift to shorter lipid chain length by cerulenin. On the other hand, one histidine kinase inhibitor, F1374-0037, showed synergy with vancomycin for S7 but not S7-D2. More experiments with *vraS* loss-of-function mutants and other antimicrobials need to be performed to narrow down possible mechanisms of killing and to see if the mechanisms directly involved the *vraTSR* system.

Finally, in Chapter 3, we found that while daptomycin exposure indeed resulted in increased shedding of membrane lipids to the media, the amount and types of released lipids did not correlate with the survival of the bacteria against daptomycin or the genotype of the bacteria. In the cases where there is improved survival, such effects appear to be dependent on experimental conditions, such as aeration, and ultimately are transient effects. Furthermore, the role of the Agr system in counteracting this effect appears to be dependent on the nature of the

Agr dysfunction and genetic backgrounds as demonstrated by the variable effects of our isogenic strains with different types of *agr* mutants. Lastly, many factors could affect the formation of extracellular vesicles released by *S. aureus*, *e.g.* phenol soluble modulins, peptidoglycan cross-linking and autolysis enzymes. Future investigations on those factors might help shed light on why some Agr-defective strains showed improved daptomycin survival while others did not.

REFERENCES

1. Jevons M. 1961. “Celbenin”-resistant staphylococci. BMJ 1:124–25.
2. Kuroda M, Ohta T, Uchiyama I, Baba T, Yuzawa H, Kobayashi I, Cui L, Oguchi A, Aoki K, Nagai Y, Lian J, Ito T, Kanamori M, Matsumaru H, Maruyama A, Murakami H, Hosoyama A, Mizutani-Ui Y, Takahashi NK, Sawano T, Inoue R, Kaito C, Sekimizu K, Hirakawa H, Kuhara S, Goto S, Yabuzaki J, Kanehisa M, Yamashita A, Oshima K, Furuya K, Yoshino C, Shiba T, Hattori M, Ogasawara N, Hayashi H, Hiramatsu K. 2001. Whole genome sequencing of meticillin-resistant Staphylococcus aureus. The Lancet 357:1225–1240.
3. Tran TT, Gomez Villegas S, Aitken SL, Butler-Wu SM, Soriano A, Werth BJ, Munita JM. 2022. New Perspectives on Antimicrobial Agents: Long-Acting Lipoglycopeptides. Antimicrob Agents Chemother 66:e02614-20.
4. Butler MS, Hansford KA, Blaskovich MAT, Halai R, Cooper MA. 2014. Glycopeptide antibiotics: Back to the future. J Antibiot (Tokyo) 67:631–644.
5. Miller WR, Bayer AS, Arias CA. 2016. Mechanism of Action and Resistance to Daptomycin in Staphylococcus aureus and Enterococci. Cold Spring Harb Perspect Med 6:a026997.
6. Hassoun A, Linden PK, Friedman B. 2017. Incidence, prevalence, and management of MRSA bacteremia across patient populations-a review of recent developments in MRSA management and treatment. Crit Care Lond Engl 21:211.
7. Centers for Disease Control and Prevention (U.S.). 2019. Antibiotic resistance threats in the United States, 2019. U.S. Department of Health and Human Services, Centers for Disease Control and Prevention, Atlanta, GA.
8. Higashi Y, Strominger JL, Sweeley CC. 1970. Biosynthesis of the Peptidoglycan of Bacterial Cell Walls. J Biol Chem 245:3697–3702.
9. Strominger JL, Tipper DJ. 1965. Bacterial cell wall synthesis and structure in relation to the mechanism of action of penicillins and other antibacterial agents. Am J Med 39:708–721.
10. 2024. CLSI M100-ED34: 2024 Performance Standards for Antimicrobial Susceptibility Testing, 34th Edition. CLSI.
11. Howden BP, Davies JK, Johnson PDR, Stinear TP, Grayson ML. 2010. Reduced vancomycin susceptibility in Staphylococcus aureus, including vancomycin-intermediate and heterogeneous vancomycin-intermediate strains: Resistance mechanisms, laboratory detection, and clinical implications. Clin Microbiol Rev 23:99–139.
12. Wootton M, Howe RA, Hillman R, Walsh TR, Bennett PM, MacGowan AP. A modified population analysis profile (PAP) method to detect hetero-resistance to vancomycin in Staphylococcus aureus in a UK hospital.
13. Smith TL, Pearson ML, Wilcox KR, Cruz C, Lancaster MV, Robinson-Dunn B, Tenover FC, Zervos MJ, Band JD, White E, Jarvis WR. 1999. Emergence of Vancomycin Resistance in *Staphylococcus aureus*. N Engl J Med 340:493–501.
14. Ploy M, Grelaud C, Martin C, De Lumley L, Denis F. 1998. First clinical isolate of vancomycin-intermediate Staphylococcus aureus in a French hospital. The Lancet 351:1212.
15. Wong SSY, Ho PL, Woo PCY, Yuen KY. 1999. Bacteremia Caused by Staphylococci with Inducible Vancomycin Heteroresistance. Clin Infect Dis 29:760–767.

16. Ariza J, Pujol M, Cabo J, Peña C, Fernández N, Liñares J, Ayats J, Gudiol F. 1999. Vancomycin in surgical infections due to meticillin-resistant Staphylococcus aureus with heterogeneous resistance to vancomycin. The Lancet 353:1587–1588.
17. Hiramatsu K, Aritaka N, Hanaki H, Kawasaki S, Hosoda Y, Hori S, Fukuchi Y, Kobayashi I. 1997. Dissemination in Japanese hospitals of strains of Staphylococcus aureus heterogeneously resistant to vancomycin. The Lancet 350:1670–1673.
18. Ledger EVK, Sabnis A, Edwards AM. 2022. Polymyxin and lipopeptide antibiotics: membrane-targeting drugs of last resort: This article is part of the Bacterial Cell Envelopes collection. Microbiology 168.
19. Zhivich A. 2017. Fighting bacterial resistance: approaches, challenges, and opportunities in the search for new antibiotics.Part 1. Antibiotics used in clinical practice: mechanisms of action and the development of bacterial resistance. Microbiol Indep Res J MIR J 4.
20. Smith JR, Roberts KD, Rybak MJ. 2015. Dalbavancin: A Novel Lipoglycopeptide Antibiotic with Extended Activity Against Gram-Positive Infections. Infect Dis Ther 4:245–258.
21. Boucher HW, Wilcox M, Talbot GH, Puttagunta S, Das AF, Dunne MW. 2014. Once-Weekly Dalbavancin versus Daily Conventional Therapy for Skin Infection. N Engl J Med 370:2169–2179.
22. Werth BJ, Vidaillac C, Murray KP, Newton KL, Sakoulas G, Nonejuie P, Pogliano J, Rybak MJ. 2013. Novel Combinations of Vancomycin plus Ceftaroline or Oxacillin against Methicillin-Resistant Vancomycin-Intermediate Staphylococcus aureus (VISA) and Heterogeneous VISA. Antimicrob Agents Chemother 57:2376–2379.
23. Barber KE, Ireland CE, Bukavyn N, Rybak MJ. 2014. Observation of "Seesaw Effect" with Vancomycin, Teicoplanin, Daptomycin and Ceftaroline in 150 Unique MRSA Strains. Infect Dis Ther 3:35–43.
24. Hines KM, Shen T, Ashford NK, Waalkes A, Penewit K, Holmes EA, McLean K, Salipante SJ, Werth BJ, Xu L. 2020. Occurrence of cross-resistance and β-lactam seesaw effect in glycopeptide-, lipopeptide- and lipoglycopeptide-resistant MRSA correlates with membrane phosphatidylglycerol levels. J Antimicrob Chemother 75:1182–1186.
25. Werth BJ, Vidaillac C, Murray KP, Newton KL, Sakoulas G, Nonejuie P, Pogliano J, Rybak MJ. 2013. Novel combinations of vancomycin plus ceftaroline or oxacillin against methicillin-resistant vancomycin-intermediate Staphylococcus aureus (VISA) and Heterogeneous VISA. Antimicrob Agents Chemother 57:2376–2379.
26. Kuroda M, Kuwahara-Arai K, Hiramatsu K. 2000. Identification of the Up- and Down-Regulated Genes in Vancomycin-Resistant Staphylococcus aureus Strains Mu3 and Mu50 by cDNA Differential Hybridization Method. Biochem Biophys Res Commun 269:485–490.
27. Cui L, Neoh H, Shoji M, Hiramatsu K. 2009. Contribution of *vraSR* and *graSR* Point Mutations to Vancomycin Resistance in Vancomycin-Intermediate *Staphylococcus aureus*. Antimicrob Agents Chemother 53:1231–1234.
28. Gardete S, Kim C, Hartmann BM, Mwangi M, Roux CM, Dunman PM, Chambers HF, Tomasz A. 2012. Genetic pathway in acquisition and loss of vancomycin resistance in a methicillin resistant Staphylococcus aureus (MRSA) strain of clonal type USA300. PLoS Pathog 8:e1002505.
29. Fischer A, Yang S-J, Bayer AS, Vaezzadeh AR, Herzig S, Stenz L, Girard M, Sakoulas G, Scherl A, Yeaman MR, Proctor RA, Schrenzel J, François P. 2011. Daptomycin resistance

mechanisms in clinically derived Staphylococcus aureus strains assessed by a combined transcriptomics and proteomics approach. J Antimicrob Chemother 66:1696–1711.
30. Gardete S, Wu SW, Gill S, Tomasz A. 2006. Role of VraSR in Antibiotic Resistance and Antibiotic-Induced Stress Response in *Staphylococcus aureus*. Antimicrob Agents Chemother 50:3424–3434.
31. Peschel A, Jack RW, Otto M, Collins LV, Staubitz P, Nicholson G, Kalbacher H, Nieuwenhuizen WF, Jung G, Tarkowski A, Van Kessel KPM, Van Strijp JAG. 2001. *Staphylococcus aureus* Resistance to Human Defensins and Evasion of Neutrophil Killing via the Novel Virulence Factor Mprf Is Based on Modification of Membrane Lipids with L -Lysine. J Exp Med 193:1067–1076.
32. Kuhn S, Slavetinsky CJ, Peschel A. 2015. Synthesis and function of phospholipids in Staphylococcus aureus. Int J Med Microbiol 305:196–202.
33. DeMars Z, Singh VK, Bose JL. 2020. Exogenous Fatty Acids Remodel Staphylococcus aureus Lipid Composition through Fatty Acid Kinase. J Bacteriol 202.
34. Parsons JB, Rock CO. 2013. Bacterial lipids: Metabolism and membrane homeostasis. Prog Lipid Res 52:249–276.
35. Short SA, White DC. 1971. Metabolism of phosphatidylglycerol, lysylphosphatidylglycerol, and cardiolipin of Staphylococcus aureus. J Bacteriol 108:219–226.
36. Koch HU, Haas R, Fischer W. 1984. The role of lipoteichoic acid biosynthesis in membrane lipid metabolism of growing *Staphylococcus aureus*. Eur J Biochem 138:357–363.
37. Emdur L, Chiu T. 1975. T H E R O L E of P H O S P H a T I D Y L G L Y C E R O L in T H E in Vitro Biosynthesis of 55:3–6.
38. Percy MG, Gründling A. 2014. Lipoteichoic Acid Synthesis and Function in Gram-Positive Bacteria. Annu Rev Microbiol 68:81–100.
39. van Heijenoort J. 2007. Lipid Intermediates in the Biosynthesis of Bacterial Peptidoglycan. Microbiol Mol Biol Rev 71:620–635.
40. Matsuhashi M, Dietrich CP, Strominger JL. 1967. Biosynthesis of the Peptidoglycan of Bacterial Cell Walls. J Biol Chem 242:3191–3206.
41. Ishii E, Eguchi Y. 2021. Diversity in Sensing and Signaling of Bacterial Sensor Histidine Kinases. Biomolecules 11:1524.
42. Stock AM, Robinson VL, Goudreau PN. 2000. Two-Component Signal Transduction. Annu Rev Biochem 69:183–215.
43. Galperin MY, Makarova KS, Wolf YI, Koonin EV. 2018. Phyletic Distribution and Lineage-Specific Domain Architectures of Archaeal Two-Component Signal Transduction Systems. J Bacteriol 200.
44. Rapun-Araiz B, Haag AF, De Cesare V, Gil C, Dorado-Morales P, Penades JR, Lasa I. 2020. Systematic Reconstruction of the Complete Two-Component Sensorial Network in Staphylococcus aureus. mSystems 5:e00511-20.
45. Gotoh Y, Eguchi Y, Watanabe T, Okamoto S, Doi A, Utsumi R. 2010. Two-component signal transduction as potential drug targets in pathogenic bacteria. Curr Opin Microbiol 13:232–239.
46. Bem AE, Velikova N, Pellicer MT, Baarlen PV, Marina A, Wells JM. 2015. Bacterial Histidine Kinases as Novel Antibacterial Drug Targets. ACS Chem Biol 10:213–224.

47. Stephenson K. 2002. Two-component and phosphorelay signal-transduction systems as therapeutic targets. Curr Opin Pharmacol 2:507–512.
48. Ortet P, Whitworth DE, Santaella C, Achouak W, Barakat M. 2015. P2CS: updates of the prokaryotic two-component systems database. Nucleic Acids Res 43:D536–D541.
49. Gumerov VM, Ulrich LE, Zhulin IB. 2024. MiST 4.0: a new release of the microbial signal transduction database, now with a metagenomic component. Nucleic Acids Res 52:D647–D653.
50. Ali L, Aziz MHA. 2024. Crosstalk involving two-component systems in Staphylococcus aureus signaling networks. J Bacteriol https://doi.org/10.1128/jb.00418-23.
51. Cock PJA, Whitworth DE. 2007. Evolution of Prokaryotic Two-Component System Signaling Pathways: Gene Fusions and Fissions. Mol Biol Evol 24:2355–2357.
52. Stewart RC. 2010. Protein histidine kinases: assembly of active sites and their regulation in signaling pathways. Curr Opin Microbiol 13:133–141.
53. Zschiedrich CP, Keidel V, Szurmant H. 2016. Molecular Mechanisms of Two-Component Signal Transduction. J Mol Biol 428:3752–3775.
54. Buschiazzo A, Trajtenberg F. 2019. Two-Component Sensing and Regulation: How Do Histidine Kinases Talk with Response Regulators at the Molecular Level? Annu Rev Microbiol 73:507–528.
55. Gao R, Stock AM. 2009. Biological Insights from Structures of Two-Component Proteins. Annu Rev Microbiol 63:133–154.
56. Jacob-Dubuisson F, Mechaly A, Betton J-M, Antoine R. 2018. Structural insights into the signalling mechanisms of two-component systems. Nat Rev Microbiol 16:585–593.
57. Haag AF, Bagnoli F. 2015. The Role of Two-Component Signal Transduction Systems in Staphylococcus aureus Virulence Regulation, p. 145–198. *In* Bagnoli, F, Rappuoli, R, Grandi, G (eds.), Staphylococcus aureus. Springer International Publishing, Cham.
58. Ramos JL, Martínez-Bueno M, Molina-Henares AJ, Terán W, Watanabe K, Zhang X, Gallegos MT, Brennan R, Tobes R. 2005. The TetR Family of Transcriptional Repressors. Microbiol Mol Biol Rev 69:326–356.
59. Sidote DJ, Barbieri CM, Wu T, Stock AM. 2008. Structure of the Staphylococcus aureus AgrA LytTR Domain Bound to DNA Reveals a Beta Fold with an Unusual Mode of Binding. Structure 16:727–735.
60. Villanueva M, García B, Valle J, Rapún B, Ruiz De Los Mozos I, Solano C, Martí M, Penadés JR, Toledo-Arana A, Lasa I. 2018. Sensory deprivation in Staphylococcus aureus. Nat Commun 9:523.
61. Martin PK, Li T, Sun D, Biek DP, Schmid MB. 1999. Role in Cell Permeability of an Essential Two-Component System in *Staphylococcus aureus*. J Bacteriol 181:3666–3673.
62. Meehl M, Herbert S, Götz F, Cheung A. 2007. Interaction of the GraRS Two-Component System with the VraFG ABC Transporter To Support Vancomycin-Intermediate Resistance in *Staphylococcus aureus*. Antimicrob Agents Chemother 51:2679–2689.
63. Hiron A, Falord M, Valle J, Débarbouillé M, Msadek T. 2011. Bacitracin and nisin resistance in *Staphylococcus aureus* : a novel pathway involving the BraS/BraR two-component system (SA2417/SA2418) and both the BraD/BraE and VraD/VraE ABC transporters. Mol Microbiol 81:602–622.
64. Prieto JM, Rapún-Araiz B, Gil C, Penadés JR, Lasa I, Latasa C. 2020. Inhibiting the two-component system GraXRS with verteporfin to combat Staphylococcus aureus infections. Sci Rep 10:17939.

65. Novick RP, Jiang D. 2003. The staphylococcal saeRS system coordinates environmental signals with agr quorum sensing. Microbiology 149:2709–2717.
66. Giraudo AT, Calzolari A, Cataldi AA, Bogni C, Nagel R. 1999. The *sae* locus of *Staphylococcus aureus* encodes a two-component regulatory system. FEMS Microbiol Lett 177:15–22.
67. Pragman AA, Yarwood JM, Tripp TJ, Schlievert PM. 2004. Characterization of Virulence Factor Regulation by SrrAB, a Two-Component System in *Staphylococcus aureus*. J Bacteriol 186:2430–2438.
68. Fedtke I, Kamps A, Krismer B, Götz F. 2002. The Nitrate Reductase and Nitrite Reductase Operons and the *narT* Gene of *Staphylococcus carnosus* Are Positively Controlled by the Novel Two-Component System NreBC. J Bacteriol 184:6624–6634.
69. Kamps A, Achebach S, Fedtke I, Unden G, Götz F. 2004. Staphylococcal NreB: an O_2-sensing histidine protein kinase with an O_2-labile iron–sulphur cluster of the FNR type. Mol Microbiol 52:713–723.
70. Sun F, Ji Q, Jones MB, Deng X, Liang H, Frank B, Telser J, Peterson SN, Bae T, He C. 2012. AirSR, a [2Fe-2S] Cluster-Containing Two-Component System, Mediates Global Oxygen Sensing and Redox Signaling in Staphylococcus aureus. J Am Chem Soc 134:305–314.
71. Brunskill EW, Bayles KW. 1996. Identification and molecular characterization of a putative regulatory locus that affects autolysis in Staphylococcus aureus. J Bacteriol 178:611–618.
72. Fournier B, Hooper DC. 2000. A New Two-Component Regulatory System Involved in Adhesion, Autolysis, and Extracellular Proteolytic Activity of *Staphylococcus aureus*. J Bacteriol 182:3955–3964.
73. Stauff DL, Torres VJ, Skaar EP. 2007. Signaling and DNA-binding Activities of the Staphylococcus aureus HssR-HssS Two-component System Required for Heme Sensing. J Biol Chem 282:26111–26121.
74. Kelliher JL, Radin JN, Kehl-Fie TE. 2018. PhoPR Contributes to Staphylococcus aureus Growth during Phosphate Starvation and Pathogenesis in an Environment-Specific Manner. Infect Immun 86:e00371-18.
75. Moscoso JA, Schramke H, Zhang Y, Tosi T, Dehbi A, Jung K, Gründling A. 2016. Binding of Cyclic Di-AMP to the Staphylococcus aureus Sensor Kinase KdpD Occurs via the Universal Stress Protein Domain and Downregulates the Expression of the Kdp Potassium Transporter. J Bacteriol 198:98–110.
76. Fuda CCS, Fisher JF, Mobashery S. 2005. β-Lactam resistance in Staphylococcus aureus: the adaptive resistance of a plastic genome. Cell Mol Life Sci 62:2617–2633.
77. Fridman M, Williams GD, Muzamal U, Hunter H, Siu KWM, Golemi-Kotra D. 2013. Two Unique Phosphorylation-Driven Signaling Pathways Crosstalk in *Staphylococcus aureus* to Modulate the Cell-Wall Charge: Stk1/Stp1 Meets GraSR. Biochemistry 52:7975–7986.
78. Ohlsen K, Donat S. 2010. The impact of serine/threonine phosphorylation in Staphylococcus aureus. Int J Med Microbiol 300:137–141.
79. Canova MJ, Baronian G, Brelle S, Cohen-Gonsaud M, Bischoff M, Molle V. 2014. A novel mode of regulation of the Staphylococcus aureus Vancomycin-resistance-associated response regulator VraR mediated by Stk1 protein phosphorylation. Biochem Biophys Res Commun 447:165–171.

80. Donat S, Streker K, Schirmeister T, Rakette S, Stehle T, Liebeke M, Lalk M, Ohlsen K. 2009. Transcriptome and Functional Analysis of the Eukaryotic-Type Serine/Threonine Kinase PknB in *Staphylococcus aureus*. J Bacteriol 191:4056–4069.
81. Burnside K, Rajagopal L. 2011. Aspects of Eukaryotic-Like Signaling in Gram-Positive Cocci: A Focus on Virulence. Future Microbiol 6:747–761.
82. Burnside K, Lembo A, Harrell MI, Gurney M, Xue L, BinhTran N-T, Connelly JE, Jewell KA, Schmidt BZ, De Los Reyes M, Tao WA, Doran KS, Rajagopal L. 2011. Serine/Threonine Phosphatase Stp1 Mediates Post-transcriptional Regulation of Hemolysin, Autolysis, and Virulence of Group B Streptococcus. J Biol Chem 286:44197–44210.
83. Jarick M, Bertsche U, Stahl M, Schultz D, Methling K, Lalk M, Stigloher C, Steger M, Schlosser A, Ohlsen K. 2018. The serine/threonine kinase Stk and the phosphatase Stp regulate cell wall synthesis in Staphylococcus aureus. Sci Rep 8:13693.
84. Janczarek M, Vinardell J-M, Lipa P, Karaś M. 2018. Hanks-Type Serine/Threonine Protein Kinases and Phosphatases in Bacteria: Roles in Signaling and Adaptation to Various Environments. Int J Mol Sci 19:2872.
85. Huemer M, Mairpady Shambat S, Hertegonne S, Bergada-Pijuan J, Chang C-C, Pereira S, Gómez-Mejia A, Van Gestel L, Bär J, Vulin C, Pfammatter S, Stinear TP, Monk IR, Dworkin J, Zinkernagel AS. 2023. Serine-threonine phosphoregulation by PknB and Stp contributes to quiescence and antibiotic tolerance in *Staphylococcus aureus*. Sci Signal 16:eabj8194.
86. Cameron DR, Ward DV, Kostoulias X, Howden BP, Moellering RC, Eliopoulos GM, Peleg AY. 2012. Serine/Threonine Phosphatase Stp1 Contributes to Reduced Susceptibility to Vancomycin and Virulence in Staphylococcus aureus. J Infect Dis 205:1677–1687.
87. Boyle-Vavra S, Yin S, Jo DS, Montgomery CP, Daum RS. 2013. VraT/YvqF is required for methicillin resistance and activation of the VraSR regulon in Staphylococcus aureus. Antimicrob Agents Chemother 57:83–95.
88. Belcheva A, Golemi-Kotra D. 2008. A close-up view of the VraSR two-component system: A mediator of Staphylococcus aureus response to cell wall damage. J Biol Chem 283:12354–12364.
89. Sengupta M, Jain V, Wilkinson BJ, Jayaswal RK. 2012. Chromatin immunoprecipitation identifies genes under direct VraSR regulation in *Staphylococcus aureus*. Can J Microbiol 58:703–708.
90. Fernandes PB, Reed P, Monteiro JM, Pinho MG. 2022. Revisiting the Role of VraTSR in Staphylococcus aureus Response to Cell Wall-Targeting Antibiotics. J Bacteriol 204.
91. Kato Y, Suzuki T, Ida T, Maebashi K. 2010. Genetic changes associated with glycopeptide resistance in Staphylococcus aureus: predominance of amino acid substitutions in YvqF/VraSR. J Antimicrob Chemother 65:37–45.
92. Hafer C, Lin Y, Kornblum J, Lowy FD, Uhlemann A-C. 2012. Contribution of Selected Gene Mutations to Resistance in Clinical Isolates of Vancomycin-Intermediate Staphylococcus aureus. Antimicrob Agents Chemother 56:5845–5851.
93. Katayama Y, Murakami-Kuroda H, Cui L, Hiramatsu K. 2009. Selection of Heterogeneous Vancomycin-Intermediate *Staphylococcus aureus* by Imipenem. Antimicrob Agents Chemother 53:3190–3196.
94. Mehta S, Cuirolo AX, Plata KB, Riosa S, Silverman JA, Rubio A, Rosato RR, Rosato AE. 2012. VraSR Two-Component Regulatory System Contributes to *mprF* -Mediated

Decreased Susceptibility to Daptomycin in *In Vivo* -Selected Clinical Strains of Methicillin-Resistant Staphylococcus aureus. Antimicrob Agents Chemother 56:92–102.
95. Kuroda M, Kuroda H, Oshima T, Takeuchi F, Mori H, Hiramatsu K. 2003. Two-component system VraSR positively modulates the regulation of cell-wall biosynthesis pathway in Staphylococcus aureus. Mol Microbiol 49:807–821.
96. Jansen A, Türck M, Szekat C, Nagel M, Clever I, Bierbaum G. 2007. Role of insertion elements and yycFG in the development of decreased susceptibility to vancomycin in Staphylococcus aureus. Int J Med Microbiol 297:205–215.
97. Friedman L, Alder JD, Silverman JA. 2006. Genetic Changes That Correlate with Reduced Susceptibility to Daptomycin in *Staphylococcus aureus*. Antimicrob Agents Chemother 50:2137–2145.
98. Howden BP, McEvoy CRE, Allen DL, Chua K, Gao W, Harrison PF, Bell J, Coombs G, Bennett-Wood V, Porter JL, Robins-Browne R, Davies JK, Seemann T, Stinear TP. 2011. Evolution of Multidrug Resistance during Staphylococcus aureus Infection Involves Mutation of the Essential Two Component Regulator WalKR. PLoS Pathog 7:e1002359.
99. Dubrac S, Msadek T. 2004. Identification of Genes Controlled by the Essential YycG/YycF Two-Component System of *Staphylococcus aureus*. J Bacteriol 186:1175–1181.
100. Dubrac S, Boneca IG, Poupel O, Msadek T. 2007. New Insights into the WalK/WalR (YycG/YycF) Essential Signal Transduction Pathway Reveal a Major Role in Controlling Cell Wall Metabolism and Biofilm Formation in *Staphylococcus aureus*. J Bacteriol 189:8257–8269.
101. Mohedano ML, Overweg K, De La Fuente A, Reuter M, Altabe S, Mulholland F, De Mendoza D, López P, Wells JM. 2005. Evidence that the Essential Response Regulator YycF in *Streptococcus pneumoniae* Modulates Expression of Fatty Acid Biosynthesis Genes and Alters Membrane Composition. J Bacteriol 187:2357–2367.
102. Mohedano ML, Amblar M, De La Fuente A, Wells JM, López P. 2016. The Response Regulator YycF Inhibits Expression of the Fatty Acid Biosynthesis Repressor FabT in Streptococcus pneumoniae. Front Microbiol 7.
103. Bayer AS, Mishra NN, Chen L, Kreiswirth BN, Rubio A, Yang S-J. 2015. Frequency and Distribution of Single-Nucleotide Polymorphisms within *mprF* in Methicillin-Resistant Staphylococcus aureus Clinical Isolates and Their Role in Cross-Resistance to Daptomycin and Host Defense Antimicrobial Peptides. Antimicrob Agents Chemother 59:4930–4937.
104. Hines KM, Waalkes A, Penewit K, Holmes EA, Salipante SJ, Werth BJ, Xu L. 2017. Characterization of the Mechanisms of Daptomycin Resistance among Gram-Positive Bacterial Pathogens by Multidimensional Lipidomics. mSphere 2:1–16.
105. Peleg AY, Miyakis S, Ward DV, Earl AM, Rubio A, Cameron DR, Pillai S, Moellering RC, Eliopoulos GM. 2012. Whole Genome Characterization of the Mechanisms of Daptomycin Resistance in Clinical and Laboratory Derived Isolates of Staphylococcus aureus. PLoS ONE 7:e28316.
106. Mishra NN, Bayer AS. 2013. Correlation of Cell Membrane Lipid Profiles with Daptomycin Resistance in Methicillin-Resistant Staphylococcus aureus. Antimicrob Agents Chemother 57:1082–1085.
107. Bertsche U, Yang S-J, Kuehner D, Wanner S, Mishra NN, Roth T, Nega M, Schneider A, Mayer C, Grau T, Bayer AS, Weidenmaier C. 2013. Increased Cell Wall Teichoic Acid Production and D-alanylation Are Common Phenotypes among Daptomycin-Resistant

Methicillin-Resistant Staphylococcus aureus (MRSA) Clinical Isolates. PLoS ONE 8:e67398.
108. Mishra NN, Bayer AS, Weidenmaier C, Grau T, Wanner S, Stefani S, Cafiso V, Bertuccio T, Yeaman MR, Nast CC, Yang S-J. 2014. Phenotypic and Genotypic Characterization of Daptomycin-Resistant Methicillin-Resistant Staphylococcus aureus Strains: Relative Roles of mprF and dlt Operons. PLoS ONE 9:e107426.
109. Sabnis A, Ledger EVK, Pader V, Edwards AM. 2018. Antibiotic interceptors: Creating safe spaces for bacteria. PLoS Pathog 14:10–15.
110. Pader V, Hakim S, Painter KL, Wigneshweraraj S, Clarke TB, Edwards AM. 2016. Staphylococcus aureus inactivates daptomycin by releasing membrane phospholipids. Nat Microbiol 2:16194.
111. Thoendel M, Kavanaugh JS, Flack CE, Horswill AR. 2011. Peptide signaling in the Staphylococci. Chem Rev 111:117–151.
112. Tracers for Membrane Labeling—Section 14.4 | Thermo Fisher Scientific - US. https://www.thermofisher.com/us/en/home/references/molecular-probes-the-handbook/fluorescent-tracers-of-cell-morphology-and-fluid-flow/tracers-for-membrane-labeling.html. Retrieved 5 September 2021.
113. Bai J, Zhu X, Zhao K, Yan Y, Xu T, Wang J, Zheng J, Huang W, Shi L, Shang Y, Lv Z, Wang X, Wu Y, Qu D. 2019. The role of ArlRS in regulating oxacillin susceptibility in methicillin-resistant *Staphylococcus aureus* indicates it is a potential target for antimicrobial resistance breakers. Emerg Microbes Infect 8:503–515.
114. Cardona ST, Choy M, Hogan AM. 2018. Essential Two-Component Systems Regulating Cell Envelope Functions: Opportunities for Novel Antibiotic Therapies. J Membr Biol 251:75–89.
115. Rapun-Araiz B, Haag AF, Solano C, Lasa I. 2020. The impact of two-component sensorial network in staphylococcal speciation. Curr Opin Microbiol 55:40–47.
116. Villanueva M, Roch M, Lasa I, Renzoni A, Kelley WL. 2021. The Role of ArlRS and VraSR in Regulating Ceftaroline Hypersusceptibility in Methicillin-Resistant Staphylococcus aureus. Antibiotics 10:821.
117. Zhang R, Ashford NK, Li A, Ross DH, Werth BJ, Xu L. 2023. High-throughput analysis of lipidomic phenotypes of methicillin-resistant Staphylococcus aureus by coupling in situ 96-well cultivation and HILIC-ion mobility-mass spectrometry. Anal Bioanal Chem 415:6191–6199.
118. Zhang R, Barreras Beltran IA, Ashford NK, Penewit K, Waalkes A, Holmes EA, Hines KM, Salipante SJ, Xu L, Werth BJ. 2021. Synergy Between Beta-Lactams and Lipo-, Glyco-, and Lipoglycopeptides, Is Independent of the Seesaw Effect in Methicillin-Resistant Staphylococcus aureus. Front Mol Biosci 8:688357.
119. Zhang R, Polenakovik H, Barreras Beltran IA, Waalkes A, Salipante SJ, Xu L, Werth BJ. 2022. Emergence of Dalbavancin, Vancomycin, and Daptomycin Nonsusceptible *Staphylococcus aureus* in a Patient Treated With Dalbavancin: Case Report and Isolate Characterization. Clin Infect Dis 75:1641–1644.
120. Werth BJ, Jain R, Hahn A, Cummings L, Weaver T, Waalkes A, Sengupta D, Salipante SJ, Rakita RM, Butler-Wu SM. 2018. Emergence of dalbavancin non-susceptible, vancomycin-intermediate Staphylococcus aureus (VISA) after treatment of MRSA central line-associated bloodstream infection with a dalbavancin- and vancomycin-containing regimen. Clin Microbiol Infect 24:429.e1-429.e5.

121. Horrevoets AJG, Verheij HM, De Haas GH. 1991. Inactivation of *Escherichia coli* outer-membrane phospholipase A by the affinity label hexadecanesulfonyl fluoride: Evidence for an active-site serine. Eur J Biochem 198:247–253.
122. Richter SG, Elli D, Kim HK, Hendrickx APA, Sorg JA, Schneewind O, Missiakas D. 2013. Small molecule inhibitor of lipoteichoic acid synthesis is an antibiotic for Gram-positive bacteria. Proc Natl Acad Sci U S A 110:3531–3536.
123. Parsons JB, Rock CO. 2011. Is bacterial fatty acid synthesis a valid target for antibacterial drug discovery? Curr Opin Microbiol 14:544–549.
124. Lee H, Boyle-Vavra S, Ren J, Jarusiewicz JA, Sharma LK, Hoagland DT, Yin S, Zhu T, Hevener KE, Ojeda I, Lee RE, Daum RS, Johnson ME. 2019. Identification of Small Molecules Exhibiting Oxacillin Synergy through a Novel Assay for Inhibition of *vraTSR* Expression in Methicillin-Resistant Staphylococcus aureus. Antimicrob Agents Chemother 63:e02593-18.
125. Fey PD, Endres JL, Yajjala VK, Widhelm TJ, Boissy RJ, Bose JL, Bayles KW. 2013. A Genetic Resource for Rapid and Comprehensive Phenotype Screening of Nonessential Staphylococcus aureus Genes. mBio 4:e00537-12.
126. Norazah A. 2012. The Presence of Heterogeneous Vancomycin-Intermediate Staphylococcus aureus (heteroVISA) in a Major Malaysian Hospital 67.
127. Monk IR, Shah IM, Xu M, Tan M-W, Foster TJ. 2012. Transforming the Untransformable: Application of Direct Transformation To Manipulate Genetically Staphylococcus aureus and Staphylococcus epidermidis. mBio 3:e00277-11.
128. Cui L, Ma X, Sato K, Okuma K, Tenover FC, Mamizuka EM, Gemmell CG, Kim M-N, Ploy M-C, El Solh N, Ferraz V, Hiramatsu K. 2003. Cell Wall Thickening Is a Common Feature of Vancomycin Resistance in *Staphylococcus aureus*. J Clin Microbiol 41:5–14.
129. McGuinness WA, Malachowa N, DeLeo FR. 2017. Vancomycin Resistance in Staphylococcus aureus. Yale J Biol Med 90:269–281.
130. Jones T, Yeaman MR, Sakoulas G, Yang S-J, Proctor RA, Sahl H-G, Schrenzel J, Xiong YQ, Bayer AS. 2008. Failures in Clinical Treatment of *Staphylococcus aureus* Infection with Daptomycin Are Associated with Alterations in Surface Charge, Membrane Phospholipid Asymmetry, and Drug Binding. Antimicrob Agents Chemother 52:269–278.
131. Mishra NN, Yang S-J, Sawa A, Rubio A, Nast CC, Yeaman MR, Bayer AS. 2009. Analysis of Cell Membrane Characteristics of In Vitro-Selected Daptomycin-Resistant Strains of Methicillin-Resistant *Staphylococcus aureus*. Antimicrob Agents Chemother 53:2312–2318.
132. Mishra NN, McKinnell J, Yeaman MR, Rubio A, Nast CC, Chen L, Kreiswirth BN, Bayer AS. 2011. *In Vitro* Cross-Resistance to Daptomycin and Host Defense Cationic Antimicrobial Peptides in Clinical Methicillin-Resistant Staphylococcus aureus Isolates. Antimicrob Agents Chemother 55:4012–4018.
133. Do Canto AMTM, Robalo JR, Santos PD, Carvalho AJP, Ramalho JPP, Loura LMS. 2016. Diphenylhexatriene membrane probes DPH and TMA-DPH: A comparative molecular dynamics simulation study. Biochim Biophys Acta BBA - Biomembr 1858:2647–2661.
134. Mishra NN, Bayer AS, Baines SL, Hayes AS, Howden BP, Lapitan CK, Lew C, Rose WE. 2021. Cell Membrane Adaptations Mediate β-Lactam-Induced Resensitization of Daptomycin-Resistant (DAP-R) Staphylococcus aureus In Vitro. Microorganisms 9:1028.
135. Lentz BR. 1989. Membrane "fluidity" as detected by diphenylhexatriene probes. Chem Phys Lipids 50:171–190.

136. Unsay JD, Cosentino K, Subburaj Y, García-Sáez AJ. 2013. Cardiolipin effects on membrane structure and dynamics. Langmuir ACS J Surf Colloids 29:15878–15887.
137. Coenye T. 2021. Do results obtained with RNA-sequencing require independent verification? Biofilm 3:100043.
138. Everaert C, Luypaert M, Maag JLV, Cheng QX, Dinger ME, Hellemans J, Mestdagh P. 2017. Benchmarking of RNA-sequencing analysis workflows using whole-transcriptome RT-qPCR expression data. Sci Rep 7:1559.
139. Koch CM, Chiu SF, Akbarpour M, Bharat A, Ridge KM, Bartom ET, Winter DR. 2018. A Beginner's Guide to Analysis of RNA Sequencing Data. Am J Respir Cell Mol Biol 59:145–157.
140. Goedhart J, Luijsterburg MS. 2020. VolcaNoseR is a web app for creating, exploring, labeling and sharing volcano plots. Sci Rep 10:20560.
141. Mani N, Baddour LM, Offutt DQ, Vijaranakul U, Nadakavukaren MJ, Jayaswal RK. 1994. Autolysis-defective mutant of Staphylococcus aureus: pathological considerations, genetic mapping, and electron microscopic studies. Infect Immun 62:1406–1409.
142. Razew A, Laguri C, Vallet A, Bougault C, Kaus-Drobek M, Sabala I, Simorre J-P. 2023. Staphylococcus aureus sacculus mediates activities of M23 hydrolases. Nat Commun 14:6706.
143. Oogai Y, Yamaguchi M, Kawada-Matsuo M, Sumitomo T, Kawabata S, Komatsuzawa H. 2016. Lysine and Threonine Biosynthesis from Aspartate Contributes to Staphylococcus aureus Growth in Calf Serum. Appl Environ Microbiol 82:6150–6157.
144. Gélinas M, Museau L, Milot A, Beauregard PB. 2021. The *de novo* Purine Biosynthesis Pathway Is the Only Commonly Regulated Cellular Pathway during Biofilm Formation in TSB-Based Medium in Staphylococcus aureus and Enterococcus faecalis. Microbiol Spectr 9:e00804-21.
145. Sause WE, Balasubramanian D, Irnov I, Copin R, Sullivan MJ, Sommerfield A, Chan R, Dhabaria A, Askenazi M, Ueberheide B, Shopsin B, Van Bakel H, Torres VJ. 2019. The purine biosynthesis regulator PurR moonlights as a virulence regulator in *Staphylococcus aureus*. Proc Natl Acad Sci 116:13563–13572.
146. Goncheva MI, Flannagan RS, Sterling BE, Laakso HA, Friedrich NC, Kaiser JC, Watson DW, Wilson CH, Sheldon JR, McGavin MJ, Kiser PK, Heinrichs DE. 2019. Stress-induced inactivation of the Staphylococcus aureus purine biosynthesis repressor leads to hypervirulence. Nat Commun 10:775.
147. Li L, Abdelhady W, Donegan NP, Seidl K, Cheung A, Zhou Y-F, Yeaman MR, Bayer AS, Xiong YQ. 2018. Role of Purine Biosynthesis in Persistent Methicillin-Resistant Staphylococcus aureus Infection. J Infect Dis 218:1367–1377.
148. Karinou E, Schuster CF, Pazos M, Vollmer W, Gründling A. 2019. Inactivation of the Monofunctional Peptidoglycan Glycosyltransferase SgtB Allows *Staphylococcus aureus* To Survive in the Absence of Lipoteichoic Acid. J Bacteriol 201.
149. Reed P, Atilano ML, Alves R, Hoiczyk E, Sher X, Reichmann NT, Pereira PM, Roemer T, Filipe SR, Pereira-Leal JB, Ligoxygakis P, Pinho MG. 2015. Staphylococcus aureus Survives with a Minimal Peptidoglycan Synthesis Machine but Sacrifices Virulence and Antibiotic Resistance. PLOS Pathog 11:e1004891.
150. Hartman BJ, Tomasz A. 1984. Low-affinity penicillin-binding protein associated with beta-lactam resistance in Staphylococcus aureus. J Bacteriol 158:513–516.

151. Pinho MG, De Lencastre H, Tomasz A. 2001. An acquired and a native penicillin-binding protein cooperate in building the cell wall of drug-resistant staphylococci. Proc Natl Acad Sci 98:10886–10891.
152. Reed P, Veiga H, Jorge AM, Terrak M, Pinho MG. 2011. Monofunctional Transglycosylases Are Not Essential for Staphylococcus aureus Cell Wall Synthesis. J Bacteriol 193:2549–2556.
153. Wang QM, Peery RB, Johnson RB, Alborn WE, Yeh W-K, Skatrud PL. 2001. Identification and Characterization of a Monofunctional Glycosyltransferase from *Staphylococcus aureus*. J Bacteriol 183:4779–4785.
154. De Oliveira MVD, Furtado RM, Da Costa KS, Vakal S, Lima AH. 2022. Advances in UDP-N-Acetylglucosamine Enolpyruvyl Transferase (MurA) Covalent Inhibition. Front Mol Biosci 9:889825.
155. Laddomada F, Miyachiro M, Dessen A. 2016. Structural Insights into Protein-Protein Interactions Involved in Bacterial Cell Wall Biogenesis. Antibiotics 5:14.
156. Egan AJF, Errington J, Vollmer W. 2020. Regulation of peptidoglycan synthesis and remodelling. Nat Rev Microbiol 18:446–460.
157. Barbuti MD, Myrbråten IS, Morales Angeles D, Kjos M. 2023. The cell cycle of *Staphylococcus aureus* : An updated review. MicrobiologyOpen 12:e1338.
158. Sherman BT, Hao M, Qiu J, Jiao X, Baseler MW, Lane HC, Imamichi T, Chang W. 2022. DAVID: a web server for functional enrichment analysis and functional annotation of gene lists (2021 update). Nucleic Acids Res 50:W216–W221.
159. Stoodley P, Sauer K, Davies DG, Costerton JW. 2002. Biofilms as Complex Differentiated Communities. Annu Rev Microbiol 56:187–209.
160. Sauer K, Stoodley P, Goeres DM, Hall-Stoodley L, Burmølle M, Stewart PS, Bjarnsholt T. 2022. The biofilm life cycle: expanding the conceptual model of biofilm formation. Nat Rev Microbiol 20:608–620.
161. Wilson C, Lukowicz R, Merchant S, Valquier-Flynn H, Caballero J, Sandoval J, Okuom M, Huber C, Brooks TD, Wilson E, Clement B, Wentworth CD, Holmes AE. 2017. Quantitative and Qualitative Assessment Methods for Biofilm Growth: A Mini-review. Res Rev J Eng Technol 6:http://www.rroij.com/open-access/quantitative-and-qualitative-assessment-methods-for-biofilm-growth-a-minireview-.pdf.
162. Ewald JD, Zhou G, Lu Y, Kolic J, Ellis C, Johnson JD, Macdonald PE, Xia J. 2024. Web-based multi-omics integration using the Analyst software suite. Nat Protoc 19:1467–1497.
163. Kanehisa M, Furumichi M, Sato Y, Kawashima M, Ishiguro-Watanabe M. 2023. KEGG for taxonomy-based analysis of pathways and genomes. Nucleic Acids Res 51:D587–D592.
164. Kaiser JC, King AN, Grigg JC, Sheldon JR, Edgell DR, Murphy MEP, Brinsmade SR, Heinrichs DE. 2018. Repression of branched-chain amino acid synthesis in Staphylococcus aureus is mediated by isoleucine via CodY, and by a leucine-rich attenuator peptide. PLOS Genet 14:e1007159.
165. Sen S, Sirobhushanam S, Johnson SR, Song Y, Tefft R, Gatto C, Wilkinson BJ. 2016. Growth-Environment Dependent Modulation of Staphylococcus aureus Branched-Chain to Straight-Chain Fatty Acid Ratio and Incorporation of Unsaturated Fatty Acids. PLOS ONE 11:e0165300.
166. Casey D, Sleator RD. 2021. A genomic analysis of osmotolerance in Staphylococcus aureus. Gene 767:145268.

167. Schwan WR, Wetzel KJ. 2016. Osmolyte transport in Staphylococcus aureus and the role in pathogenesis. World J Clin Infect Dis 6:22–27.
168. Kaenjak A, Graham JE, Wilkinson BJ. 1993. Choline transport activity in Staphylococcus aureus induced by osmotic stress and low phosphate concentrations. J Bacteriol 175:2400–2406.
169. Graham JE, Wilkinson BJ. 1992. Staphylococcus aureus osmoregulation: roles for choline, glycine betaine, proline, and taurine. J Bacteriol 174:2711–2716.
170. Kiamco MM, Atci E, Khan QF, Mohamed A, Renslow RS, Abu-Lail N, Fransson BA, Call DR, Beyenal H. 2015. Vancomycin and maltodextrin affect structure and activity of Staphylococcus aureus biofilms; Vancomycin and maltodextrin affect structure and activity of Staphylococcus aureus biofilms. Biotechnol Bioeng 112:2562–2570.
171. van der Waal SV, van der Sluis LWM, Özok AR, Exterkate R a. M, van Marle J, Wesselink PR, de Soet JJ. 2011. The effects of hyperosmosis or high pH on a dual-species biofilm of Enterococcus faecalis and Pseudomonas aeruginosa: an in vitro study. Int Endod J 44:1110–1117.
172. Sultana ST, Call DR, Beyenal H. 2016. Maltodextrin enhances biofilm elimination by electrochemical scaffold. Sci Rep 6:36003.
173. Makhlin J, Kofman T, Borovok I, Kohler C, Engelmann S, Cohen G, Aharonowitz Y. 2007. *Staphylococcus aureus* ArcR Controls Expression of the Arginine Deiminase Operon. J Bacteriol 189:5976–5986.
174. Pruitt EL, Zhang R, Ross DH, Ashford NK, Chen X, Alonzo F, Bush MF, Werth BJ, Xu L. 2023. Elucidating the impact of bacterial lipases, human serum albumin, and FASII inhibition on the utilization of exogenous fatty acids by *Staphylococcus aureus*. mSphere 8:e00368-23.
175. Pee CJE, Pader V, Ledger EVK, Edwards AM. 2019. A FASII Inhibitor Prevents Staphylococcal Evasion of Daptomycin by Inhibiting Phospholipid Decoy Production. Antimicrob Agents Chemother 63:e02105-18.
176. Zhanel GG, Schweizer F, Karlowsky JA. 2012. Oritavancin: Mechanism of Action. Clin Infect Dis 54:S214–S219.
177. Frey AJ, Feldman DR, Trefely S, Worth AJ, Basu SS, Snyder NW. 2016. LC-quadrupole/Orbitrap high-resolution mass spectrometry enables stable isotope-resolved simultaneous quantification and 13C-isotopic labeling of acyl-coenzyme A thioesters. Anal Bioanal Chem 408:3651–3658.
178. Emdur L, Chiu T. 1975. The role of phosphatidylglycerol in the in vitro biosynthesis of teichoic acid and lipoteichoic acid. FEBS Lett 55:216–219.
179. Seo HS, Cartee RT, Pritchard DG, Nahm MH. 2008. A New Model of Pneumococcal Lipoteichoic Acid Structure Resolves Biochemical, Biosynthetic, and Serologic Inconsistencies of the Current Model. J Bacteriol 190:2379–2387.
180. Bayer AS, Schneider T, Sahl H. 2013. Mechanisms of daptomycin resistance in *Staphylococcus aureus* : role of the cell membrane and cell wall. Ann N Y Acad Sci 1277:139–158.
181. Parsons JB, Frank MW, Jackson P, Subramanian C, Rock CO. 2014. Incorporation of extracellular fatty acids by a fatty acid kinase-dependent pathway in *S taphylococcus aureus*. Mol Microbiol 92:234–245.

182. Shen T, Hines KM, Ashford NK, Werth BJ, Xu L. 2021. Varied Contribution of Phospholipid Shedding From Membrane to Daptomycin Tolerance in Staphylococcus aureus. Front Mol Biosci 8:679949.
183. Rosenthal S, Decano AG, Bandali A, Lai D, Malat GE, Bias TE. 2018. Oritavancin (Orbactiv): A New-Generation Lipoglycopeptide for the Treatment Of Acute Bacterial Skin and Skin Structure Infections. P T Peer-Rev J Formul Manag 43:143–179.
184. Chambers HF, Hartman BJ, Tomasz A. 1985. Increased amounts of a novel penicillin-binding protein in a strain of methicillin-resistant Staphylococcus aureus exposed to nafcillin. J Clin Invest 76:325–331.
185. Werth BJ, Ashford NK, Penewit K, Waalkes A, Holmes EA, Ross DH, Shen T, Hines KM, Salipante SJ, Xu L. 2021. Dalbavancin exposure in vitro selects for dalbavancin-non-susceptible and vancomycin-intermediate strains of methicillin-resistant Staphylococcus aureus. Clin Microbiol Infect 27:910.e1-910.e8.
186. Nair SR, Cherubin CE. 1978. Use of Cefoxitin, New Cephalosporin-Like Antibiotic, in the Treatment of Aerobic and Anaerobic Infections. Antimicrob Agents Chemother 14:866–875.
187. Yang S-J, Xiong YQ, Boyle-Vavra S, Daum R, Jones T, Bayer AS. 2010. Daptomycin-Oxacillin Combinations in Treatment of Experimental Endocarditis Caused by Daptomycin-Nonsusceptible Strains of Methicillin-Resistant *Staphylococcus aureus* with Evolving Oxacillin Susceptibility (the "Seesaw Effect"). Antimicrob Agents Chemother 54:3161–3169.
188. Renzoni A, Kelley WL, Rosato RR, Martinez MP, Roch M, Fatouraei M, Haeusser DP, Margolin W, Fenn S, Turner RD, Foster SJ, Rosato AE. 2017. Molecular Bases Determining Daptomycin Resistance-Mediated Resensitization to β-Lactams (Seesaw Effect) in Methicillin-Resistant Staphylococcus aureus. Antimicrob Agents Chemother 61:e01634-16.
189. Donaldson LW. 2008. The NMR Structure of the *Staphylococcus aureus* Response Regulator VraR DNA Binding Domain Reveals a Dynamic Relationship between It and Its Associated Receiver Domain. Biochemistry 47:3379–3388.
190. Leonard PG, Golemi-Kotra D, Stock AM. 2013. Phosphorylation-dependent conformational changes and domain rearrangements in *Staphylococcus aureus* VraR activation. Proc Natl Acad Sci 110:8525–8530.
191. Kumar JV, Tseng T, Lou Y, Wei S, Wu T, Tang H, Chiu Y, Hsu C, Chen C. 2022. Structural insights into DNA binding domain of vancomycin-resistance-associated response regulator in complex with its promoter DNA from *Staphylococcus aureus*. Protein Sci 31:e4286.
192. Kim D, Paggi JM, Park C, Bennett C, Salzberg SL. 2019. Graph-based genome alignment and genotyping with HISAT2 and HISAT-genotype. Nat Biotechnol 37:907–915.
193. Li H, Handsaker B, Wysoker A, Fennell T, Ruan J, Homer N, Marth G, Abecasis G, Durbin R, 1000 Genome Project Data Processing Subgroup. 2009. The Sequence Alignment/Map format and SAMtools. Bioinformatics 25:2078–2079.
194. Liao Y, Smyth GK, Shi W. 2014. featureCounts: an efficient general purpose program for assigning sequence reads to genomic features. Bioinformatics 30:923–930.
195. Love MI, Huber W, Anders S. 2014. Moderated estimation of fold change and dispersion for RNA-seq data with DESeq2. Genome Biol 15:550.

196. Garrett TA, Guan Z, Raetz CRH. 2007. Analysis of Ubiquinones, Dolichols, and Dolichol Diphosphate-Oligosaccharides by Liquid Chromatography-Electrospray Ionization-Mass Spectrometry, p. 117–143. *In* Methods in Enzymology. Elsevier.
197. Garrett TA, Kordestani R, Raetz CRH. 2007. Quantification of Cardiolipin by Liquid Chromatography-Electrospray Ionization Mass Spectrometry, p. 213–230. *In* Methods in Enzymology. Elsevier.
198. Bligh EG, Dyer WJ. 1959. A RAPID METHOD OF TOTAL LIPID EXTRACTION AND PURIFICATION. Can J Biochem Physiol 37:911–917.
199. Fuchs S, Mehlan H, Bernhardt J, Hennig A, Michalik S, Surmann K, Pané-Farré J, Giese A, Weiss S, Backert L, Herbig A, Nieselt K, Hecker M, Völker U, Mäder U. 2018. Aureo Wiki‑The repository of the Staphylococcus aureus research and annotation community. Int J Med Microbiol 308:558–568.
200. Muraih JK, Pearson A, Silverman J, Palmer M. 2011. Oligomerization of daptomycin on membranes. Biochim Biophys Acta BBA - Biomembr 1808:1154–1160.
201. Muraih JK, Harris J, Taylor SD, Palmer M. 2012. Characterization of daptomycin oligomerization with perylene excimer fluorescence: Stoichiometric binding of phosphatidylglycerol triggers oligomer formation. Biochim Biophys Acta BBA - Biomembr 1818:673–678.
202. Pogliano J, Pogliano N, Silverman JA. 2012. Daptomycin-Mediated Reorganization of Membrane Architecture Causes Mislocalization of Essential Cell Division Proteins. J Bacteriol 194:4494–4504.
203. Yang S-J, Kreiswirth BN, Sakoulas G, Yeaman MR, Xiong YQ, Sawa A, Bayer AS. 2009. Enhanced Expression of dltABCD Is Associated with the Development of Daptomycin Nonsusceptibility in a Clinical Endocarditis Isolate of Staphylococcus aureus. J Infect Dis 200:1916–1920.
204. Mishra NN, Yang S-J, Chen L, Muller C, Saleh-Mghir A, Kuhn S, Peschel A, Yeaman MR, Nast CC, Kreiswirth BN, Crémieux A-C, Bayer AS. 2013. Emergence of Daptomycin Resistance in Daptomycin-Naïve Rabbits with Methicillin-Resistant Staphylococcus aureus Prosthetic Joint Infection Is Associated with Resistance to Host Defense Cationic Peptides and mprF Polymorphisms. PLoS ONE 8:e71151.
205. Bayer AS, Mishra NN, Sakoulas G, Nonejuie P, Nast CC, Pogliano J, Chen K-T, Ellison SN, Yeaman MR, Yang S-J. 2014. Heterogeneity of *mprF* Sequences in Methicillin-Resistant Staphylococcus aureus Clinical Isolates: Role in Cross-Resistance between Daptomycin and Host Defense Antimicrobial Peptides. Antimicrob Agents Chemother 58:7462–7467.
206. Cafiso V, Bertuccio T, Purrello S, Campanile F, Mammina C, Sartor A, Raglio A, Stefani S. 2014. dltA overexpression: A strain-independent keystone of daptomycin resistance in methicillin-resistant Staphylococcus aureus. Int J Antimicrob Agents 43:26–31.
207. Jiang J-H, Bhuiyan MS, Shen H-H, Cameron DR, Rupasinghe TWT, Wu C-M, Le Brun AP, Kostoulias X, Domene C, Fulcher AJ, McConville MJ, Howden BP, Lieschke GJ, Peleg AY. 2019. Antibiotic resistance and host immune evasion in *Staphylococcus aureus* mediated by a metabolic adaptation. Proc Natl Acad Sci 116:3722–3727.
208. Otto M. 2014. Phenol-soluble modulins. Int J Med Microbiol 304:164–169.
209. Peschel A, Otto M. 2013. Phenol-soluble modulins and staphylococcal infection. Nat Rev Microbiol 11:667–673.

210. Boles BR, Horswill AR. 2008. agr-Mediated Dispersal of Staphylococcus aureus Biofilms. PLoS Pathog 4:e1000052.
211. Tsompanidou E, Sibbald MJJB, Chlebowicz MA, Dreisbach A, Back JW, Van Dijl JM, Buist G, Denham EL. 2011. Requirement of the *agr* Locus for Colony Spreading of *Staphylococcus aureus*. J Bacteriol 193:1267–1272.
212. Gurung M, Moon DC, Choi CW, Lee JH, Bae YC, Kim J, Lee YC, Seol SY, Cho DT, Kim SI, Lee JC. 2011. Staphylococcus aureus Produces Membrane-Derived Vesicles That Induce Host Cell Death. PLoS ONE 6:e27958.
213. Wang X, Thompson CD, Weidenmaier C, Lee JC. 2018. Release of Staphylococcus aureus extracellular vesicles and their application as a vaccine platform. Nat Commun 9:1379.
214. Sakoulas G, Eliopoulos GM, Moellering RC, Wennersten C, Venkataraman L, Novick RP, Gold HS. 2002. Accessory Gene Regulator (*agr*) Locus in Geographically Diverse *Staphylococcus aureus* Isolates with Reduced Susceptibility to Vancomycin. Antimicrob Agents Chemother 46:1492–1502.
215. Hall Snyder AD, Werth BJ, Nonejuie P, McRoberts JP, Pogliano J, Sakoulas G, Yim J, Singh N, Rybak MJ. 2016. Fosfomycin Enhances the Activity of Daptomycin against Vancomycin-Resistant Enterococci in an *In Vitro* Pharmacokinetic-Pharmacodynamic Model. Antimicrob Agents Chemother 60:5716–5723.
216. Benvenuto M, Benziger DP, Yankelev S, Vigliani G. 2006. Pharmacokinetics and Tolerability of Daptomycin at Doses up to 12 Milligrams per Kilogram of Body Weight Once Daily in Healthy Volunteers. Antimicrob Agents Chemother 50:3245–3249.